

**MICROFLUIDIC CELL PROCESSING FOR PERSONALIZED AND
REGENERATIVE MEDICINE**

A Dissertation
Presented to
The Academic Faculty

by

Nicholas Edwin Stone

In Partial Fulfillment
of the Requirements for the Degree
Doctor of Philosophy in the
Woodruff School of Mechanical Engineering

Georgia Institute of Technology
August 2021

COPYRIGHT © 2021 BY NICHOLAS STONE

MICROFLUIDIC CELL PROCESSING FOR PERSONALIZED AND REGENERATIVE MEDICINE

Approved by:

Dr. Todd Sulchek, Advisor
Woodruff School of Mechanical
Engineering
Georgia Institute of Technology

Dr. Ross Ethier
Woodruff School of Mechanical
Engineering
Georgia Institute of Technology

Dr. John McDonald
School of Biological Sciences
Georgia Institute of Technology

Dr. Budd Tucker
Department of Ophthalmology
University of Iowa

Dr. Alexander Alexeev
Woodruff School of Mechanical
Engineering
Georgia Institute of Technology

Date Approved: June 9, 2021

ACKNOWLEDGEMENTS

First, I would like to thank my advisor, Dr. Todd Sulchek for giving me a home in his lab and the opportunity to work on such an interesting and fulfilling project. He has always been very supportive, and his invaluable insight has been a great aid in completing the work contained in this thesis. I would also like to thank all of my committee members. Dr. Budd Tucker welcomed a graduate student from another institution into his lab and gave me the opportunity to apply our microfluidic technologies to iPSC manufacturing and the treatment of inherited degenerative blindness. He has also been a bottomless well of support and advice, and I will be forever grateful for the huge positive impact he has made on me personally and professionally. I would also like to thank Dr. John McDonald for giving me a strong background in cancer biology and for all the insight and support he has offered me over the years. Dr. Ross Ethier, in addition to helping me acquire a scary number of pig eyes in the early stages of my retinal work also showed a great interest in my project, for which I am very thankful. Finally, I'd like to thank Dr. Alexander Alexeev for all of the great conversations we had about microfluidic device design over the years, and for his continual support of me and this work.

I would also like to thank all of the professionals in the ME department office who have helped me so much over the years. I would particularly like to thank Ms. Glenda Johnson and Dr. Wayne Whiteman, who provided me with invaluable support on many occasions during my time at Georgia Tech.

Next, I would like to thank all my Sulchek labmates for being my family at Georgia Tech. Katie Young, in addition to providing valuable insight on cancer biology was always

willing to pitch in when I needed an extra pair of hands (or extra brain). Her passion for and dedication to helping others both through her research and in her private life is an inspiration. Alan Liu always kept me caffeinated, and was an invaluable resource on AFM. I'll always remember our beers at Cypress and hotpot dinners, both of which were highlights of my time in Atlanta. Anna Liu, for being a great friend, for managing the Sulchek lab's small army of undergraduate researchers and for developing CellVECT, a technology which holds great promise for application to iPSC-derived photoreceptor manufacturing. Abhishek Raj, for both his help on the ascites sorting project and for being a great resource for brainstorming sorting issues. Aaron Enten, for his boundless enthusiasm. Tong Yu, for all of her help on the transfection work. Peter Shankles, for his passion for coffee as well as his device design and manufacturing expertise. Katily Ramírez Mendez, for trying to teach me to dance. Betsy Campbell, Kathryn Murray, Tom Bongiorno, Muhymin Islam, Mike Bellavia, Bushra Tasadduq, Dan Potter, Shawn Newlan, Srinivas Hanasoge, and Avi Gupta for being great friends and colleagues, looking forward to seeing all of you at conferences for years to come!

I would also like to thank all my labmates in the Tucker lab for making me feel so welcome. Katie Cranston, without whom nothing would work, for keeping the lights on and the fires out, for her kindness and patience as well as for all the delicious baked goods. Jessica Cooke for teaching me about the wonders of Trizol, as well as for her perspective and wit. Erin Burnight, who is always willing to teach a mechanical engineer new tricks (like running gels) as well as for her sense of humor. Laura Bohrer, for all the help with cell culture and for helping me remain optimistic even when the experiments are not working. Drew Voigt, for melting down eyes like a champ while simultaneously being a

bioinformatics guru and a seriously nice guy. Adam DeLuca, for teaching me to write code all those years ago, for your bioinformatics expertise, and for always being up for beers after work. Kelly Mulfaul for being a great friend, and for being a constant example of hard work, determination, and scientific ability. Dalyz Ochoa and Brynnon Harman for always reminding me that they could beat me up, if they wanted. Kristin Anfinson, for always being willing to split me off some cells and for being patient when the robot is misbehaving. Jessica Fick, for making sure I always play by the rules. Christy Ralston, for not murdering me when I steal her pipet-aid. Nate, for showing interest in AFM. Emily Kaalberg, Arwin Shrestha, and Mallory Ulferts for their humor and positivity.

I would also like to thank my friends, who add so much joy to my life. Lucas Henneman, Ashton Imlay and Miriam Gutman for making small apartments feel like castles and strange cities feel like home. Gaby Hernández for being a constant source of companionship and sympathy, both from down the street and from across the country. Judah Gruen and Arhanti Sadanand, for making me feel like part of your family, and for not making too much fun of me when I came over to dinner with a load of laundry. Laura Carpenter, for letting me be the third wheel. Adam Sullivan and Aaron Seegmiller, for keeping me sane during a pandemic. Colin Kenny, for his perspective on life and science. Yoshi Sei, Candice Hovell Hester, Michael Toth, Angel Santiago-Lopez, and Song Ih Ahn, for fighting the good fight. Christen Anton, Matt Wittman, Dan Halpert, John Harrison, Andrew Rohrberger, Jack Murtagh, Haley Bruns and Thomas Pollack, for always being there. My life would not be the same without you guys.

Finally I would like to thank my family. Your support and encouragement has been a constant for my entire life, and gave me the ability to take risks (like grad school) which I

never would have been able to otherwise. Edwin Stone, for always doing what he thinks is right, even when it makes his life harder. Mary Stone, for her humor and support, as well as for always being a model of dedication and hard work. Carolyn Reddick, for her commitment to excellence in everything she does. Will Reddick, for being my brother even when we disagree. I love you all so much!

TABLE OF CONTENTS

ACKNOWLEDGEMENTS	iii
LIST OF FIGURES	x
LIST OF SYMBOLS AND ABBREVIATIONS	xii
AUTHOR CONTRIBUTION STATEMENT	xiv
SUMMARY	xvi
CHAPTER 1. Introduction	1
1.1 Specific Aim 1: Isolation of metastatic ovarian cancer cells from primary abdominal ascites samples.	4
1.1.1 Summary	4
1.1.2 Significance	5
1.2 Specific Aim 2: Sort photoreceptor cells from a heterogenous population of human retinal cells without relying on the use of cell surface antigens and antibodies.	5
1.2.1 Summary	5
1.2.2 Significance	6
1.3 Specific Aim 3: Use microfluidics to deliver large functional constructs to patient derived iPSCs in a one-step mechanical process	6
1.3.1 Summary	6
1.3.2 Significance	7
CHAPTER 2. Microfluidic processing of stem cells for autologous cell replacement	9
2.1 Abstract	9
2.2 Introduction	10
2.3 Cell Sorting Techniques	11
2.3.1 Label Based Strategies	11
2.3.2 Label Free Strategies	15
2.4 Transfection Techniques	20
2.4.1 Viral Transduction	21
2.4.2 Chemical Transduction Techniques	21
2.4.3 Electroporation	22
2.4.4 Microfluidic Transfection	22
2.5 Future Perspectives	26
2.6 Summary	28
CHAPTER 3. Label-free microfluidic enrichment of cancer cells from non-cancer cells in ascites	29
3.1 Abstract	29
3.2 Introduction	30

3.3	Methods	34
3.3.1	Device Design and Fabrication	34
3.3.2	Cell line preparation and sorting	34
3.3.3	Trajectory Analysis	35
3.3.4	Ascites Sorting for NGS Sequencing	36
3.3.5	Ascites Sorting for Immunocytochemistry	36
3.4	Results	38
3.5	Discussion	48
CHAPTER 4. Label-free microfluidic enrichment of photoreceptor cells		50
4.1	Abstract	50
4.2	Introduction	51
4.3	Methods	53
4.3.1	Human iPSC derived photoreceptor precursor cell line generation and culture	53
4.3.2	Lentiviral vector generation	54
4.3.3	Immunocytochemical analysis	55
4.3.4	AFM and force curve analysis	55
4.3.5	Human donor retina dissociation	56
4.3.6	Quantitative RT-PCR	57
4.3.7	Microfluidic device fabrication and cell sorting	57
4.4	Results	58
4.4.1	Design and optimization of a microfluidic retinal cell sorting device	58
4.4.2	Separation of RPE and iPSC-derived photoreceptor precursor cell lines via microfluidic cell sorting.	65
4.4.3	Microfluidic sorting of mature human donor derived retinal cells	67
4.5	Discussion	69
CHAPTER 5. Use microfluidics to deliver large functional constructs to patient-derived iPSCs in a one-step mechanical process		75
5.1	Abstract	75
5.2	Introduction	75
5.3	Methods	78
5.3.1	Atomic force microscopy	78
5.3.2	iPSC culture and maintenance	79
5.3.3	Microscopic analysis	79
5.3.4	iPSC size analysis	79
5.4	Results	80
5.5	Conclusions	90
CHAPTER 6. Conclusions		91
6.1	Aim 1: Label-free microfluidic enrichment of cancer cells from non-cancer cells in ascites	91
6.1.1	Summary	91
6.1.2	Future directions	93
6.2	Specific Aim 2: Label-free microfluidic enrichment of photoreceptor cells	93
6.2.1	Summary	93
6.2.2	Future directions	95

6.3	Specific Aim 3: Use microfluidics to deliver large functional constructs to patient derived iPSCs in a one-step mechanical process	95
6.3.1	Summary	95
6.3.2	Future directions	96
6.4	Summary	97
APPENDIX A.	Optimization of microfluidic sorting devices	98
APPENDIX B.	Design improvements for transfection devices	100
APPENDIX C.	List of publications	102
REFERENCES		104

LIST OF FIGURES

Figure 1	Overview of specific aims.	4
Figure 2	CD73 expression in the adult and developing fetal human retina.	14
Figure 3	Next-generation microfluidic cell sorting strategies.	17
Figure 4	Next-generation microfluidic cell devices.	24
Figure 5	Sorting of primary ascites samples.	38
Figure 6	Device Overview.	40
Figure 7	Trajectory analysis of ovarian cancer cell lines.	41
Figure 8	Sorting of ovarian cancer cell lines.	43
Figure 9	Sensitivity, specificity and accuracy analysis.	45
Figure 10	Sorting of Primary Ascites Samples.	47
Figure 11	Method for generating iPSC-derived photoreceptor precursor cell line.	54
Figure 12	Microfluidic cell sorting device designed for sorting of retinal cells.	60
Figure 13	Generation of a stable human iPSC-derived photoreceptor precursor cell line.	62
Figure 14	Mechanical characterization of retinal cell lines.	63
Figure 15	Optimization of cell enrichment parameters.	65
Figure 16	Sorting of ARPE-19 and hiPS-PPCs using a microfluidic cell sorting device.	66
Figure 17	Microfluidic sorting of retinal cells obtained from human donor eyes.	69
Figure 18	Figure 18. Mechanistic model of convective microfluidic delivery of macromolecules to cells.	82
Figure 19	Microfluidic transfection as compared to lipofectamine.	83
Figure 20	iPSC Morphology at various cell densities	85

Figure 21	Measured iPSC size for iPSCs derived from several different patients.	86
Figure 22	iPSC size at various culture conditions.	87
Figure 23	iPSC size immediately after dissociation and after 3 hours in suspension.	88
Figure 24	iPSC morphology at the center and edge of iPSC colonies.	89
Figure 26	Figure 26. Symmetric constrictions for transfection devices.	101
Figure 27	Figure 27. Hydrodynamic focusing channels for sheathless operation of transfection devices.	101

LIST OF SYMBOLS AND ABBREVIATIONS

AAV	Adeno-associated virus
AFM	Atomic force microscopy
cGMP	Current good manufacturing practice
CRISPR	Clustered regularly interspaced short palindromic repeats
CTC	Circulating tumor cell
DLD	Deterministic lateral displacement
DNA	Deoxyribonucleic acid
ECM	Extracellular matrix
EDTA	Ethylenediaminetetraacetic acid
ELISA	Enzyme-linked immunosorbent assay
FACS	Fluorescence activated cell sorting
FBS	Fetal bovine serum
FDA	Food and drug administration
FISH	Fluorescence <i>in situ</i> hybridization
FN	False negative
FP	False positive
GFP	Green fluorescent protein
HDR	Homology directed repair
hiPC	Human induced pluripotent cell
hiPC-PPC	Human induced pluripotent cell derived photoreceptor cell
iPSC	Induced pluripotent stem cell
iPSC-PPC	Induced pluripotent stem cell derived photoreceptor cell

IRB	Institutional review board
MACS	Magnetic activated cell sorting
NGS	Next generation sequencing
NHEJ	Non-homologous end joining
PBS	Phosphate buffered saline
PCR	Polymerase chain reaction
PDMS	Polydimethylsiloxane
qPCR	Quantitative polymerase chain reaction
RNA	Ribonucleic acid
RPE	Retinal pigment epithelium
rt-PCR	Reverse transcription-polymerase chain reaction
sgRNA	Single guide RNA
TALEN	Transcription activator-like effector nuclease
TG2	Transglutaminase 2
TN	True negative
TP	True positive

AUTHOR CONTRIBUTION STATEMENT

I, Nicholas Stone, am the principal author of all of the manuscripts presented in this thesis (chapters 2-5), but multiple other authors have made invaluable contributions to this work. My advisor, Dr. Todd Sulchek and my committee member Dr. Budd Tucker have co-authored all of the manuscripts contained in this work, and the specific contributions of each author to each manuscript are described below. Chapter 3 is a published manuscript, chapters 2 and 4 are in press, and chapter 5 is in preparation.

Chapter 2, “Microfluidic processing of stem cells for autologous cell replacement”. Dr. Budd Tucker, Dr. Todd Sulchek and myself wrote the manuscript and prepared Figure 3 and Figure 4. The RNA-seq data analysis presented in Figure 2, along with preparation of the figure itself was performed by Andrew Voigt and Dr. Robert Mullins.

Chapter 3, “Label-Free Microfluidic Enrichment of Cancer Cells from Non-Cancer Cells in Ascites”. Dr. Budd Tucker, Dr. Todd Sulchek, Dr. Abhishek Raj, Katie Young and I wrote the manuscript. Katie Young collected the data displayed in Figure 7B and assisted me and Dr. Abhishek Raj in performing the ascites sorting presented in Figure 10. Katie Young also assisted me in preparing the NGS libraries sequenced for Figure 9. In addition to his help with the ascites sorting, Dr. Raj performed the sorting and data analysis for Figure 8, as well as the sensitivity analysis presented in Figure 9. Dr. Benedict Benigno collected the ascites specimens used in this work. Dr. Adam Deluca performed the data analysis for the NGS data presented in Figure 10. Dr. Muhymin Islam fabricated the molds for the microfluidic chips used in this work. I prepared all of the figures other than Figure 9A and performed all other experiments.

Chapter 4, “Label-Free Microfluidic Enrichment of Photoreceptor Cells”. Dr. Budd Tucker, Dr. Todd Sulchek and I wrote the manuscript. Dr. Tucker prepared Figure 11, Figure 12, and Figure 13. Dr. Joseph Giacalone generated the iPSC-PPC cell line used in this manuscript and performed the characterization presented in Figure 13. Andrew Voigt prepared the dissociated human retina, the sorting of which is the focus of Figure 17. Dr. Srinivas Hanasoge fabricated the molds for the microfluidic devices used in this study. I performed all other experiments and prepared all remaining figures.

Chapter 5, “Use microfluidics to deliver large functional constructs to patient derived iPSCs in a one-step mechanical process”. Dr. Todd Sulchek, Dr. Budd Tucker and I wrote the manuscript. Dr. Tucker, Dr. Laura Bohrer and Dr. Jessica Cooke cultured the cells used in this work. Dr. Bohrer captured the micrographs presented in Figure 19, Dr. Tucker prepared Figure 20 and Figure 24. Dr. Peter Shankles and Tong Yu fabricated the devices used in this work. I performed all microfluidic transfection and size characterization experiments and prepared all other figures.

SUMMARY

Cell processing lies at the heart of modern medicine. While in the past, the treatment of diseases such as cancer was based mostly on the cancer's tissue of origin and histological classification, today these decisions are also informed by detailed functional and molecular characterization of a patient's own cancer cells, a practice commonly referred to as 'personalized medicine'. Treatments for cancer and other diseases have also recently evolved to use manufactured cell therapies derived from the patient's own tissue. For example, recent therapies for cancers such as leukemia reprogram immune cells harvested from a patient to target malignant cells, and regenerative medicine techniques seek to manufacture patient-derived cells capable of replacing tissue lost due to injury or inherited degenerative conditions.

While these new therapies are targeted at a wide variety of different conditions, they all share a dependence on efficient processing of patient cells, which often takes the form of either cell sorting or transfection. For example, for personalized medicine techniques to be effective, clinicians must have access to a patient's malignant cells. While cells from a solid tumor can be harvested via biopsy, depending on where the tumor is in the body, performing this type of biopsy can be an invasive procedure. One alternative is a 'liquid biopsy', where instead of removing a piece of a patient's primary tumor, a liquid sample such as blood or abdominal fluid is taken from the patient. While this type of procedure is generally significantly less invasive than a traditional biopsy, it does not yield a pure population of the patient's malignant cells. These cells are often a minority population in these liquid samples, surrounded by contaminating, non-malignant cells such

as blood and immune cells. To increase the sensitivity of any molecular or functional assays that caregivers plan to perform on these harvested cells, techniques are needed to sort the cancer cells needed for analysis from contaminating healthy cells.

Cell sorting is also required for manufacture of regenerative medicines. One such application is induced pluripotent stem cell (iPSC) derived autologous cell replacement therapies. In this approach, cells (usually fibroblasts harvested from a skin biopsy) are transformed into iPSCs through forced expression of a series of transcription factors. These iPSCs are then differentiated into cells capable of replacing tissue in the patient that has been lost due to injury or inherited degenerative disease. For example, in the case of inherited degenerative blindness one possible treatment is the implantation of manufactured patient-derived photoreceptors to replace those that the patient has lost over the course of their disease. While these approaches hold great promise, one issue with current cell manufacturing techniques is the limited control that scientists have over the lineage of differentiated cells. For instance, modern protocols for the generation of photoreceptor cells from patient derived iPSCs do not generate pure populations of photoreceptors. Instead, all of the cell types which make up the retina are generated, usually organized very similarly to the way they are *in vivo*. Given that not all of these cells are desired for transplantation, some mechanism is needed to separate the potent cells desired for transplant from the contaminating cells.

While mature cell sorting technologies exist, they have limitations that make them less than ideal for personalized and regenerative medicine. The two most mature technologies are known as fluorescence activated cell sorting (FACS) and magnetic activated cell sorting (MACS). In both techniques, labels are attached to cells using

antibodies that recognize markers present on cell surfaces. In FACS, these antibodies are conjugated to fluorophores, allowing the presence of the antibodies to be detected on the surfaces of the cells using optical techniques. Sorting is then accomplished with a fluidic system that passes cells one at a time through a series of lasers and photodetectors, after which the cells are deposited into different collection tubes based on the presence or absence of several different markers. The MACS approach, on the other hand, uses antibodies conjugated to paramagnetic beads. After labeling cells with these beads, tagged cells can be separated from untagged cells using a permanent magnet.

While both of these techniques can be very specific and operate at high throughput, their reliance on antibody labels makes them difficult to apply in some personalized and regenerative medicine applications. For example, in cancer applications there is often no unique marker present on the surface of cancer cells, and any markers that do exist can differ dramatically from patient to patient. Further, even if the required markers do exist, it is possible that conjugating an antibody to cell surface receptors could alter the behavior of cells in downstream functional assays. Similarly, in regenerative medicine applications where unique cell surface markers exist, conjugation of antibodies to cells destined for implantation into a patient constitutes a significant safety concern.

To address these concerns, ‘label-free’ sorting techniques (i.e. techniques that do not require antibody labels) are required. In recent years, this need has spurred the development of several such label-free techniques, many of which are implemented as microfluidic chips. While there are label-free techniques that are not based on a microfluidic platform, the microfluidic approach offers several key advantages. First, microfluidic devices based on standard microfabrication techniques can be manufactured

very cheaply, meaning that these devices can be designed as single-use disposables. In addition to making these approaches very inexpensive to incorporate into existing cell manufacturing workflows, there is also a significant safety benefit, given that the use of disposables drastically reduces the risk of cross-contaminating cells being manufactured for one patient with those destined for another. In addition, given the very small size of these devices, they are amenable to massive parallelization. This allows engineers and scientists developing these platforms to optimize the design at relatively small scale and then dramatically increase throughput once the design of the system has been optimized.

Another form of cell processing often required for the manufacture of cell therapies is transfection, the delivery of cargo into cells. For instance, when manufacturing cell therapies for the treatment of inherited blindness, the genetic defect which originally caused the onset of disease must be corrected in any cells destined for transplant to prevent the therapeutic cells from suffering the same fate as the patient's native cells. Similarly, in immune therapies for cancer, macromolecules must be delivered to the therapeutic cells in order to target them against the patient's cancer. Similarly to cell sorting, several techniques for cell transfection have been developed and commercialized, but these 'gold-standard' approaches have limitations which restrict their usefulness to manufacturing cell therapies. Current 'gold-standard' approaches include viral transfection, electroporation and lipofection.

Viral transduction is a robust technique, capable of very high transfection efficiency. In this technique, nucleic acid sequences that encode proteins that alter cell behavior when expressed are packaged into viruses, which then inject their payload into cells. While this approach is very well characterized and efficient, it suffers from several

important drawbacks. First, packaging the desired message into viruses is not a simple process, and requires specialized equipment and highly trained personnel. Second, when these viruses are engineered to incorporate their payload into host cells, there is a risk of mutagenesis, which could cause transformed cells to form tumors. Finally, there is an upper limit on the size of constructs that can be packaged into viral vectors. This limit is smaller than many therapeutically relevant genes. For instance, USH2A, mutations in which are responsible for multiple forms of inherited blindness, is too large to be packaged into the most clinically favorable viruses.

Non-viral techniques, such as lipofection and electroporation, are not subject to these packaging limitations, but have their own drawbacks. First, while it is possible to use these techniques to deliver constructs that cannot be packaged into viruses, the delivery efficiency of these techniques drops significantly with increasing payload size. Therefore, while it is possible to use these systems to deliver large genes such as USH2A, these approaches have very low transfection efficiency for these large payloads. In addition, both of these techniques require the use of proprietary reagents which pose a significant regulatory burden in terms of proving their safety for use in human subjects.

Due to these drawbacks, the research community has recently developed reagent-free microfluidic transfection platforms that accomplish delivery into cells through mechanical perturbation of the cells. In addition to evading the regulatory burdens associated with lipofection and electroporation, these platforms are also not subject to the packaging size limitation posed by viruses. Further, as discussed above with respect to microfluidic sorting platforms these approaches can be implemented as low-cost disposable chips which is desirable in terms of safety and allows easy incorporation into

existing cell manufacturing pipelines without requiring the purchase of large, expensive equipment that must be thoroughly decontaminated after each use. New transfection platforms are needed that exhibit high transfection efficiency that is not a function of construct size for correcting disease-causing mutations in large genes in cells destined for transplant into a patient.

In this thesis, I will detail the development of microfluidic platforms capable of solving significant issues in current cell processing pipelines for personalized and regenerative medicine applications. After a review of methods currently being developed by the community to address the issues in ‘gold-standard’ techniques, I will present my recent intellectual and technological contributions to this effort. First, I will describe my development of a label-free, microfluidic approach for the isolation of metastatic cancer cells from liquid biopsies of ovarian cancer patients, demonstrating how this technology can enhance both diagnostics and prognostics in cancer treatment. Next, I will demonstrate how microfluidics can be used to separate dissociated human retina into therapeutically relevant subpopulations as an example of how these techniques can be used to separate cells with a desired phenotype from cells of related lineages to enhance the potency of iPSC derived cell therapies. Finally, I will present my work on the development of microfluidic methodologies to enable high-efficiency, reagent-free delivery of macromolecules to iPSC cells. Taken together, this work demonstrates the promise of microfluidics to revolutionize the fields of cancer treatment, cell manufacturing and regenerative medicine.

CHAPTER 1. INTRODUCTION

Today, many therapeutic approaches rely on the efficient processing of patient cells. Personalized medicine, which promises to revolutionize oncologic care and regenerative medicine to treat many diverse conditions, depends on the processing of a patient's own cells using a variety of techniques. For most cancers, gathering cells via biopsy is an invasive process, meaning it is often preferable to isolate a patient's metastatic cells from samples which can be obtained relatively non-invasively such as blood or other liquid patient samples. But in many liquid biopsies of patient cell samples, such as from abdominal ascites or pulmonary effusions, the cells of interest generally make up a small percentage of the heterogeneous cell population present in the sample causing high rates of false negative specimens. Therefore, the first step in most personalized medicine approaches is the isolation of the cells of interest from some mixed population of normal and oncologic cells. In addition, the last step in many cell therapies is the isolation of potent cells required for treatment from contaminating cells. This can be performed using a variety of approaches, including flow activated cell sorting (FACS), magnetic activated cell sorting (MACS), as well as new microfluidic approaches including ours, in which high-throughput mechanical manipulation is used to sort cells by their mechanical properties.

While MACS and FACS can be quite selective, they generally require the cells of interest to express some type of unique surface protein that can be tagged using antibodies, which increase the cost and complexity of the assay. In some cases, these markers are not expressed solely on the cells of interest, making these approaches much harder to apply successfully to obtain sufficient purity. Novel label-free microfluidic methods, including

our platform, can allow us to sort based on cellular mechanical properties that may be sufficiently distinct to the target cells to avoid relying on the presence of cell surface markers. Label free approaches would be ideal to isolate tumor cells with unreliable or absent cell surface antigens, such as metastatic ovarian cancer cells from liquid abdominal ascites samples.

In regenerative medicine applications, since therapeutic stem cells are transplanted into patients to regenerate tissue, an additional safety concern is at stake in separations. In therapeutic cell engineering, all reagents applied to the cells must be guaranteed to be safe in order to gain regulatory approval. As antibodies used for labeling are derived from animal sources, they pose an additional risk and regulatory burden. Therefore, label free sorting of the therapeutic cells from a heterogeneous culture is desirable. In a project focused on cell replacement-based treatment of inherited retinal degenerative blindness, we generate retinal photoreceptor cells destined for retinal transplantation by differentiating patient-derived induced pluripotent stem cells (iPSCs). Retinal differentiation protocols, while very effective in generating photoreceptor cells, also produce contaminating retinal cell types such as retinal pigmented epithelium, retinal ganglion and bipolar interneurons, which are less useful therapeutically and should be removed prior to transplantation. Sorting these cells using gold-standard approaches such as FACS and MACS, which as indicated above rely upon the use of antibodies, would drastically increase cell manufacturing labor, patient risk and the regulatory burden of the therapy. In addition, conjugating antibodies to the cells destined for transplant could compromise the effectiveness of the treatment.

In addition to its utility for cell sorting, we further have discovered that high-throughput mechanical manipulation of cells, specifically rapid, repeated cellular compression, can facilitate delivery of large macromolecules and other therapies into the cell interior [1], [2]. For this platform, delivery is accomplished via convective, rather than diffusive transport, meaning that delivery efficiency is not a strong function of the size of the construct being delivered into the cells. The delivery of large nucleic acids provides an ideal solution to the challenge of CRISPR-based correction of genetic defects that cause inherited eye disease. Multicistronic CRISPR constructs, which contain guide RNAs, homology-directed repair (HDR) templates and antibiotic selection cassettes, can be well over 14,000 base pairs in length, resulting in transfection efficiencies of lower than 1% when using lipofectamine. Using our new discovery of convective transport of genetic cargo, mediated by a microfluidics-based approach, we find that transfection can be achieved without the use of chemical reagents which will result in safer treatments and lower regulatory burden.

The long-term goal of this research is to enable high-throughput purely mechanical processing of cells for therapeutic applications. To achieve this goal, I will leverage a microfluidic platform which applies repeated, high speed compressions to single cells in the pursuit of three specific aims, a summary of which is presented in Figure 1.

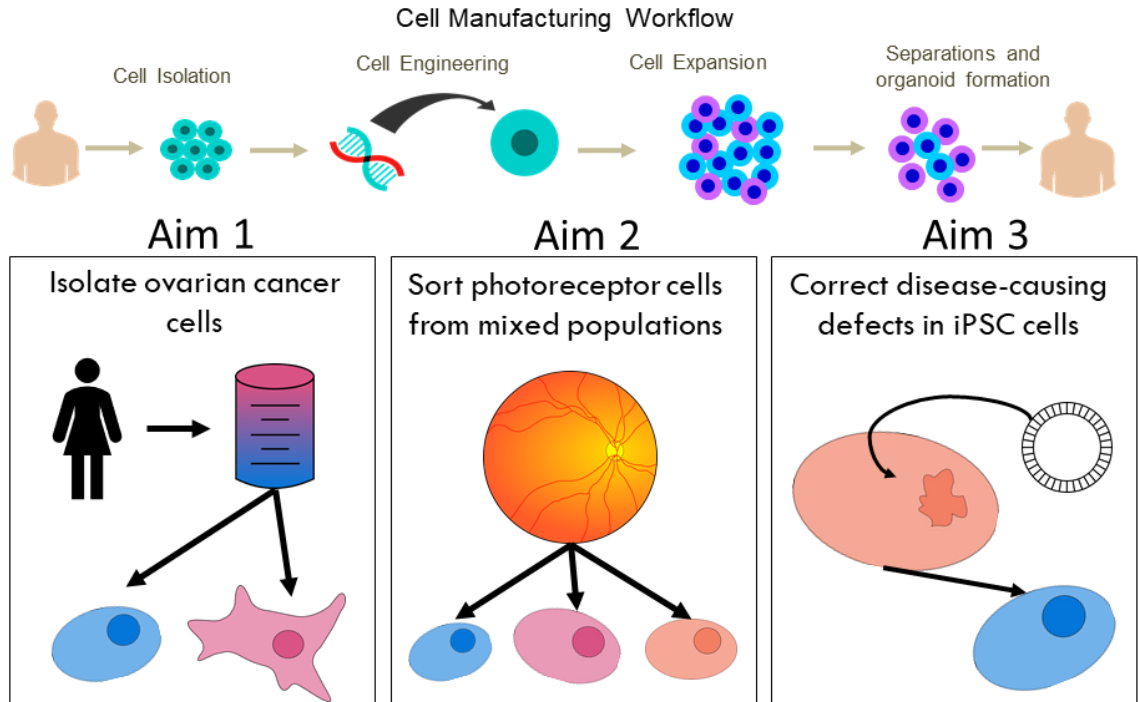


Figure 1. Overview of specific aims. Each aim addresses a need in modern cell manufacturing workflows (top). Aim one demonstrates isolation of cancer cells from patient liquid biopsies. In aim two, I demonstrate how microfluidics can be used to sort photoreceptors from dissociated human retina, as a model for how mixed cell populations can be sorted to increase the potency of manufactured cell therapies. In aim three I explore how microfluidics could be used to make transfection more efficient in cell engineering applications.

1.1 Specific Aim 1: Isolation of metastatic ovarian cancer cells from primary abdominal ascites samples.

1.1.1 Summary

A microfluidic sorting device was designed and tested to isolate metastatic ovarian cancer cells from the abdominal ascites of patients with advanced ovarian cancer. In order to optimize the device's sensitivity to the differences between cells with differing levels of malignancy and metastatic potential, we first flowed pure populations of representative cell lines through the device and assess the trajectory of each cell type using high-speed

microscopy. We then proceeded to optimize the sorting of a malignant cell line from a non-malignant cell line to determine device parameters (constriction size) and experimental conditions (flow rate) that allow for the most specific sorting of cells based upon their metastatic potential. Finally, we sorted the heterogeneous cell population present in the abdominal ascites of patients with late stage ovarian cancer. Our ability to sort these cells was assessed by examining the rate of P53 mutations present in the cell populations as well as by staining the sorted populations for TG2, overexpression of which is associated with malignancy in ovarian cancer.

1.1.2 Significance

In this aim, we demonstrate the first ever label-free microfluidic enrichment of primary ovarian cancer cells from patient ascites samples. Our success in this effort shows that label-free microfluidic cell sorting has the potential to increase the sensitivity of functional and molecular characterization of cancer cells for personalized medicine applications by enabling the preparation of purified samples of cancer cells from liquid biopsies without depending on cell surface markers.

1.2 Specific Aim 2: Sort photoreceptor cells from a heterogeneous population of human retinal cells without relying on the use of cell surface antigens and antibodies.

1.2.1 Summary

To optimize sensitivity to the biomechanical differences between cell types present in human retina we performed the first mechanical characterization of two representative

retinal cell lines, a retinal pigmented epithelial cell line (ARPE-19) and a human iPSC derived photoreceptor precursor cell line (iPSC-PPC). After discovering that the two cell lines representative of important retinal cell types were mechanically distinct, we proceeded to sort the two cell lines and assessed enrichment via flow cytometry. Finally, we used the optimized microfluidic device to sort dissociated postmortem human retinal cells. Sorting performance was assessed using qPCR to demonstrate enrichment of different retinal cell subpopulations at different outlets of the microfluidic device.

1.2.2 Significance

In this aim, we demonstrate the first-ever label-free microfluidic fractionation of dissociated human retina into biologically meaningful subpopulations. This success indicates that label-free microfluidic cell sorting could be used to isolate photoreceptors from the mixed population of cells produced by modern iPSC retinal differentiation protocols. Such label-free isolation of photoreceptors has the promise to increase the potency of cell therapies for inherited retinal degenerative blindness without the use of animal-derived antibodies and other reagents that could compromise the safety of the treatment.

1.3 Specific Aim 3: Use microfluidics to deliver large functional constructs to patient derived iPSCs in a one-step mechanical process

1.3.1 Summary

To enable the design of a microfluidic transfection platform for the delivery of multicistronic plasmids encoding humanized Cas-9, guide RNAs and homology-dependent

repair (HDR) templates for correction of mutations in iPSCs generated from patients with inherited retinal degenerative blindness microscopic size analysis was carried out. Based on this data we designed devices with a range of gap sizes and demonstrated delivery of a large multicistronic CRISPR/Cas9 construct that was comparable to the gold-standard lipofectamine. To enhance transfection efficiency further, an extensive characterization of the size of patient-derived iPSCs under a variety of conditions was carried out on cells in suspension. In addition to revealing which factors need to be controlled in order to minimize batch-to-batch variability in iPSC size, this work revealed that a significant degree of heterogeneity in terms of size exists in every population of iPSCs measured in this study. In order to enable high-efficiency transfection of these heterogeneous populations, we propose the design of a multistage microfluidic platform which consists of a microfluidic sorter upstream of a convective mechanical transfection stage as future work. The sorter will be used to split heterogeneous iPSC populations into subpopulations much more homogenous in size. These subpopulations will then be transfected using transfection channels optimized for each subpopulation, enabling high-efficiency delivery of large macromolecules to iPSCs.

1.3.2 Significance

In this aim, we demonstrated the first ever convective microfluidic delivery of CRISPR genome-editing reagents to patient-derived iPSCs. Further, we performed the first ever extensive characterization of the size of iPSCs in suspension, which resulted in the discovery of significant size heterogeneity in patient derived iPSCs. This discovery suggests that multistage microfluidic devices which sort cell by size before transfection

could dramatically increase the efficiency of microfluidic delivery of large constructs to patient-derived iPSCs.

CHAPTER 2. MICROFLUIDIC PROCESSING OF STEM CELLS FOR AUTOLOGOUS CELL REPLACEMENT

2.1 Abstract

Autologous photoreceptor cell replacement is one of the most promising approaches currently under development for the treatment of inherited retinal degenerative blindness. Unlike endogenous stem cell populations, induced pluripotent stem cells (iPSCs) can be differentiated into both rod and cone photoreceptors in high numbers, making them ideal for this application. That said, in addition to photoreceptor cells, state of the art retinal differentiation protocols give rise to all of the different cell types of the normal retina, the majority of which are not required and may in fact hinder successful photoreceptor cell replacement. As such, following differentiation photoreceptor cell enrichment will likely be required. In addition, to prevent the newly generated photoreceptor cells from suffering the same fate as the patient's original cells, correction of the patient's disease-causing genetic mutations will be necessary. In this review we discuss literature pertaining to the use of different cell sorting and transfection approaches with a focus on the development and use of novel next generation microfluidic devices. We will discuss how gold standard strategies have been used, the advantages and disadvantages of each, and how novel microfluidic platforms can be incorporated into the clinical manufacturing pipeline to reduce the complexity, cost and regulatory burden associated with clinical grade production of photoreceptor cells for autologous cell replacement.

2.2 Introduction

Development of patient-derived induced pluripotent stem cells, next-generation sequencing and genome editing technologies have fueled the field of personalized medicine, which can be defined broadly as use of the patient's own data to inform diagnosis and develop customized treatments. Autologous cell replacement is at the leading edge of this field. The most promising autologous cell replacement strategies currently under development rely on the use of induced pluripotent stem cells (iPSCs), which require tissue-specific differentiation prior to transplantation. For instance, we and others have shown that following subretinal transplantation, iPSC-derived photoreceptor precursor cells are able to restore retinal function in animal models of retinal degenerative blindness [3]–[12]. Following decades of development, the vast majority of the differentiation protocols reported faithfully recapitulate normal retinal development, which means that they give rise to each of the different cell types found in the retina [12]–[42]. For therapeutic photoreceptor cell replacement, enrichment of photoreceptor precursor cells away from the unwanted cell types (i.e., retinal ganglion cells, bipolar inter neurons, retinal pigmented epithelial (RPE) cells, etc.) will be desirable.

In addition to requiring the use of sorting technologies, autologous stem cell therapies for inherited diseases are also likely to require a method for delivering reagents to the interior of cells in order to modify their genome prior to differentiation and transplantation. For instance, when using patient-derived induced pluripotent stem cells to generate photoreceptors for the treatment of inherited retinal degenerative blindness, the disease-causing genetic defect that initially resulted in photoreceptor cell dysfunction and death will likely need to be repaired prior to transplantation. As we and others have shown, repair

can be accomplished by delivering macromolecules such as Cas9 and homology dependent repair (HDR) sequences to patient derived iPSCs followed by clonal selection and cell line expansion [43]–[45].

In this review, we will discuss common techniques for both cell sorting and transfection and show how current ‘gold standard’ methods compare with new state of the art microfluidic approaches for stem cell processing. In doing so we will discuss how novel microfluidic strategies have the potential to decrease the cost, complexity and regulatory burden associated with conventional approaches.

2.3 Cell Sorting Techniques

2.3.1 Label Based Strategies

Currently, fluorescence-activated cell sorting (FACS) and magnetic-activated cell sorting (MACS) constitute the gold standard of cell sorting approaches. Both techniques are selective and capable of processing cells with very high throughput. Selectivity is most commonly conferred via the use of antibodies designed to target specific cell surface antigens.

For FACS, cells are first labeled using fluorescent antibodies, dyes or genetic reporters. They are then passed one cell at a time through a series of lasers, which each excite the cell at a specific wavelength. The light emitted by these fluorophores is then detected by photodetectors, which allow for the identification of the fluorescent signal present. Based on the markers detected, a FACS machine can then deposit different cell populations into separate containers using electrostatic force to deflect single cell liquid

droplets. This approach has been used widely for mouse photoreceptor cell isolation and subsequent subretinal transplantation. For instance, several groups have used reporter mouse strains engineered to express green fluorescent protein under control of the NRL promoter to isolate photoreceptor precursor cells at various stages of retinal development to evaluate the role of cellular maturation on functional integration following transplantation [46]–[48]. Similarly, using genetically modified pluripotent stem cell fluorescent reporter lines, several groups have adopted this sorting strategy for evaluating human retinal development in vitro and to identify photoreceptor precursor cells following isolation and subretinal transplantation in vivo [49]–[51]. Unfortunately, this strategy relies on endogenous expression of a cell type-specific fluorophore and as such is unlikely to be useful for clinical application. This is especially true for photoreceptor cell replacement where endogenous expression of a fluorescent protein such as GFP would likely interfere with normal visual function.

Unlike FACS, MACS relies exclusively on the use of antibodies to attach paramagnetic beads to the surface of cells, which allows these cells to be pulled out of suspension using a strong magnet. Once isolated, antibody bound beads can be released and cells used for downstream applications. For instance, several groups have used cluster of differentiation antigen 73 (CD73) antibody-bound magnetic beads to isolate photoreceptor precursor cells that retain the ability to integrate into the rodent retina following transplantation [52]–[56]. Like many cell surface markers, CD73 has been reported to be expressed on a variety of different cell types [57]–[59]. For enhanced specificity, Lakowski and colleagues demonstrated that a panel of 5 cluster of differentiation antigens (i.e., CD73+, CD24+, CD133+, Cd47+ and CD15-) could be used to isolate photoreceptor precursor cells from

embryonic stem cells [57]. Unfortunately, the MACS approach is not well suited for multiple marker-mediated isolation of specific cell populations as selecting for multiple markers would require sequential isolation, increasing the difficulty of the procedure while also increasing cell loss. As such, the above-described study was performed using FACS. Interestingly, as shown in Figure 2, in both developing fetal and adult human retina CD73 appears to be predominantly expressed on a subset of Rod photoreceptor cells. While the lack of expression in non-photoreceptor cell types in the human retina is desirable, the fact that CD73 does not appear to be expressed by cone photoreceptor cells, even during early retinal development, is of concern for cell replacement, as cone photoreceptor cells will be required to restore high acuity vision. Interestingly, Gagliardi and colleagues convincingly demonstrate that human CD73 enriched photoreceptor precursors have the ability to give rise to cells expressing blue and red/green cone opsin following subretinal transplantation [52]. As such, additional lineage tracing studies to demonstrate the fate of CD73-positive progenitor cells are needed if this approach is to be used clinically.

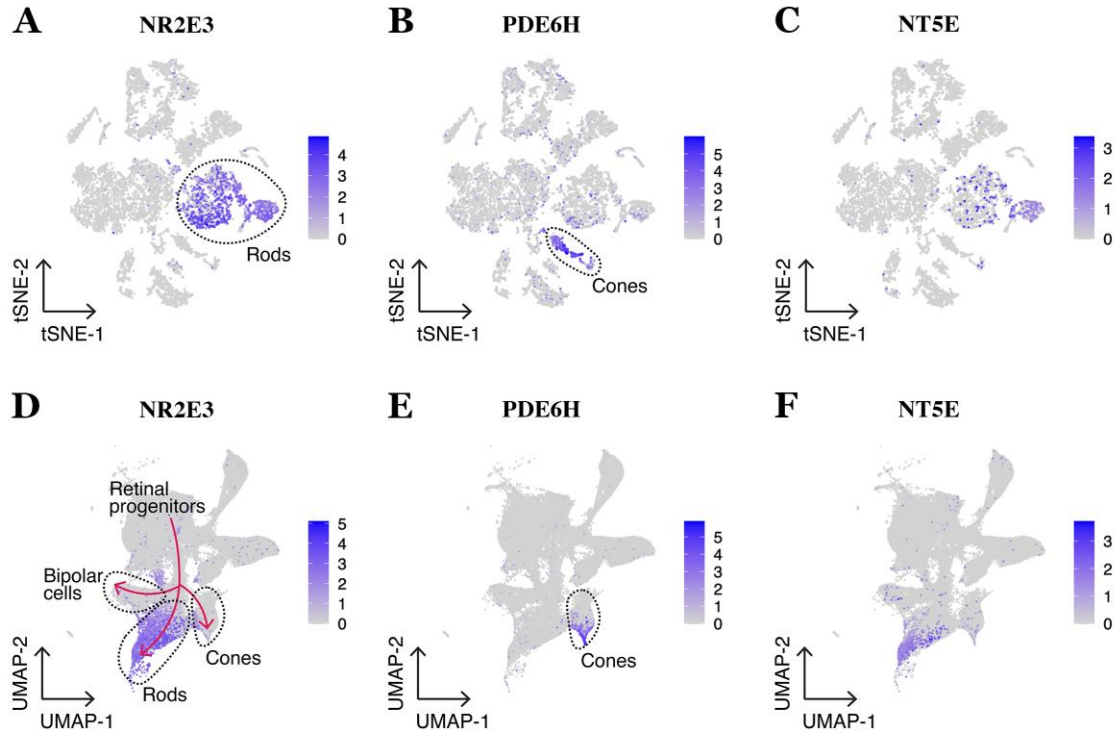


Figure 2. CD73 expression in the adult and developing fetal human retina. A-C: Single-cell RNA sequencing of adult human retinal cells [60] demonstrates that the NT5E gene that encodes CD73 is expressed by a select population of mature rod photoreceptor cells only. **D-F:** Re-processed single-cell RNA sequencing of developing fetal human retinal cells [61] demonstrates that NT5E is predominantly expressed by committed rod photoreceptor cells, with very infrequent expression in retinal progenitor cells and developing cone photoreceptor cells.

While MACS and FACS can be useful for cell sorting, as indicated above, to be clinically relevant, cell surface antigens and corresponding antibodies are required. Unfortunately, in many cases targetable antigens either do not exist or are not expressed solely on the cell type of interest, making these approaches challenging to apply successfully. For instance, until recently cell surface antigens useful for isolation of corneal limbal stem cells remained elusive. Although we were able to demonstrate that ABCB5 was expressed on limbal stem cells and could be used for cellular enrichment to successfully treat animal models of limbal stem cell deficiencies, this marker is not Limbal stem cell specific [62]–[64].

Similarly, markers that are often used for stem cell-derived vascular endothelial cell enrichment (e.g., CD31) are expressed on a variety of different endothelial cell populations and monocytic cells, making them less than ideal for isolation of tissue specific vascular subtypes [65]–[67].

2.3.2 Label Free Strategies

In regenerative medicine, therapeutic stem cells or their progeny are typically transplanted into patients to rebuild injured tissues. For clinical cell replacement, all reagents applied to the cells must be fully characterized and guaranteed to be safe in order to gain regulatory approval. The use of fluorescent and/or magnetic bead bound antibodies that target specific cell surface antigens for cell sorting, increases the labor and regulatory burden associated with clinical translation. For instance, conjugation of antibodies to cells destined for transplant followed by sorting is both time consuming and has the potential to alter cell function and compromise both safety and the effectiveness of the treatment. In addition, FACS, which requires a complex specialized piece of equipment, presents significant manufacturing challenges. For autologous cell replacement for instance, FACS protocols must reliably prevent cross contamination of patient derived cell lines following sequential sorting. This would likely require a complete sterilization between each sorting run. Sorting strategies that utilize pre-sterilized single use devices that do not require specialized reagents would be much more desirable. To address concerns associated with label-based cell enrichment, a variety of different label-free microfluidic cell sorting approaches are being developed. Microfluidic sorting methods are typically designed to sort cells based on physical characteristics such as diameter and stiffness, which avoids reliance on the presence of unique cell surface antigens and reagents. These platforms are generally

implemented as cheap, disposable chips driven by an external pump (e.g., syringe pump or peristaltic pump). Such label free approaches are ideal for isolation of cells with unreliable or absent cell surface antigens and terminally differentiated stem cell progeny that are destined for clinical cell replacement. Two of the most commonly used microfluidic device designs published to date are 1) deterministic lateral displacement (DLD) and 2) hydrodynamic focusing. There are also many label free cytometry approaches being developed, such as ghost cytometry [68], impedance cytometry [69] and deformability cytometry [70] which will likely play an important role in cellular analysis going forward. However, these platforms have not yet been integrated into cell sorters, so we will not be covering them in depth in this review.

2.3.2.1 Deterministic Lateral Displacement

As shown in Figure 3A, in deterministic lateral displacement (DLD) a series of microposts are used to move cells perpendicular to the direction of fluid flow in a manner related to their size and stiffness. Several groups have successfully used this approach to separate a variety of different cell types [71]–[73]. For instance, Xavier and colleagues recently demonstrated how this approach could be used to isolate skeletal progenitor cells from human bone marrow [71]. Specifically, they showed that by using DLD they could successfully isolate skeletal progenitor cells, which were stiffer than leukocytes and contained within the larger cell fraction of bone marrow. These isolated progenitor cells retained their ability to form clones in cultures indicating that they retained their stem cell potential. One of the drawbacks of DLD however, is that it is susceptible to clogging. As cell debris and/or aggregates cannot easily escape the active region of the DLD device they

become trapped, disrupting the flow pattern required for sorting, which in turn negatively impacts enrichment efficiency.

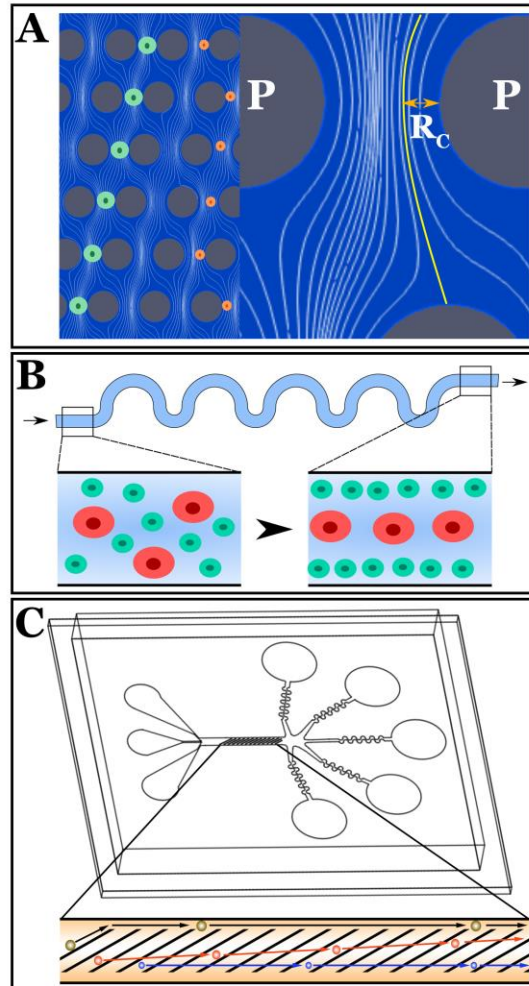


Figure 3. Next-generation microfluidic cell sorting strategies. A-C: Microfluidic cell sorting strategies that utilize deterministic lateral displacement (A, adapted from [74], streamlines obtained via CFD simulation), hydrodynamic focusing (B, Adapted from [75]) and cellular compression with lateral deflection (C). For DLD, cells start in a given streamline. If the cell is larger than a critical size, it is displaced laterally into a new streamline due to interaction with the posts (P). For hydrodynamic focusing, the balance between a wall interaction force, a shear gradient lift force and Stokes drag dictates the presence of equilibrium positions for cells suspended in a liquid. Over time, cells will tend to occupy equilibrium positions within the channel, resulting in size-based focusing. For cellular compression with lateral deflection, the sorting platform consists of a series of diagonal constrictions designed to deflect cells laterally relative to the main direction of flow in a manner related to their size and mechanical properties.

2.3.2.2 Hydrodynamic Focusing

Hydrodynamic focusing uses hydrodynamic forces to cause cells to come to an equilibrium position in a channel. As illustrated in Figure 3B, this equilibrium position is determined by balancing of lift and drag forces, which is a function of cell size and biomechanical properties (i.e., stiffness and viscosity). Like DLD, hydrodynamic focusing has been used successfully to sort a variety of different cell types, including endogenous stem cells [76]–[78]. For instance, Hur and colleagues were able to show how hydrodynamic focusing could be used to isolate adrenal cortical progenitor cells from a mixed cell population obtained from digestions of murine adrenal glands [76]. Separation was accomplished by exploiting the differing strengths of cell-cell adhesion between undifferentiated precursors and differentiated somatic cells. Given that the cell-cell junctions are stronger between differentiated cells than undifferentiated cells, a digestion protocol was developed which resulted in complete dissociation of progenitor cells leaving the differentiated somatic cells in larger clumps. The clumps and single cells could then be hydrodynamically sorted by size to effectively separate progenitor cells from the contaminating somatic cells with little to no reduction in viability (i.e., not significantly different from unsorted control samples). As enriched adrenal progenitor cells could subsequently be expanded in culture, it is conceivable that these cells could be given back to the patient from whom they were derived in order to restore adrenal function. One drawback of this technique is that it takes relatively large differences in cell size and/or stiffness to result in detectable differences in equilibrium position.

2.3.2.3 Our Platform

Due to the issues mentioned above, neither DLD nor hydrodynamic focusing are ideal for sorting of pluripotent stem cell derived photoreceptor precursor cells from each of the different cell types derived following retinal differentiation [16], [23]–[33], [79]–[84]. Specifically, following retinal organoid dissociation clusters of RPE and/or inner retinal cell types is common, as such the potential for DLD device clogging is high. Similarly, the differences in size between retinal cells that are liberated from organoids are less than ideal for efficient hydrodynamic sorting. To address these concerns, we recently developed the microfluidic cell sorting platform illustrated in Figure 3C. Using this device cells are exposed to repeated compressions by a series of thin ridge constrictions oriented diagonally to the direction of flow. In our hands, these repeated compressions do not have a significant impact on cell viability [85]. As cells interact with these constrictions, which are designed to be smaller than the cell's diameter, they deflect laterally in the device in a manner related to their size and stiffness. The performance of this platform is dependent on the gap size and as such must be reoptimized for each application. The design of the constrictions allows cell debris and aggregates to move along the constrictions into a gutter and exit the device without causing clogs. At the end of the device there are 5 independent wells from which sorted cell populations can be collected. To evaluate the utility of this platform, we recently performed a series of experiments using iPSC derived photoreceptor precursor and RPE cell lines as well as human donor retina [86]. When photoreceptor precursor and RPE cells were mixed at a ratio of 37% RPE to 63% photoreceptor precursor cell and injected into the device at a concentration of 2×10^6 cells per mL, we were able to reliably separate the photoreceptor precursor cells from the RPE cells. Similarly, when human donor retina

was dissociated and sorted using the device, we were able to isolate independent samples enriched for RPE (largest fraction in well 1), rod and cone photoreceptor cells (largest fraction in well 4) and inner retinal neurons, including retinal ganglion cells (enriched in wells 1-3) [86]. Although we believe that there is still room for further improvement, these findings demonstrate that retinal cells can be separated into discrete populations by exploiting differences in cell size, stiffness and viscosity [87]–[89] (i.e., without the need for antigen specific antibodies or fluorescent markers). Moreover, naturally occurring stem cells may be processed in a similar manner to enrich for desired cell phenotypes [90].

2.4 Transfection Techniques

Since autologous iPSCs possess the same genome as the patient from whom they are derived, the use of these cells for treatment of inherited disease will likely require correction of the disease-causing genetic variants that resulted in death of the target cell type prior to differentiation. Genome editing approaches that utilize zinc finger nucleases, Talens or CRISPR/Cas9 to induce double strand DNA breaks and homology directed repair of target genetic loci, have been used for this purpose [91]–[93]. In addition, next-generation CRISPR technologies including base editors, primer editors and RNA-targeting Cas effectors, which can be used to restore gene function in the absence of double strand DNA break induction, are promising new approaches [94]. For these strategies to work, delivery of nucleic acid and/or protein to patient derived iPSCs, followed by genetic screening and expansion of genetically corrected clones, is required. Although several strategies for delivering genome editing reagents to iPSCs exist, the most widely used are 1) viral transduction, 2) chemical transfection and 3) electroporation.

2.4.1 *Viral Transduction*

Viral transduction takes advantage of the native ability of viruses to insert their DNA into infected cells. By replacing the genetic material required for replication, viruses can be engineered to deliver sequences of interest to a variety of different cell types with high efficiency. For instance, adeno associated viruses (AAV) are used extensively in both pre-clinical and clinical settings to safely deliver therapeutic DNA to photoreceptor cells and mitigate disease progression [95]–[99]. Unfortunately, the packaging capacity of AAVs is limited to approximately 4.7kb, making them less useful for delivery of the genome editing reagents required to induce homology directed repair in patient derived iPSCs in vitro since CRISPR/Cas9 and repair templates exceed this limit. For this reason, lentiviruses, which have a payload of approximately 8kb, have been widely used for genome editing of patient derived iPSCs [100]–[103]. Although successful, the major drawback associated with the use of lentivirus is that they carry increased risk of inducing insertional mutagenesis resulting from random insertion of the genetic payload into the host cell’s genome [104]. In addition, viruses are only useful for delivery of nucleic acids, which precludes their use for CRISPR mediated genome editing via delivery of ribonuclear proteins, which are often significantly more efficient [105], [106].

2.4.2 *Chemical Transduction Techniques*

Chemical reagents such as lipofectamine are quite common for delivery of macromolecules given that they are not subject to the packaging size limitation that viruses are subject to. These techniques involve conjugating a positively charged carrier with target nucleic acids. This positively charged complex is then attracted to the cell membrane, whereby it is taken

up via endocytosis. One of the greatest advantages of this approach is the ease and speed with which it can be utilized. Specifically, unlike viral transduction, which requires engineering of a viral plasmid and packaging into viral particles by trained technical staff using well characterized safety protocols, lipofection can be safely performed using almost any expression plasmid.

2.4.3 Electroporation

As with lipofection, electroporation also avoids concerns associated with cargo size limits. Electroporation works via exposure of cells to large electric fields that cause pores to form transiently in the cell membrane through which macromolecules can enter. Both lipofection and electroporation have been used extensively by us and others for CRISPR mediated correction of patient derived iPSCs with excellent success [91], [107]. The major drawback of both techniques is that they use proprietary reagents that would be subject to FDA regulation when used for clinical cell replacement. As these reagents are not typically produced under and compliant with cGMP the regulatory burden associated with their use is high.

2.4.4 Microfluidic Transfection

To address these concerns, we and others have pioneered the use of novel microfluidic approaches designed to deliver macromolecules to cells without the need for specialized reagents. In general, microfluidic transfection strategies rely on physical deformation of a cell to induce pore formation. Macromolecules (nucleic acids, proteins, etc.) are then delivered by either diffusion or convective transport. These transfections are generally very

fast (less than an hour of processing time) after which the cells can be re-plated and expanded for downstream selection, clonal expansion and validation.

2.4.4.1 Microfluidic Transfection Mediated By Diffusive Transport

In 2008, Hallow and colleagues demonstrated that fluid shear forces can be used to deliver a macromolecule cargo into cell lines [108]. In 2012 Sharei and colleagues reported the development of a microfluidic cellular transfection device that was designed to deliver macromolecules to cells by passing them through a narrow constriction at high flow rates [109]. By squeezing the cells into a small channel, the authors demonstrated that they could cause pores to form in the cell membrane through which a payload suspended in the surrounding buffer could be passed into the cell through diffusive transport (Figure 4A). By using mechanical forces to induce pore formation, this approach removes the need for proprietary reagents necessary for common transfection strategies such as lipofection and electroporation. In addition, devices are relatively simple, which allows for mass production and distribution as single use disposable units eliminating the need for complex pieces of equipment and worry about cross contamination of independent patient samples. Collectively these advantages are significant when trying to deploy the technology under current Good Manufacturing Practice (cGMP) for autologous clinical cell replacement. This approach, however, is not without its drawbacks. Most importantly, given that the payload enters the cell through passive, diffusive transport, delivery efficiency when using this technique is inversely related to payload size. For instance, when delivering fluorescent dextran molecules of varying size to murine embryonic stem cells, Sharei et al. demonstrated a drop in delivery efficiency from approximately 50% for 3kDa dextran to approximately 25% when 70kDa dextran was used [109].

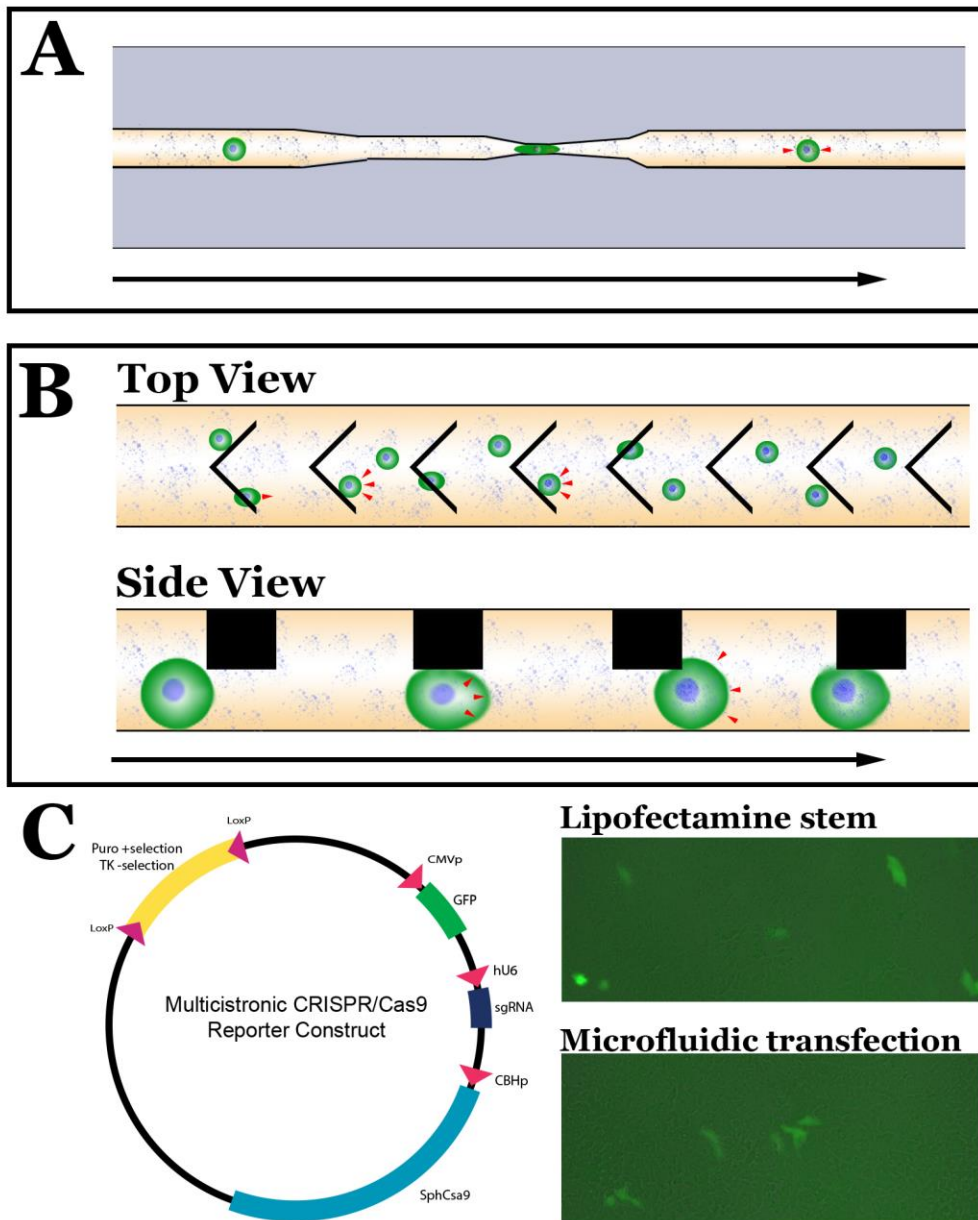


Figure 4. Next-generation microfluidic cell devices. **A-B:** Schematics depicting diffusive (**A**) and convective (**B**) microfluidic cell transfection device designs. Red arrowheads denote net direction of macromolecular transport across the cell membrane. Black arrow denotes direction of fluid flow. **C:** Schematic and preliminary data demonstrating microfluidic delivery of a large multicistronic construct containing sgRNAs, Cas9, GFP reporter and associated promoters to patient-derived iPSCs. Delivery of the same construct using Lipofectamine Stem, which we have previously used for CRISPR correction of patient iPSCs [93], has been included for comparison.

2.4.4.2 Microfluidic Transfection Mediated By Convective Transport

To address issues associated with reduced delivery efficiencies with increased cargo size, our group recently developed another microfluidic delivery platform, which subjects cells to repeated, rapid compressions [85]. During these rapid compressions, the volume of the compressed cell decreases, followed by partial volume recovery between compressions (Figure 4B). As shown in Figure 4C, in preliminary experiments we have been able to deliver a large multicistronic CRISPR construct containing gene-specific sgRNA sequences, Cas9 and a GFP report construct with associated promoters, to human patient derived iPSCs at an efficiency similar to that obtained using Lipofectamine Stem. As CRISPR mediated genomic correction of iPSCs is typically achieved by transient transfection followed by clonal selection and expansion [110], [111], high transfection efficiency is not a requirement for genomic correction. That said, unlike the above-described approach, the volume changes created using this device cause active, convective transport of the payload suspended in the surround buffer across the cell membrane. The most important consequence of this convective delivery mechanism is that delivery efficiency is not a strong function of payload size. For instance, a relatively constant delivery efficiency of greater than 80% was demonstrated for delivery of dextrans that were 4kDa and 2000 kDa in size to K562 myelogenous leukemia cells. With some optimization (see future perspectives section below) we believe that efficient transfection of patient derived iPSCs will be possible. As with the diffusive transfection approach described above, use of this convective transfection strategy does not require specialized reagents or proprietary materials. Likewise, devices can be readily fabricated and provided as sterilized

single use devices, which is ideal for manufacturing of autologous cell replacement products.

In addition to cGMP compatibility, both the techniques described above are amenable to massive parallelization. Due to the small size of each individual channel, many channels can be fabricated on a single chip with shared inputs and outputs, drastically increasing throughput without increasing device cost or the usability of the platform.

2.5 Future Perspectives

While the microfluidic techniques presented in this paper have the potential to enable the manufacture of safe, high potency cell therapies, there are some shortfalls, which the community is continuing to address. First, while label-free microfluidic sorting strategies have advantages over ‘gold standard’ techniques in terms of cost and safety, they are still not as selective as FACS or MACS. While we expect the performance of these new devices to continue to improve, it may be that microfluidic cell sorting will never perform as well as antibody-based methods, provided that appropriate markers exist. It is the belief of the authors that emerging label-free microfluidic sorting techniques can complement ‘gold-standard’ techniques by serving as an alternative when either, 1) appropriate targets for antibody labels do not exist, 2) the conjugation of antibodies to cells pre-sort could interfere with the cell’s utility in downstream applications, 3) sterilizing multi-use instrumentation becomes burdensome or 4) the cost of purchasing/operating large commercial sorters becomes prohibitive.

As discussed above, the performance of microfluidic transfection technologies is highly dependent on proper selection of device geometry to ensure sufficient deformation of cells

to facilitate transfection without destroying the cells or clogging the device. While this optimization is more straightforward with a relatively homogeneous cell population, things rapidly become complicated when attempting to transfect heterogeneous samples. One can imagine that for a fixed device geometry, cells of differing size in a mixed population will respond differently. The smallest cells in the population may not be adequately deformed to allow for transfection, while the largest cells may be damaged due to excessive deformation or simply clog the device, resulting in loss of valuable cell product and time. It is possible that this issue can be addressed by ‘pre-sorting’ a heterogeneous cell population into more homogeneous fractions, and then transfecting each fraction containing useful cells using separate devices.

In addition to the technical limitations of emerging technologies, there is also the issue that new microfluidic sorting and transfection platforms currently do not exist as ‘out of the box’ solutions. This is especially problematic when attempting to implement the technology into an existing clinical production pipeline. Unlike existing technologies such as FACS that have been in widespread use and are familiar to the FDA, implementation of novel microfluidic devices will likely require extensive validation and pose a significant regulatory burden. Generally, device geometries and process parameters need to be re-tuned for new applications, and this optimization generally must be done by someone familiar with the platform of interest. While these issues will likely become less pronounced as the technologies mature, we believe that increased communication and collaboration between the stem cell and microfluidics communities is essential in ensuring that these new microfluidic platforms are developed and distributed in a way that is most

beneficial to the research needs of the stem cell community and most translatable to the treatment of patients.

2.6 Summary

Autologous photoreceptor cell replacement for the treatment of inherited retinal degenerative blindness is at the forefront of personalized medicine. Unfortunately, complexities associated with this approach present significant manufacturing challenges. In general, biologics manufacturing is designed for mass production of a single product to treat a large number of individuals (e.g., vaccine production). Autologous photoreceptor cell replacement requires that a unique line of iPSCs be generated, genetically corrected, and differentiated for every patient in need, in order to prevent immune rejection. Following differentiation, photoreceptor precursor cells must be isolated and delivered independent of the other retinal cell types that are generated during the differentiation process. Although many of the reagents required for manufacturing of autologous iPSC-photoreceptor cells are cGMP compliant, gold standard approaches used for genetic correction of patient derived iPSCs and sorting of photoreceptor precursor cells following differentiation require reagents and equipment that are not well suited to clinical manufacturing. As described in this review, novel microfluidic strategies are being developed for both cellular enrichment and transfection that do not require specialized reagents and complex equipment. By incorporating these microfluidic strategies into autologous photoreceptor cell manufacturing pipelines we believe that it will be possible to greatly reduce the cost, protocol complexity and regulatory burden associated with production of autologous photoreceptor cells for treatment of retinal degenerative blindness.

CHAPTER 3. LABEL-FREE MICROFLUIDIC ENRICHMENT OF CANCER CELLS FROM NON-CANCER CELLS IN ASCITES

3.1 Abstract

The isolation of a patient's metastatic cancer cells is the first, enabling step toward treatment of that patient using modern personalized medicine techniques. Whereas traditional standard-of-care approaches select treatments for cancer patients based on the histological classification of cancerous tissue at the time of diagnosis, personalized medicine techniques leverage molecular and functional analysis of a patient's own cancer cells to select treatments with the highest likelihood of being effective. Unfortunately, the pure populations of cancer cells required for these analyses can be difficult to acquire, given that metastatic cancer cells typically reside in fluid containing many different cell populations. Detection and analyses of cancer cells therefore require separation from these contaminating cells. Conventional cell sorting approaches such as Fluorescence Activated Cell Sorting (FACS) or Magnetic Activated Cell Sorting (MACS) rely on the presence of distinct surface markers on cells of interest which may not be known nor exist for cancer applications. In this work, we present a microfluidic platform capable of label-free enrichment of tumor cells from the ascites fluid of ovarian cancer patients. This approach sorts cells based on differences in biomechanical properties, and therefore does not require any labeling or other pre-sort interference with the cells. The method is also useful in the cases when specific surface markers do not exist for cells of interest. In model ovarian cancer cell lines, the method was used to separate invasive subtypes from less invasive subtypes with an enrichment of ~6-fold. In ascites specimens from ovarian cancer patients,

we found the enrichment protocol resulted in an improved purity of P53 mutant cells indicative of the presence of ovarian cancer cells. We believe that this technology could enable the application of personalized medicine based on analysis of liquid biopsy patient specimens, such as ascites from ovarian cancer patients, for quick evaluation of metastatic disease progression and determination of patient-specific treatment.

3.2 Introduction

Metastasis is the primary cause of cancer-related death. The American Cancer Society has predicted 21,750 new diagnoses of ovarian cancer and 13,940 deaths due to ovarian cancer in 2020 [112]. Metastasis plays a large role in ovarian cancer related mortality, given that 75% of ovarian cancer patients already have metastatic disease at the time of diagnosis, resulting in a five year survival rate of only 48.6% [112], [113].

Detecting and analyzing metastasizing cancer cells in locations of the body in which the cancer cells are a minority population remains a challenge. A consequence of the inability to identify and isolate rare metastatic cells for molecular characterization and drug testing is the inability to optimize chemotherapies; this contributes to the lack of progress in addressing metastatic cancers. A variety of techniques have been developed to enrich cancer cells, usually requiring conjugation of antibodies to surface antigens, which may not be specific to the cells of interest. For example, a magnetic bead capture and isolation immunoassay [114], [115], while sensitive to ovarian cancer cells, is expensive to implement and requires the use of antibodies against specific surface markers that may not be present on cancer cells or may also exist on healthy cells. Similar limitations exist with fluorescence activated cell sorting (FACS). While an adherence assay has been developed

to enrich ovarian cancer cells [116], which does not rely on the use of antibody conjugation and sorting, this method requires 2-3 days for cells to be adhered, washed, and cultured.

To improve the accuracy of downstream analyses of metastatic cells, there is a need for label-free and high-throughput methods for enriching cancer cells within fluids, which includes effusions, ascites, lymph, and blood. The benefits of obtaining more highly purified cancer cell samples include increased sensitivity to gene expression diagnostics. Higher purity samples will then result in accelerated cancer biology research and improved treatments by clinicians through more accurate and sensitive outcomes of analytical techniques. Enriching cancer cells will also enable molecular readout methods, for example ELISA, PCR, and FISH, to enhance scientific discovery, such as determining whether prognostic markers of primary tumors differ from cells in effusions [117]. Ovarian cancer is a particularly important pathology for enrichment techniques, considering the general poor quality of existing biomarkers [118]–[120]. For example, one marker used to assess malignancy in ovarian cancer is TGM2, but unfortunately the resulting protein TG2 is expressed in a wide variety of tissues and detectable in all organs [121].

Detection of circulating tumor cells can rely on differences in tumor cell biomechanical properties, especially cell size. Moreover, other cell biomechanical properties have shown use as biomarkers for enriching cancer cells from non-cancer cells. Using several different experimental techniques, abnormalities in the biophysical properties of tumor cells have been widely studied in primary and cultured cells [122]–[124] with specific examples including prostate cancer [125], bladder cancer [126], breast cancer [127]–[129], esophageal cancer [130], thyroid cancer [131], oral cancer [132], ovarian cancer [133], pancreatic cancer [134], and leukemia [135], [136]. The molecular mechanisms for the

change in cell stiffness are likely a result of remodeling of cytoskeletal pathways [137] and nuclear composition [138]. The mechanical properties of exfoliated cancer cells have been shown to undergo drastic alterations compared to and distinct from healthy counterparts. Cross et al. have quantified breast cancer cell stiffness, by a parameter called Young's modulus, and showed a correlation of stiffness with cell malignancy [139]. In their work, the stiffness of metastatic cancer cells taken from the pleural fluids of patients with breast cancer is more than 70% softer, with a standard deviation over five times narrower, than benign reactive mesothelial cells. Similar results were obtained using different methodologies by Guck et al. in breast epithelial cells [127]. These results suggest biomechanical analysis can distinguish cancerous cells from noncancerous cells, even if their morphologies are similar [140]. In prior work studying the mechanical properties of ovarian cancer cell lines, we have used atomic force microscopy (AFM) to show that more invasive ovarian cancer cells are softer than less invasive cells [137] and nonmalignant epithelial cells, indicating that cell stiffness may be a useful biomarker for use in diagnosis of ovarian cancer and isolation of metastatic cells.

While several microfluidic approaches have been described for the high frequency measurement of cell stiffness [127], [135], [141], the number of methods available for sorting of mechanically distinct cell types is fairly restricted. Several approaches have been developed to sort cells based on size [142], [143]. Two approaches for sorting cells by size include hydrodynamic focusing and ferrohydrodynamic cell separation. In hydrodynamic focusing, cells are pumped at high speed down microfluidic channels. A balance of forces due to drag and wall induced lift then dictate that cells occupy equilibrium positions in the channel which are a function of their size and biomechanical properties. This approach,

while high throughput and simple, suffers from low sensitivity given that changes in cell size only cause a moderate change in equilibrium position. Another size-based sorting method is ferrohydrodynamic cell separation. When using this approach, cells are immersed in a ferrofluid and pumped through a channel which is placed in a magnetic field. The interactions of this ferrofluid with the magnetic field induce a buoyancy force on the cells proportional to their volume. Stiffness-based sorting methods primarily rely on one of two approaches: 1) confined geometries (i.e. pillars), which slow the flow of stiff cells [144] or 2) inertial focusing, which cause stiff cells to translate laterally in the channel with respect to soft cells due to nonlinear effects in channel flow [76], [145]. A limitation of the pillar approach is that samples are processed relatively slowly with low throughput. A limitation of the inertial focusing approach is that the sensitivity to cell stiffness is small, as soft and stiff cells displace only a fraction of a cell diameter. The limited sensitivity requires more precise flow control, making it difficult to obtain multiple, biophysically distinct outputs and improved fractionation of heterogeneous cells. To address the need for a high-throughput label-free enrichment strategy for malignant ovarian cancer cells, we demonstrate the optimization and use of a microfluidic device for the isolation of malignant cells from primary ascites samples. The device design is similar to those used previously to isolate retinal cells and stem cells [146], [147]. The microfluidic device itself is biologically inert and sorts cells based on their mechanical and physical properties into biologically meaningful fractions. These fractions can be tailored based upon modification of the device parameters and flow conditions. To facilitate the optimization of this platform for different sorting applications we have developed a computational model that couples the resistance to cell deformation, determined from cell size and measured Young's

modulus, as well as hydrodynamical forces of the flow (3D flow trajectories) to model the trajectories of the cell under the ridge. The results are described in more detail in [148].

3.3 Methods

3.3.1 Device Design and Fabrication

The microfluidic sorting devices were fabricated using standard photolithography and replica molding process. Silicon masters fabricated using photolithography were prepared to mold a polydimethylsiloxane (PDMS) chip replicating the microchannel design. The PDMS chip was prepared with inlet and outlet holes formed with a biopsy punch and bonded onto a glass slide using oxygen-plasma bonding (Harrick Plasma, USA). The fabricated devices were passivated using 1% BSA solution by incubating for one hour at 37°C to reduce the non-specific adhesion of cells with the channel surface. The number of ridges and the angle was chosen to be 14 and 30° respectively, based upon an optimization of hydrodynamic and elastic forces [148]. The gap size was chosen to be 9 μm to provide sufficient compression for sorting while not causing excessive cell deflection in stiffer populations.

3.3.2 Cell line preparation and sorting

Ovarian cancer cell lines were used to optimize the microfluidics processing. OVCAR-3 and HEY-A8 were originally provided by Dr. G. Mills (MD Anderson Cancer Center, Houston, TX) and cultured in the laboratory using RPMI-1640 media with 10% FBS and 1% penicillin-streptomycin. Once the cells were 70% confluent, they were washed with phosphate buffered saline (PBS) (without calcium and magnesium) and dyed using

following procedure. OVCAR-3 and HEY-A8 cells were dyed with Cell Tracker Deep Red and Cell Tracker Green CMFDA respectively as per the protocol provided by the manufacturer (ThermoFisher). Then, the cells were trypsinized and mixed with the flow buffer (35% Percoll, 1% BSA, 1% EDTA and 0.006% Tween in PBS[-,-]) at a concentration of approximately 5×10^6 cells/mL and infused into the device at a flow rate determined to result in the best separation of cell samples. Each device inlet was connected to a syringe pump (PHD-2000, Harvard Apparatus) using plastic tubing, Luer lock adapters and blunt Luer lock needles. The cell sample was then infused at a flow rate of 15 μ L/min. Flow buffer was infused into the left and the right sheath inlets at 25 and 10 μ L/min respectively to position the cell flow stream optimally off-center in the channel. The sorted cells were collected at the outlets using pipette tips and counted using flow cytometry.

3.3.3 Trajectory Analysis

The trajectories of the ovarian cancer cell types were recorded using high-speed optical microscopy (Vision Research Phantom v9.0). Videos from each cell type were analyzed using ImageJ to identify where individual cells came into contact with each ridge. Video pixels were converted to microns and video tilt between the primary flow direction and video orientation were corrected using a custom R program. This program (<https://github.com/nstone8/Manual-Tracking>) was used to convert the locations at which the cell impacted each ridge into cumulative deflection per ridge data to characterize trajectory of each cell type.

3.3.4 Ascites Sorting for NGS Sequencing

Primary ascites specimens were obtained from two patients from Northside Hospital (Atlanta, Georgia) (Figure 1.1). All patients provided written, informed consent for this study, which was approved by the Central Institutional Review Board of the Georgia Institute of Technology (protocol number H16135) and adhered to the tenets set forth in the Declaration of Helsinki. These specimens were processed with a cell strainer (pluriSelect) to remove solid tissue and large cell aggregates greater than 20um in size (Figure 1.2). Cells were collected via centrifugation (Figure 1.3) and resuspended in flow buffer containing 35% Percoll, 1% BSA, 1% EDTA and 0.006% Tween in PBS[-,-] and pumped through our device at a total flow rate of 50 ul/min (Figure 1.4). Cells were then collected from the outlets and frozen at -80 °C for sequencing analysis. Genomic DNA was then isolated from the sorted cells using a Nucleospin Tissue kit (Machery-Nagel). Next Generation Sequencing (NGS) libraries for sequencing TP53 were prepared using an Accel-Amplicon Comprehensive TP-53 kit (Swift Biosciences) (Figure 5.5). Samples were then barcoded using unique adapter sequences, pooled and sequenced on a single micro flow cell of an Illumina MiSeq (Figure 5.6). A known disease-causing mutation (c.455dup) was observed in the sequencing data of both patients along with wild type reads.

3.3.5 Ascites Sorting for Immunocytochemistry

Primary ascites specimens were obtained from one patient from Northside Hospital (Atlanta, Georgia) under an approved Institutional Review Board (IRB H16135) (Figure 5.1). This specimen was processed with a cell strainer (pluriSelect) to remove solid tissue and large cell aggregates greater than 20 um in size (Figure 5.2). Cells were collected via

centrifugation (Figure 5.3) and resuspended in flow buffer (35 % Percoll, 1 % BSA, 1% EDTA and Tween in PBS[-,-]) and pumped through our device at a total flow rate of 27.5 ul/min (Figure 5.4). Cells were collected from the device outlets and spun onto coverslips and fixed using 4% paraformaldehyde (PFA) for 10 minutes at room temperature. The fixed cells were permeabilized by incubating the cells in 0.1% Triton X-100 in PBS for 10 minutes at room temperature. The permeabilized cells were then incubated in blocking solution containing 1% BSA, 22.52 mg/ml glycine and 0.1% Tween-20 in PBS to block non-specific interactions. The cells were finally incubated in a 1:100 dilution of the mouse monoclonal primary antibody against transglutaminase 2 (ab2386, Abcam) for 1 hour at room temperature and then incubated in a 1:200 dilution of the donkey polyclonal secondary antibody against mouse IgG (ab150105, Abcam) for 1 hour at room temperature. Finally, the cells were counterstained using Hoechst. The cells were then imaged using an imaging plate reader (Biotek) and the relative brightness of each cell was quantified using the plate reader software.

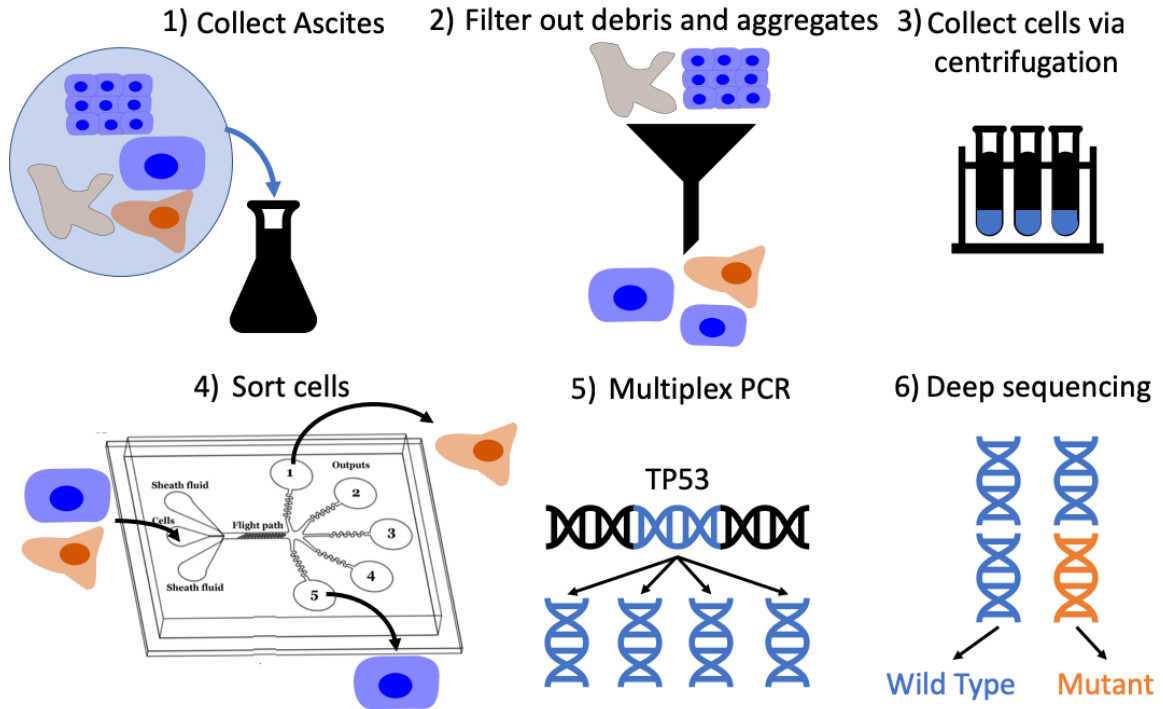


Figure 5. Sorting of primary ascites samples. An outline of the ascites sorting experiment: **1)** Ascites containing nonmalignant cells (blue), cell aggregates, malignant cells (orange) and cell debris (grey) were collected from a patient. **2)** Debris and aggregates were removed by filtration. **3)** Cells were collected from the ascites via centrifugation. **4)** Malignant cells were sorted from normal cells using our microfluidic platform. **5)** The TP53 gene was selectively amplified from the genomic DNA isolated from each sorted fraction. **6)** The proportion of cancer cells present in a sorted fraction was assessed by measuring the fraction of mutant reads present in the TP53 gene of genomic DNA isolated from each sample.

3.4 Results

The purpose of this study was to develop a microfluidic device capable of sorting metastatic ovarian cancer cells from liquid patient samples by leveraging biomechanical differences between target cancer cells and contaminating nonmalignant cells. As depicted in Figure 6, the device has 3 input ports, one for cells flanked by two for sheath liquid, which were used to organize the cells into a narrow stream aimed at the ‘top’ edge of the ridges. After entering the device, cells traveled through a rectangular microchannel

containing periodic diagonal constrictions. Larger, stiffer cells tended to translate along the constrictions (down in Figure 6) towards outlets 1-3, whereas smaller, softer cells simply passed through to outlets 4-5. Therefore, cells with different biomechanical properties were directed towards different outlets, of which there were 5 in total. Performance of this device for a given application depended on careful selection of device geometry and flow rate in order to find a productive balance between hydrodynamic and mechanical forces operating on the cell. Generally, the mechanical contribution to cell trajectories can be increased by decreasing the size of the gap between the bottom of the ridges and the floor of the channel whereas the hydrodynamic contribution to cell trajectories can be increased by increasing the flow rate. When hydrodynamic forces dominate, either by selecting too large of a gap size or too high of a flow rate, the cells will simply follow the streamlines in the device and no sorting will occur. If mechanical forces dominate, either through selection of too small of a gap size or too low of a flow rate cells will not be able to transit the constrictions and clogs will occur that prevent successful operation of the device.

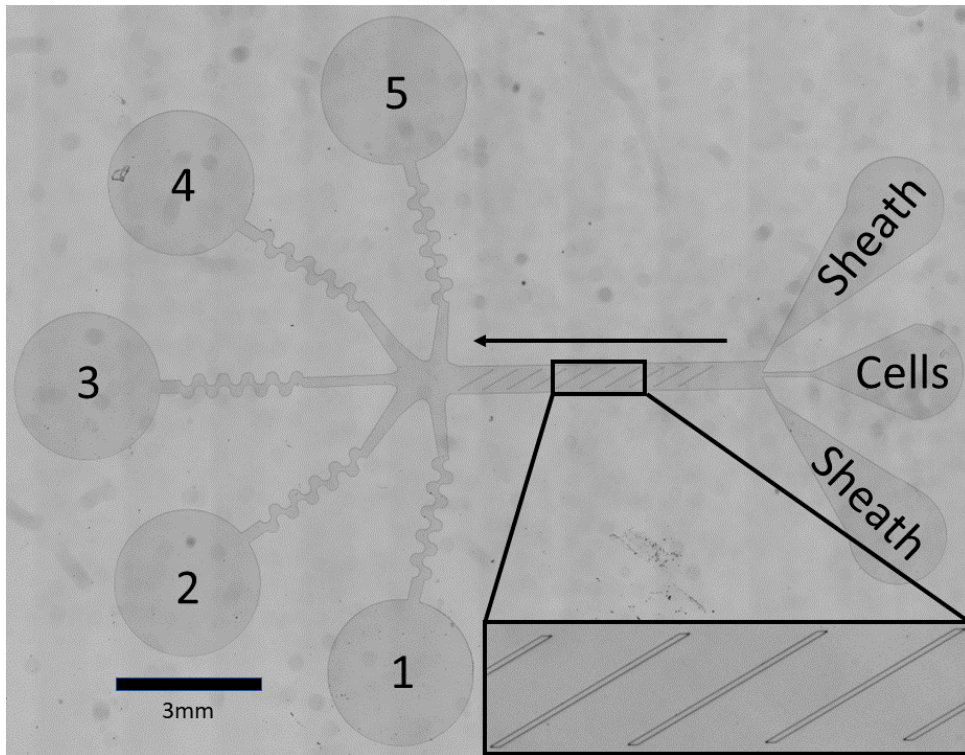


Figure 6. Device Overview. The device consists of three inlets and five outlets connected by a sorting channel. Sheath fluid is pumped into the outer two inlets in order to focus the cells from the center inlet to their desired initial lateral position in the device, which in this application was the ‘top’ edge of the ridges (the side of the ridges closest to outlet 5). The cells then flow into the sorting chamber, where they interact with periodic diagonal constrictions (inset) which are designed to force cells to deform in order to pass under them. Large, stiff cells will tend to translate along the ridge (down in the figure, towards outlets 1-3) whereas small, soft cells will pass under the ridges without deflecting and be collected in outlets 4-5.

Our first objective was to optimize the sorting device to be sensitive to the mechanical differences between ovarian cells with varying malignancy. We used high speed microscopy analysis to track cell lines of varying metastatic potential. As shown in Figure 7, at a total flow rate of 30 $\mu\text{l}/\text{min}$ differences in deflection between nonmalignant (IOSE) and malignant (HEY, HEY-A8 and OVCAR-3) cell types were observed. In addition, a substantial difference in cell trajectory was observed between cell lines with low (OVCAR3) and high (HEY-A8) metastatic potential. Therefore, biomechanical sorting

was sensitive to mechanical differences between ovarian cancer cells of different metastatic potential. The dynamic range of the separation was not sufficient to substantially isolate HEY and HEY-A8 cells in this configuration.

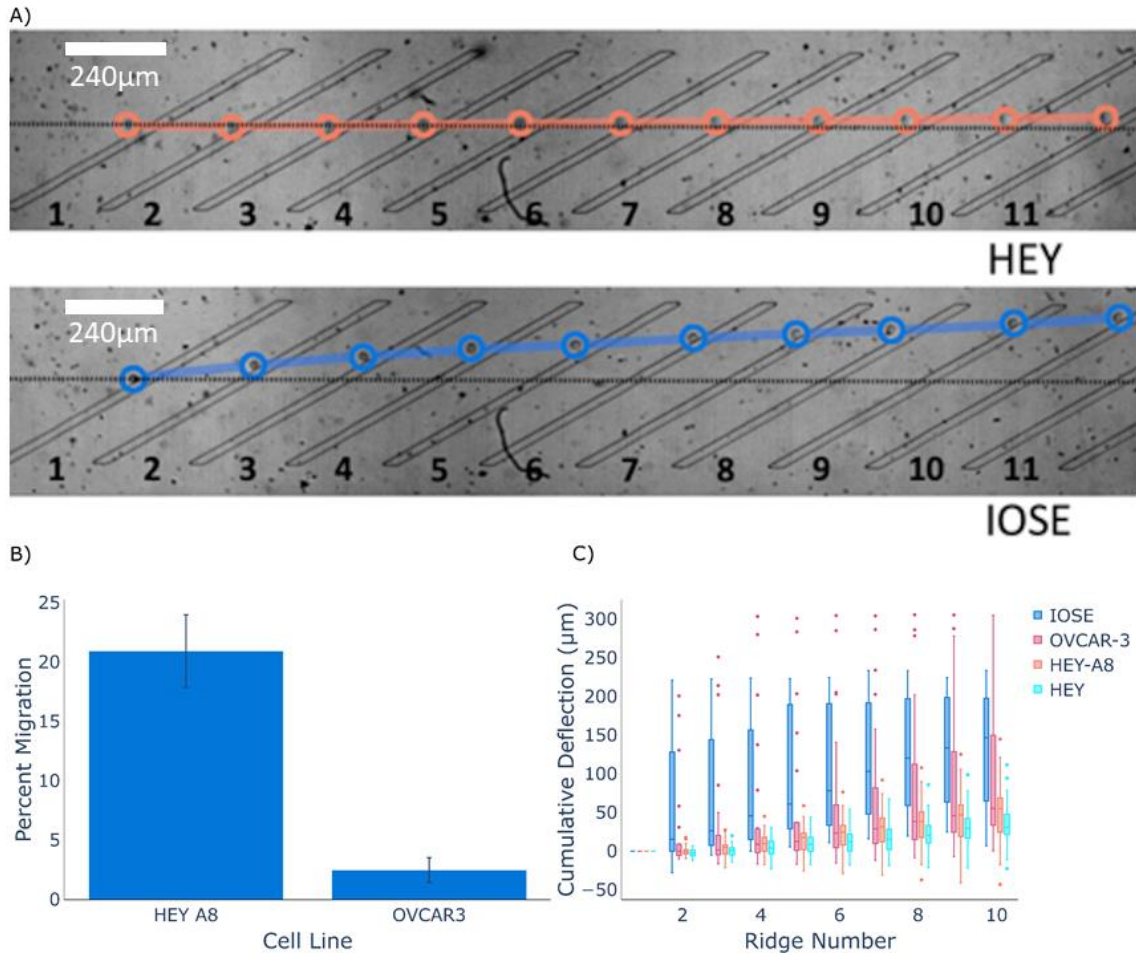


Figure 7. Trajectory analysis of ovarian cancer cell lines. A) Characteristic trajectories of a metastatic ovarian cancer cell line (HEY) vs a nonmetastatic ovarian cancer cell line (IOSE) **B)** Migration assay showing the relative invasiveness of the HEY and OVCAR-3 cell line. **C)** The trajectories of a variety of ovarian cancer cell lines analyzed to show the cumulative cell deflection at each ridge. Cells with a lower metastatic ability (IOSE, OVCAR3) deflected more than cells with a higher metastatic ability (HEY, HEY-A8)

After finding that the cell trajectories demonstrated the device's sensitivity to mechanical differences between ovarian cancer cell lines with differences in metastatic potential, we set out to establish that cell types of different metastatic potential can be separated. OVCAR-3 and HEY-A8 cells were labeled, mixed and infused into the device. The cells were sorted into 5 different outlets. As shown in Figure 8, a majority of the OVCAR-3 cells translated towards the stiff outlet (Outlets 1 & 2) while the HEY A8 cells translated into soft outlets (Outlets 4 & 5). From flow cytometry analysis of the sorted subpopulations, the enrichment factor of the target cell type was calculated using the following equation:

$$\frac{(\text{Number of } X \text{ cells/Number of } Y \text{ cells})_{\text{Outlet}}}{(\text{Number of } X \text{ cells/Number of } Y \text{ cells})_{\text{Inlet}}}$$

As shown in Figure 8, the enrichment factor for HEY-A8 cells increased from outlet 1 to 4 while the enrichment factor for OVCAR-3 cells decreased from outlet 1 to 4. Thus, OVCAR-3 cells were highly enriched at outlet 1 and HEY-A8 was highly enriched at outlet 4. Specifically, we were able to achieve enrichment factors of ~100-fold for OVCAR-3 and ~6-fold for HEY-A8. Very few cells were sorted into outlet 5 where only the smallest and softest cells would be expected.

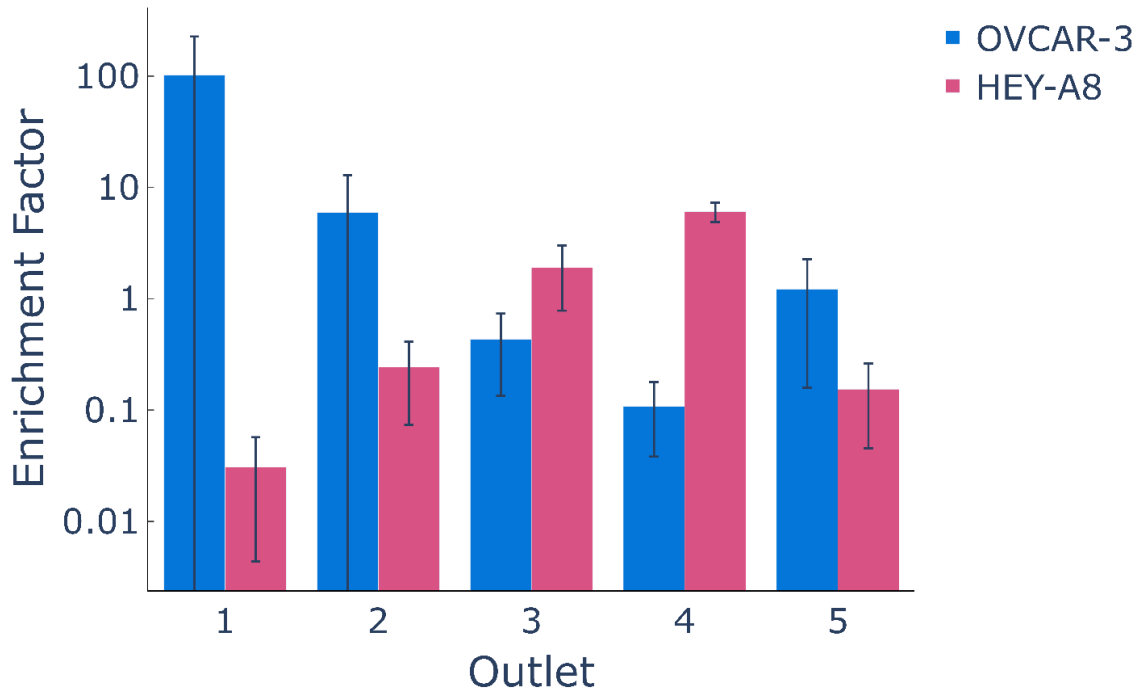


Figure 8. Sorting of ovarian cancer cell lines. In order to assess if our platform was capable of sorting cells with varying degrees of metastatic potential, we used our device to separate highly invasive cells (HEY-A8) from noninvasive cells (OVCAR-3). We were able to achieve enrichment factors of ~100-fold for OVCAR-3 and ~6-fold for the softer HEY-A8. Outlet 5 contained relatively few cells and would not be used in a clinical application.

A sensitivity analysis was performed on the sorted populations of metastatic HEY-A8 cells and less metastatic OVCAR-3 cells to evaluate the accuracy of biomechanical sorting. The number of cells at various outlets were divided based on the conditions as shown in the confusion matrix (Figure 9A). Further, Figure 9A shows the true positive (TP), false positive (FP), true negative (TN) and false negative (FN) corresponding to all five outlets, as determined from the outlet of the device (condition) and flow cytometry analyses of cell stains (test). The number of HEY-A8 cells was considered as TPs for outlets 4 and 5 while the number of OVCAR-3 cells were considered to be TPs for outlets 1 and 2.

Sensitivity is the proportion of true positives correctly sorted by the device, defined by the equation $Sensitivity = \frac{TP}{TP+FN}$. Sorting with high sensitivity indicates that most of the desired cells have been collected at a particular outlet. As shown in Figure 8, most of the softer cells (HEY-A8) have been collected at outlets 4 or 5 and most of the stiff cells (OVCAR-3) have been collected at outlets 1 or 2.

Specificity is the proportion of true negatives correctly sorted by the device, defined by the equation $Specificity = \frac{TN}{TN+FP}$. A sorting experiment with high specificity indicates that most of the non-desired cells at the corresponding outlets have not been sorted at the outlet. For example, most of OVCAR-3 cells have not been collected at outlets 4 and 5, and most of HEY-A8 cells have not been collected at outlets 1 and 2. Accuracy is the proportion of true cells (TPs or TNs) in a sorted population. It indicates the degree of veracity of the sorting test, defined by the equation $Accuracy = \frac{TN+TP}{TN+TP+FN+FP}$. Figure 9B shows the calculated sensitivity, specificity and accuracy for 3 trials of cell separation using the microfluidic device and evaluating several outlet combinations. The separation with the device has a maximum sensitivity of 0.67, specificity of 0.99, and accuracy of 0.84.

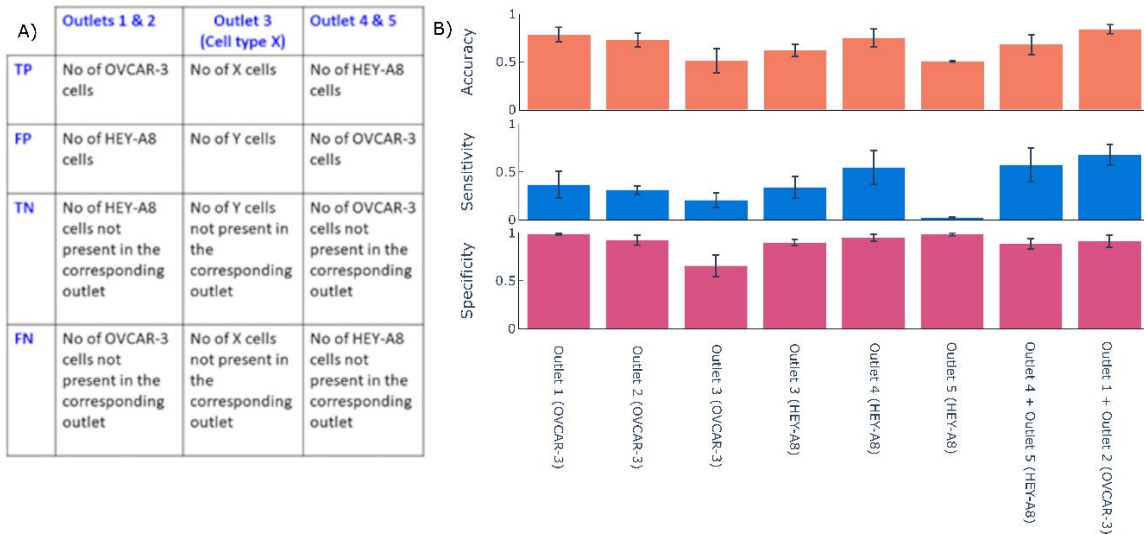


Figure 9. Sensitivity, specificity and accuracy analysis. **A)** Definitions of true positive, true negative, false positive and false negative used for our sensitivity analysis. **B)** The sensitivity, specificity and accuracy of sorting cells using our platform for each outlet, as well as for combinations of some neighboring outlets. The cell line in parentheses in the x axis label indicates which cells were considered true positives in the analysis.

To determine if microfluidic sorting is capable of separating cell populations of clinical interest from heterogeneous specimens, we obtained ascites from two patients with advanced metastatic ovarian cancer from Northside Hospital in Atlanta, GA under an informed consent IRB protocol (H16135). Cells were resuspended in flow buffer and subjected to biomechanical sorting. The sorted fractions were collected from each of the 5 output ports and were stained for TG2, a protein whose overexpression has been shown to be a feature of ovarian cancer [149]. This sorting resulted in cell fractions enriched for high-TG2 cells, consistent with an enrichment of metastatic cancer cells (Figure 10). In addition, next-generation sequencing (NGS) libraries were prepared to enable deep sequencing of the TP53 gene, mutations in which are commonly observed in ovarian cancer [150]. As shown in Figure 10, the proportion of mutant reads and TG2 fluorescence intensity in the sorted populations change at different device outlets indicating separation of the

heterogeneous input into biologically relevant subpopulations. Mutations in P53 were enriched at outlets 1 and 2 , whereas in outlets 4 and 5, cells containing P53 mutations were substantially removed, indicating a transfer of cancer cells to outlets 1 and 2. These results were consistent for both patients and indicate that the microfluidic cell sorting device is capable of selectively enriching cells with TP53 mutations associated with ovarian cancer cells in a label-free manner. A surprising feature of this result is that the cancer cells were enriched in outlets 1-2 for the primary cell sort, where metastatic cancer cells were enriched in outlets 3-4 in our cell line experiments. We believe this occurred because the cell line isolation was driven by differences in stiffness whereas the primary cell sorting was driven by differences in cell size. In the cell line experiment both cell lines were of similar size, but the cells with higher metastatic ability were softer, leading to them being sorted into outlets 3-4. In the primary cell experiment we believe sorting was driven by differences in cell size, where our cells of interest (CTCs) were larger than contaminating blood and immune cells. Therefore, our larger cells of interest deflected more than the smaller contaminating cells, resulting in enrichment of our cancer cells in outlets 1-2.

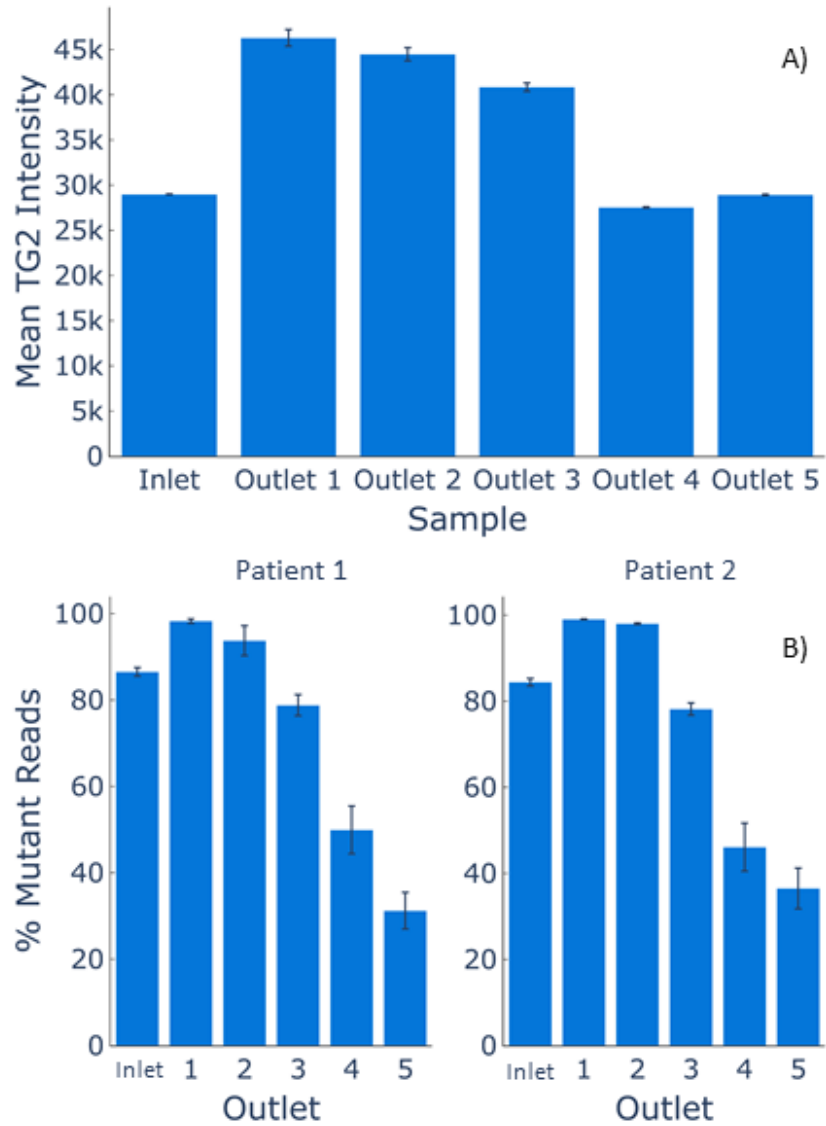


Figure 10. Sorting of Primary Ascites Samples. To assess the usefulness of our platform in a clinical setting, we used our device to sort metastatic cells from patient ascites samples. Enrichment of putative cancer cells (TP53 mutant, high TG2 intensity) was achieved in outlet 1 and 2 for **A)** one patient as quantified via immunocytology and **B)** two separate patients as quantified via sequencing.

3.5 Discussion

Personalized medicine is an exciting opportunity in cancer treatment that promises to increase the effectiveness of cancer therapy by accounting for differences between each patient's specific disease. However, application of personalized medicine depends on the clinician's ability to identify the specific characteristics of a patient's cancer cells. The collection of a minority of tumor cells from complex liquid biopsies has been proposed as an effective yet minimally invasive approach to collecting metastatic cells from patients for testing. However, for testing to be economically feasible, technologies are required to perform high-throughput sorting of cancer cells from patient samples. Alternatively, it is possible to use high-cost next generation sequencing methods to analyze rare subsets of tumor cells, but a much higher sequencing depth, at greater cost, will be required unless an enrichment strategy is utilized. By simply examining the contents of the enriched 'cancer' outlet post-sort, our device can potentially serve as a diagnostic tool, as the cancer burden could be examined by the ratio of cancer to noncancer cells present in a sample. Further, functional or drug-sensitivity assays are also possible to examine isolated cells during downstream testing of pharmacological agents [151], [152]. Current 'gold standard' sorting techniques rely on expensive antibody-based conjugation of fluorescent markers or magnetic beads to the cells. Antibody-based strategies may affect the behavior of cells in downstream testing, whereas label-free approaches cause relatively little change to sorted cells. In addition, current gold standard technologies are particularly difficult to apply to the problem of ovarian cancer due to the lack of specific extracellular markers.

In this work, we have demonstrated a label-free, high throughput sorting platform for the isolation of malignant cells from primary ascites samples. We have shown that our device

is sensitive to ovarian cancer cell lines with various degrees of metastatic potential and performed extensive characterization of our ability to sort these cell lines. Finally, we have demonstrated our ability to specifically enrich metastatic cancer cells from liquid patient samples, both by staining for the protein marker TG2 and by quantifying mutations in the cancer repressor gene TP53. Our platform constitutes an enabling step for the testing of metastatic cells for personalized medicine applications. By cheaply and quickly isolating metastatic cells from complex patient samples, we will enable downstream assays for drug response and functional assays as well as point-of-care diagnostics.

CHAPTER 4. LABEL-FREE MICROFLUIDIC ENRICHMENT OF PHOTORECEPTOR CELLS

4.1 Abstract

Inherited retinal degenerative disorders such as retinitis pigmentosa and Usher syndrome are characterized by progressive death of photoreceptor cells. To restore vision to patients blinded by these diseases, a stem cell-based photoreceptor cell replacement strategy will likely be required. Although retinal stem cell differentiation protocols suitable for generating photoreceptor cells exist, they often yield a rather heterogenous mixture of cell types. To enrich the donor cell population for one or a few cell types, scientists have traditionally relied upon the use of antibody-based selection approaches. However, these strategies are quite labor intensive and require animal derived reagents and equipment that are not well suited to current good manufacturing practices (cGMP). The purpose of this study was to develop and evaluate a microfluidic cell sorting device capable of exploiting the physical and mechanical differences between retinal cell types to enrich specific donor cell populations such as Retinal Pigment Epithelial (RPE) cells and photoreceptor cells. Using this device, we were able to separate a mixture of RPE and iPSC-derived photoreceptor precursor cell lines into two substantially enriched fractions. The enrichment factor of the RPE fraction was 2 and that of the photoreceptor precursor cell fraction was 2.7. Similarly, when human retina, obtained from 3 independent donors, was dissociated and passed through the sorting device, the heterogeneous mixture could be reliably sorted into RPE and photoreceptor cell rich fractions. In summary, microfluidic cell sorting is a promising approach for antibody free enrichment of retinal cell populations.

4.2 Introduction

Inherited retinal degenerative diseases such as retinitis pigmentosa, Leber congenital amaurosis and Usher syndrome are collectively a major cause of incurable blindness in the developed world. A unifying feature of this group of disorders is progressive death of the light sensing photoreceptor cells of the outer neural retina. These diseases are genetically very heterogeneous and as a result many specific treatments will likely be required to treat patients affected with them. For example, of the more than 40 different genes that have been reported to cause retinitis pigmentosa, only a few cause more than 1% of the disease in the total population [92].

For patients who receive a molecular diagnosis early in the course of their disease and still have a large number of photoreceptor cells remaining, it may be possible to restore gene function and prevent disease progression with some form of viral or nanoparticle-mediated gene replacement. To evaluate the efficacy of such gene-based therapeutics, scientists have traditionally relied upon the use of animal models. Unfortunately, for many retinal degenerative disorders, animal models that faithfully recapitulate critical aspects of the disease phenotype do not exist. For instance, structural differences between human and non-primate photoreceptor cells have resulted in rodent models of Usher syndrome that fail to develop retinal degeneration [153]. To overcome this problem some investigators are beginning to employ patient-derived induced pluripotent stem cell (iPSC) culture systems. By using patient-derived iPSCs to generate retinal neurons, either as 3D laminated organoids [12], [17], [20], [154] or as a 2D monolayer of cells [14], [155], one can often identify disease specific phenotypes that can be used to evaluate treatment efficacy [17], [92], [97], [156], [157]. A limitation of this approach is that stem cell differentiation

protocols often yield a rather heterogeneous mixture of cell types. Thus, to be able to evaluate therapeutic efficacy in a single cell population such as human photoreceptor cells, some type of cell isolation or enrichment method is often needed.

For patients with advanced retinal degenerative disease, who have lost the majority of their photoreceptor cells, restorative stem cell-based photoreceptor cell replacement will likely be required. For this approach, the need for cellular enrichment is even greater. Specifically, as many patients with inherited retinal degeneration retain both RPE and inner retinal neurons for years after complete loss of their photoreceptor cells [158], photoreceptor cell enrichment methods that reduce the number of unneeded RPE and inner retinal neurons in the transplanted cell population would be useful. To date, scientists have primarily used antibodies to cell surface antigens coupled with magnetic bead pull down or fluorescence activated cell sorting (FACS) to enrich specific cell types in a heterogeneous mixture [56], [57], [159], [160]. Although potentially useful, these approaches require the use of expensive reagents and equipment that are not ideally suited for current good manufacturing practices (cGMP). In addition, for applications such as isolating photoreceptors from a mixed population of retinal cells, reliable extracellular markers may not exist.

In this study, we demonstrate the use of a novel microfluidic cell sorting device to perform antibody-free sorting of a mixed population of retinal cells into biologically meaningful fractions. The microfluidic device itself is biologically inert and sorts cells based on their mechanical and physical properties and thus does not require the use of antibodies or similar non-cGMP-compliant reagents [148], [161]. In our hands the use of similar devices have little impact on cell viability [2]. The device itself is quite small, making it readily

useable within standard biological safety cabinets in existing cGMP spaces. In addition to being useful for disease modelling purposes, this approach could also be used for cGMP-compliant purification of patient-derived retinal cells in regenerative medicine applications.

4.3 Methods

4.3.1 Human iPSC derived photoreceptor precursor cell line generation and culture

Retinal progenitor cells were generated as previously described [12], [13]. In brief, as per Fig. Figure 11A, iPSCs, derived from a normal non-diseased individual, were maintained on recombinant human laminin 521 coated tissue culture plates and fed with Essential 8 medium supplemented with rhFGF2. For 3-D differentiation, hiPSCs were passaged with TrypLE, centrifuged, and resuspended in 3-D differentiation medium supplemented with Y-27632 ROCK inhibitor and IWR1e. From this suspension, 1×10^4 cells were added per well to a 96 well ultra-low adhesion tissue culture plate. On days 2–10, the 3-D differentiation media was supplemented with 1% ECM. On day 12, spheres were transferred to 100 mm ultralow attachment culture dishes. On days 14–17, the 3-D differentiation medium was supplemented with 1% ECM mixture, 40 nM CHIR99021, and 100 nM SAG. On day 18, the media was switched to neural retina medium. At day 45, 30–50 spheres were dissociated using Accutase. Cell suspensions were then counted and plated on Matrigel coated wells. For immortalization, 24 h after plating, cells were washed with fresh neural retina media and transduced with a lentiviral cocktail containing vectors driving CRX (Figure 11B) and NRL (Figure 11C) to induce photoreceptor cell fate commitment, and GRK1 promoter driving hTERT (Figure 11D) for immortalization. Five

days following transduction, immortalized photoreceptor precursor cells were pharmacologically selected via blasticidin selection (2 $\mu\text{g}/\text{ml}$ for 14 days). Immortalization was achieved via CRX/NRL induced activation of the GRK1 promoter, which in turn drives hTERT expression.

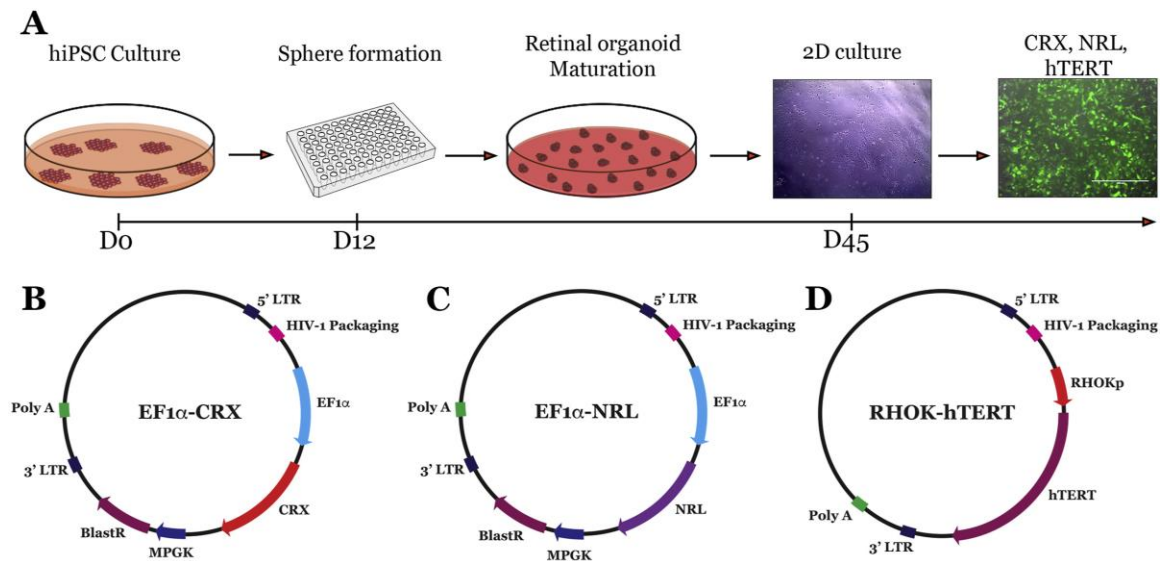


Figure 11. Method for generating iPSC-derived photoreceptor precursor cell line. A-D: Schematic diagrams depicting the methods used for iPSC-PPC line generation (A) and the lentiviral vectors used for forced expression of CRX (B), NRL (C) and cell line immortalization (D).

4.3.2 Lentiviral vector generation

Lentiviral vectors were generated in a stepwise fashion. The EF1 alpha promoter and GRK1 promoter were subcloned in the pENTR™ 5'-TOPO™ vector. HTERT, CRX, and NRL were subcloned into the pENTR™/D-TOPO™ vector. Then using LR clonase, three lenti viral vectors were generated: 1) GRK1p-hTERT, 2) EF1alpha- NRL, and 3) EF1alpha- CRX. Of note, both EF1alpha- NRL and EF1alpha- CRX vectors contained the

MPGK promoter driving blasticidin resistance cassette which was used to select for transduced cells.

4.3.3 Immunocytochemical analysis

ARPE-19 and human iPSC-derived photoreceptor precursor cells (hiPS-PPCs) were fixed in 4% PFA and stained using our previously published protocols [12]. ARPE-19 cells were stained using mouse anti-MITF (Exalpha Biologicals), mouse anti-RPE65 and mouse anti-ZO1 (Thermo Fisher) antibodies. HiPS-PPCs were stained using goat biotinylated-anti-OTX2 (R&D Systems), goat biotinylated-anti-NRL (R&D Systems), mouse anti-rhodopsin (EMD Millipore), sheep anti-CRX (R&D Systems), rabbit anti-rabbit NR2E3 (EMD Millipore), and rabbit anti-recoverin (EMD Millipore) antibodies. Primary antibodies were detected using the species-appropriate, fluorescently conjugated Alexa Fluor secondary antibodies [Life Technologies/Thermo Fisher Scientific; goat anti-mouse 488, goat anti-rabbit 568, Streptavidin 647 and donkey anti-sheep 647]. Cell nuclei were counterstained using DAPI. Cells were imaged using a Leica DM 2500 SPE confocal microscope (Leica Microsystems).

4.3.4 AFM and force curve analysis

To obtain global stiffness measurements of each cell line, 7.32 μm spherical polystyrene particles were attached to tipless silica nitride cantilevers (Bruker Probes) using a two-part epoxy, which was dried overnight prior to use. To characterize the mechanical properties of each cell, we used force spectroscopy to obtain force-indentation curves with an atomic force microscope (AFM) (Asylum Research) with an integrated optical microscope (Nikon) on a vibration isolation table using our previously published protocols [137],

[162]. Before each day of measurements, the AFM was calibrated by taking a single force curve on a clean FluoroDish (World Precision Instruments) to determine the deflection inverse optical lever sensitivity (i.e., the voltage read in the photodetector for a given amount of cantilever deflection) for each cantilever. Next, the Sader calibration method was used to obtain cantilever spring constants (k is approximately 5–20 pN/nm) based on the thermal vibration of the cantilevers. For cell measurements, the cantilever probe was visually aligned with the cell center and moved with a velocity of 1 $\mu\text{m/s}$ to indent the cell with increasing compressive force until a force trigger of 10 nN was reached. The cantilever was held in position for 10 s to allow viscous relaxation of the cell before reversing the direction of the cantilever's velocity.

We calculated the cellular reduced Young's modulus [163] based upon the Hertzian model of non-adhesive elastic contact between two bodies. The contact point was estimated by the intersection of the flat, undeformed region of the force curve with a line fit to the region of the force curve corresponding to the cantilever's contact with the cell. Next, we identified the true contact point by iteratively testing the points around the estimated contact point with the minimal residual difference between the measured force curve and a non-linear fit described by the governing Hertz contact mechanics equation between an elastic sphere and an elastic half space. We additionally fit the dwell region of the force curve to a biexponential decay curve to identify fast and slow viscous time constants [164].

4.3.5 Human donor retina dissociation

Human donor eyes were acquired through the Iowa Lion's Eye Bank, with consent from the donors' next of kin and in full accordance with the Declaration of Helsinki. For each

donor, 8-mm trephine punch biopsies were acquired and retina, RPE, and choroid was dissected away from the underlying sclera. Retinal, RPE and choroidal tissue were pooled and incubated in 20 units/mL of papain with 0.005% DNase (Worthington Biochemical Corporation, Lakewood NJ) for 1.25 h at 37 °C with gentle agitation. Dissociated cells were filtered through a 70 µm filter to remove aggregates before resuspension in PBS [+ ,+] containing 0.1% BSA, 30% Percoll, 0.006% Tween-20 and 100U/mL DNase I. Cells were resuspended to a concentration of 5–10 million cells/mL using the Countess II FL Automated Cell Counter (ThermoFisher Scientific, Waltham MA) before cell sorting.

4.3.6 Quantitative RT-PCR

Cell type specific transcript expression was assessed using TaqMan probes targeted against BEST1, RPE65, recoverin, rhodopsin, PKC α and POU4F2 (Life Technologies/Thermo Fisher Scientific). Total RNA was isolated using Trizol (Life Technologies/Thermo Fisher Scientific) according to manufacturer's instructions. One microgram of RNA was reverse transcribed using the Superscript VILO cDNA Synthesis Kit (Life Technologies/Thermo Fisher Scientific; Cat #: 11754050). Quantitative RT-PCR was performed using a QuantStudio 6 Flex Real-time PCR system (Life Technologies/Thermo Fisher Scientific). A probe set targeting beta-actin was used as a loading control.

4.3.7 Microfluidic device fabrication and cell sorting

Devices were manufactured using standard soft lithography techniques to cast PDMS on molds consisting of SU-8 photoresist patterned on silicon wafers, as described previously [151], [152]. The size of the gap between each ridge and the surface of the device (see Figure 12) was selected based on measured cell size. For the cell line sorting experiments,

a device with 9 μm gaps was fabricated. For the human retina sorting experiments, a device with 2 μm gaps was fabricated. The dimensions of the mold ridge heights were measured with profilometry (Dektak 150 profiler) and optical microscopy. Five outlet devices were tested to evaluate the accuracy of fractionation of the heterogeneous cells to isolate target retinal cell types. The mold pattern was translated to polydimethylsiloxane (PDMS), inlet and outlet holes were punched with biopsy punch, and the chip bonded to glass. Cells were transferred to a syringe and infused into the microfluidic device through Teflon tubing using a syringe pump (PHD 2000, Harvard Apparatus, and BS-300, Braintree Scientific) at specified flow rates (15-45 $\mu\text{l}/\text{min}$). In experiments in which cell trajectories were recorded, an inverted bright-field microscope (Eclipse Ti, Nikon) was used equipped with a high-speed camera (Phantom v7.3, Vision Research) [88], [89], [165]. In experiments on fluorescently labeled cell lines, cells were labeled with CellTracker™ deep red (ARPE-19) and green (hiPS-PPCs) (Molecular Probes Inc.) according to manufacturer protocols. After loading the cells with the dye, the accuracy of sorting could be quantified using flow cytometry (BD Biosciences, LSR II).

4.4 Results

4.4.1 Design and optimization of a microfluidic retinal cell sorting device

The purpose of this study was to develop a microfluidic device, capable of exploiting differences in mechanical and physical properties of retinal cells, to enrich for specific cell types. As depicted in Figure 12, this device was designed with 3 input ports, one for loading a mixed cell population and the remaining two for injection of sheathing fluid to generate flow through the center of the device. The input ports are connected to a flight path chamber

with a number of diagonal fins separated from the base by small gaps that serve to channel cells toward one of 5 different output ports where the enriched cell populations are collected.

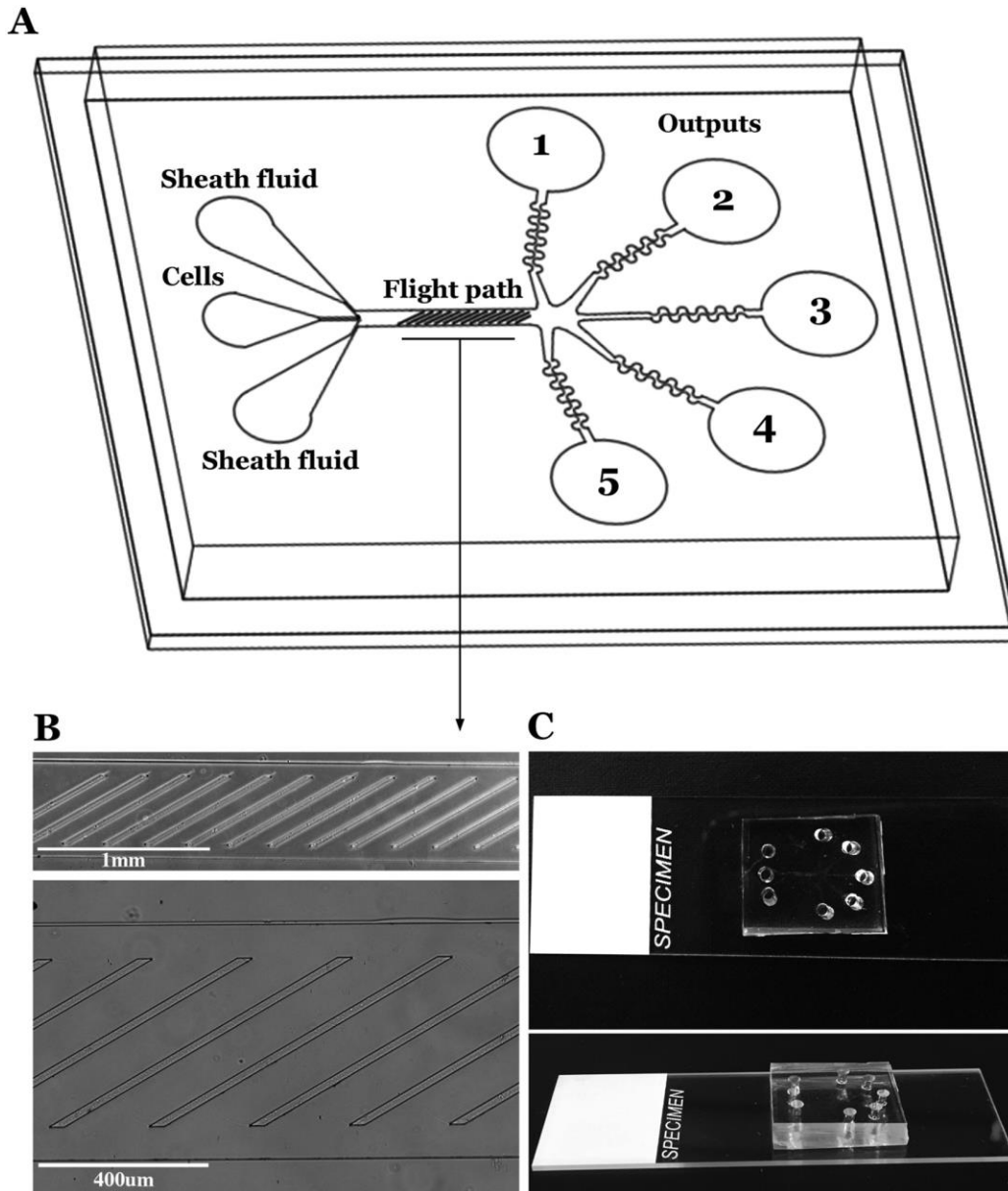


Figure 12. Microfluidic cell sorting device designed for sorting of retinal cells. A: Schematic diagram depicting the design of the microfluidic cell sorting device. **B:** Phase micrograph of the cell sorting device flight path – area containing diagonal ridges designed to deflect cells to the left or right side of the device based on each cell's size, modulus, and viscosity. Upper panel scale bar = 1 mm. Lower panel scale bar = 400 μm . **C:** Photograph of a cell sorting device demonstrating its size and design.

Our first goal was to determine whether RPE cells could be separated from iPSC-derived photoreceptor precursor cells. In order to determine the degree of enrichment that results from passage through the device, it is necessary to know the exact proportion of each cell type in the starting population. Human iPSC derived retinal organoids and samples of primary retinal tissue both vary in the percentage of each cell type present and are therefore less suitable for this experiment than homogeneous stable cell lines. Although several excellent immortalized human RPE cell lines exist (e.g., ARPE-19 and hTERT RPE-1), similar photoreceptor precursor cell lines are not available. As such, for these experiments a photoreceptor precursor cell line (hiPS-PPC) was generated as per the methods section. As expected, the transgenes CRX and NRL were robustly expressed following lentiviral transduction (Figure 13A). As shown in Figure 13B, expression of the retinal progenitor cell marker SOX2, and the photoreceptor cell markers S Opsin, M/L Opsin, RP1, recoverin and RPGR ORF15 was detectable via rt-PCR in cultures of immortalized human iPSC-derived photoreceptor precursor cells for at least 20 passages. Likewise, the photoreceptor precursor cell markers OTX2 (Figure 13C) and recoverin (Figure 13D), and the rod photoreceptor cell marker rhodopsin (Figure 13E) could be detected via immunocytochemical staining.

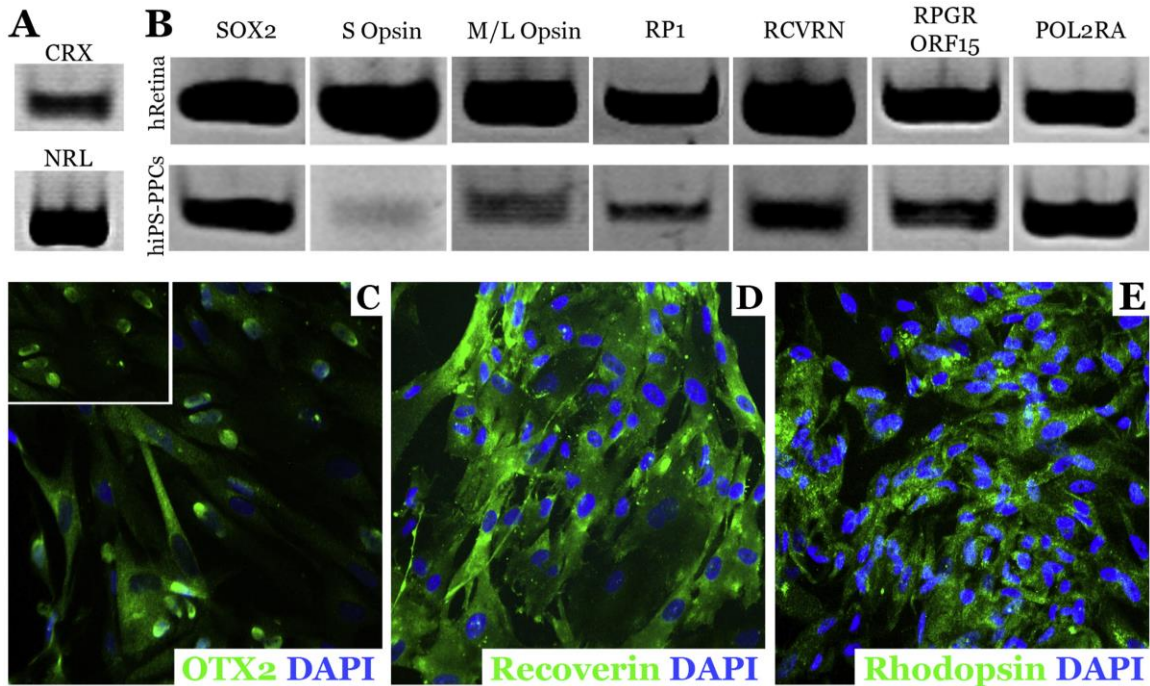


Figure 13. Generation of a stable human iPSC-derived photoreceptor precursor cell line. **A:** rt-PCR analysis performed using RNA isolated from human iPSC-PPCs following lentiviral transduction. **B:** rt-PCR analysis performed using RNA isolated from human donor retina (hRetina) as a control and iPSC-PPCs. POLR2A was included as a loading control. **C-E:** Immunocytochemical analysis of immortalized hiPS-PPCs using antibodies targeted against OTX2, recoverin and rhodopsin.

To determine whether this newly generated iPSC-derived photoreceptor precursor cell line and the commonly used RPE cell line, ARPE-19, differed enough in their mechanical properties to be sorted using our device, we first measured the stiffness and viscosity of each line using atomic force microscopy (AFM) (Figure 14A–B). As shown in Figure 14, ARPE-19 cells are smaller (C), slightly stiffer (D) and more viscous (E & F) than human iPSC derived photoreceptor precursor cells (hiPS-PPCs), suggesting that these populations could be different enough to be sortable using this microfluidic approach.

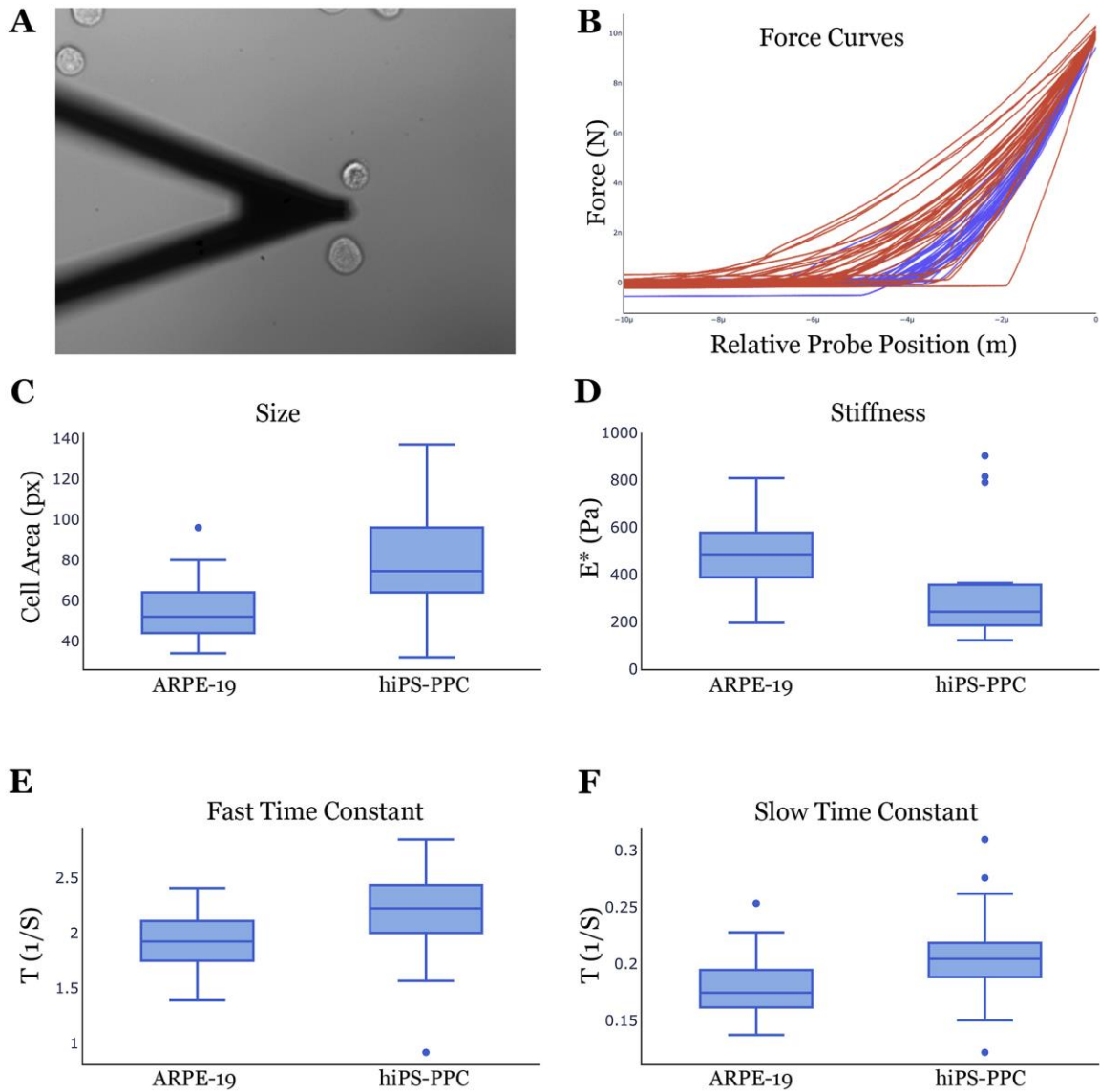


Figure 14. Mechanical characterization of retinal cell lines. **A:** Representative phase micrograph depicting the AFM probe as it approaches cells for mechanical analysis. **B:** force curves obtained following mechanical analysis of ARPE-19 (blue lines) and hiPS-PPCs (red lines). **C:** Area of ARPE-19 and hiPS-PPCs as they approach and pass beneath each ridge within the device as measured *via* high speed microscopy. **D:** Modulus (Pa) of ARPE-19 and hiPS-PPCs. **E-F:** Fast and slow time constant (i.e. measure of viscosity) for ARPE-19 and hiPS-PPCs. Collectively these data show that human ARPE-19 cells are smaller, stiffer and less viscous than human hiPS-PPCs

To determine the optimal conditions for sorting and to evaluate the degree of enrichment, ARPE-19 and human iPSC-derived photoreceptor precursor cells were first injected individually into the sorting device via a syringe pumped at a constant rate of either 15 $\mu\text{L}/\text{min}$, 30 $\mu\text{L}/\text{min}$ or 45 $\mu\text{L}/\text{min}$. Cellular trajectories were tracked for each cell line using high-speed microscopy and the characteristic deflections that occurred as the cells passed beneath each ridge of the device are shown in Figure 15. The slowest injection rate, 15 $\mu\text{L}/\text{min}$, resulted in the greatest variability in per ridge deflection (Figure 15A). This variability was much less when cells were injected at a constant rate of 45 $\mu\text{L}/\text{min}$, but at this rate, the difference in mean cumulative deflection between the two cell lines was the smallest of the 3 injection rates tested (Figure 15C). The greatest difference in characteristic deflections between the two cell lines and the smallest variability in per ridge deflection was seen at a flow rate of 30 $\mu\text{L}/\text{min}$ (Figure 15B). Thus, this injection rate was chosen for the subsequent cell-line enrichment experiments.

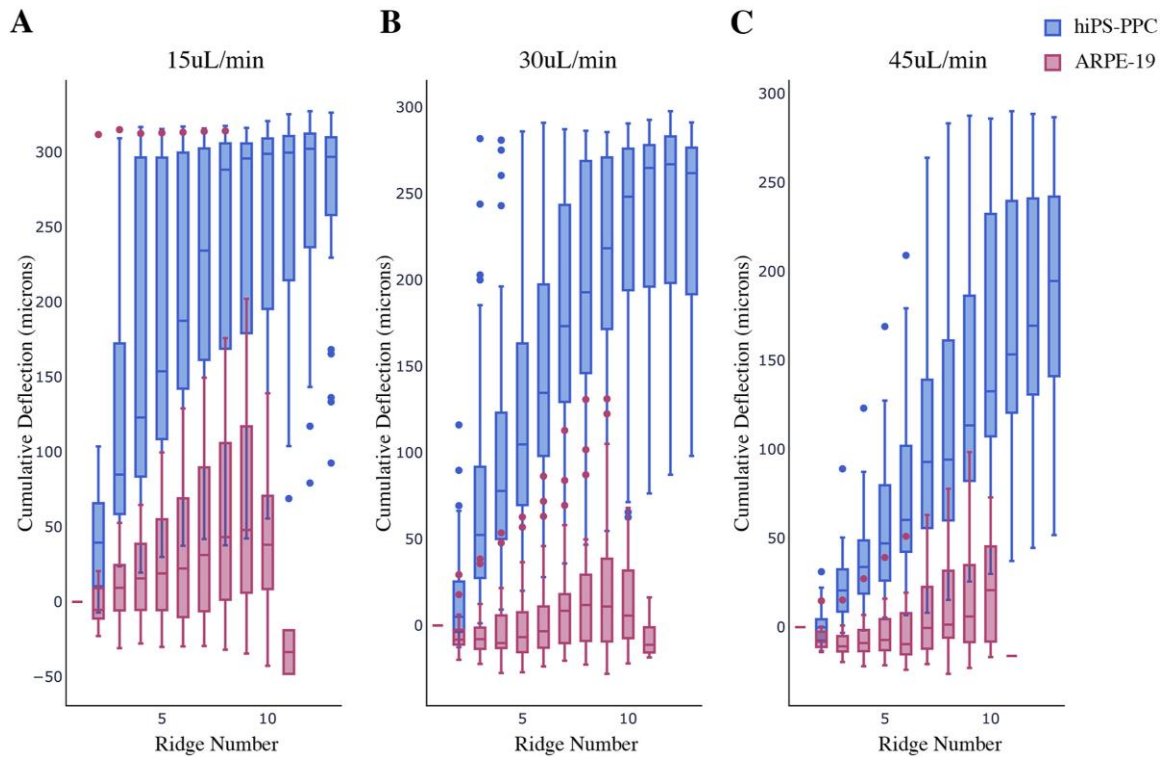


Figure 15. Optimization of cell enrichment parameters. A-C: Ridge induced deflections as a function of injection speed (**A** = 15 $\mu\text{L}/\text{min}$, **B** = 30 $\mu\text{L}/\text{min}$, **C** = 45 $\mu\text{L}/\text{min}$). The largest cumulative deflection difference with least amount of overlap between ARPE-19 and iPS-PPCs was detected at a constant injection rate of 30 $\mu\text{L}/\text{min}$ (**B**). Note: the box marks the limits of the 1st and 3rd quartile, the line within the box represents the median and the whiskers represent the maximum and minimum values detected.

4.4.2 Separation of RPE and iPSC-derived photoreceptor precursor cell lines via microfluidic cell sorting.

To test whether the device could be used to enrich for specific retinal cell populations, ARPE-19 and hiPS-PPCs were fluorescently labeled and then mixed at a 1:1.7 ratio and injected through the device via a syringe pump at a constant rate of 30 $\mu\text{L}/\text{min}$. As indicated above, knowing the precise makeup of the starting population (i.e., 37% ARPE-19 and 63% iPS-PPCs) was critical in order to determine the enrichment factor for each cell type at each of the device's output ports.

As shown in Figure 16, at these conditions we were able to achieve enrichment values of 2 for ARPE-19 and 2.7 for hiPS-PPCs. Specifically, outlet 1, which we predicted would contain larger cells with the greatest deflection rates, was heavily enriched for hiPS-PPCs. Outlet 4, which we predicted would contain smaller cells that had lower deflection rates was highly enriched for ARPE-19 cells. Outlet 5 had very few of either cell type.

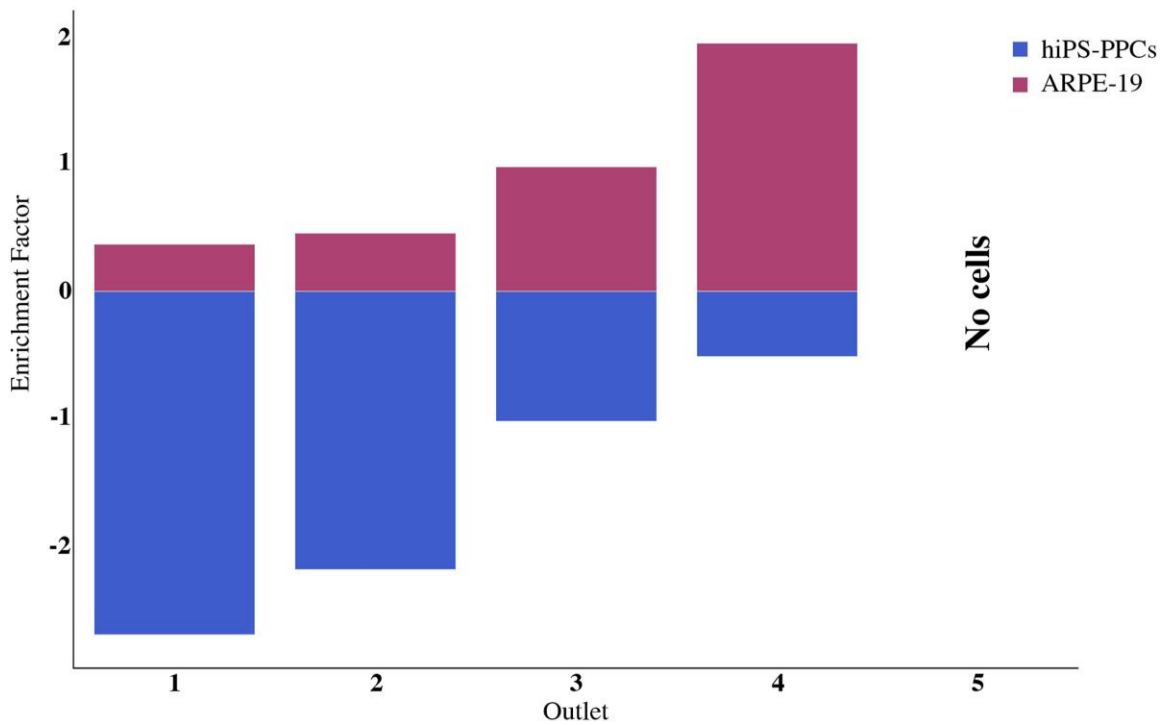


Figure 16. Sorting of ARPE-19 and hiPS-PPCs using a microfluidic cell sorting device. Following microfluidic cell sorting, outlet 1 contained the greatest number of hiPS-PPCs and the lowest number of ARPE-19 cells (hiPS-PPCs enrichment factor = 2.75). Conversely outlet 4 contained the greatest number of ARPE-19 cells and the lowest number of hiPS-PPCs (ARPE-19 enrichment factor = 1.97). As outlet 5 did not contain a significant number of either cell type the enrichment factor was not plotted.

4.4.3 *Microfluidic sorting of mature human donor derived retinal cells*

To determine if a similar microfluidic cell sorting strategy could be used to sort mature retinal cells, new devices were fabricated that contained the same number of ridges but a ridge gap size of 2 μm , which was selected based upon the average size of all cell types that would be present in the input cell population. For this experiment, human donor eyes were dissected, the neural retinal and RPE cell layers were harvested, and the tissues were mixed and dissociated into a single cell suspension. As the contribution of each of the different retinal cell types in the starting population was unknown, it was not possible to calculate an enrichment factor in this experiment. Instead, quantitative RT-PCR using primers targeted against transcripts specific to several of the dominant retinal cell populations was performed on the fractions collected from each of the 5 output ports. As in the cell line sorting experiment described above, the dissociated heterogeneous input cell population was injected via a syringe pump at a rate of 30 $\mu\text{L}/\text{min}$. As shown in Figure 17, expression of RPE, photoreceptor and inner retinal cell markers varied based on outlet, indicating separation of the heterogeneous input into biologically relevant subpopulations. Specifically, cells expressing the RPE cell markers BEST1 (Figure 17A) and RPE65 (Figure 17B) were most abundant in outlet 1. The abundance of these markers decreased dramatically in outlet 2, and little to no RPE marker expression was detected in outlets 3 through 5. The photoreceptor cell markers recoverin (expressed in both rods and cones) and rhodopsin (expressed exclusively in rods), were virtually absent in outlet 1 (Figure 17C and D). While recoverin was expressed at equal levels in outlets 2 through 4 (Figure 17C), rhodopsin expression was increased in outlet 2 and was higher again in outlets 3 and 4 (Figure 17D). Interestingly, both recoverin and rhodopsin were expressed at low levels in

outlet 5, similar to what was observed in outlet 1 (Figure 17C and D), indicating that most photoreceptor cells were captured in outlets 2, 3 and 4. In contrast to cultured cells, in this experiment the RPE cells are the largest and/or stiffest cells present in the input population. As such the finding that the larger, stiffest cells were deflected to the left toward outlets 1–3 and the smaller and/or softer cells were deflected toward the right into outlets 3–5 held true. Expression of PKC α , a bipolar cell marker, was detected at low levels in outlet 1, increased to a similar level in outlets 2 and 3 and was detected at the highest levels in outlet 4 (Figure 17E). The ganglion cell marker POU4F2 was detected at low levels across all 5 outlets, with a slight skew toward outlets 1–3 (Figure 17E). Collectively, these data demonstrate that a microfluidic cell sorting device can be used to successfully enrich for specific retinal cell populations in a label-free manner.

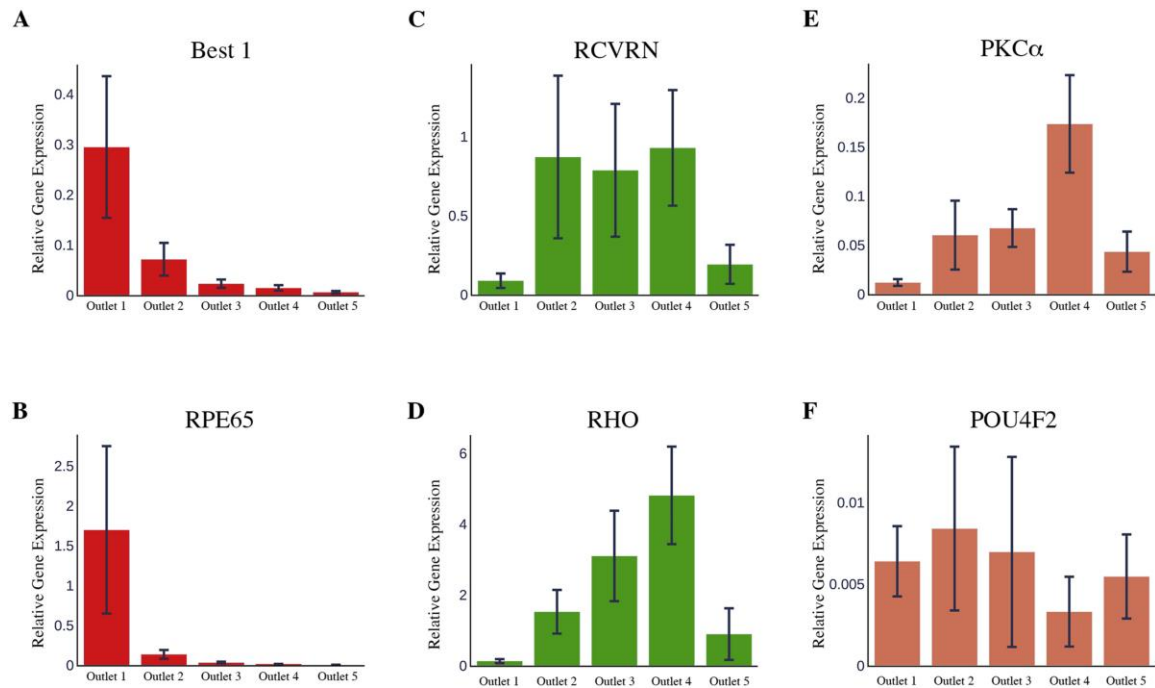


Figure 17. Microfluidic sorting of retinal cells obtained from human donor eyes. A-F: Quantitative RT-PCR analysis of human retina using primers targeting BEST1 (A), RPE65 (B), recoverin (C), rhodopsin (D), PKC α (E) and POU2F4 (F) following microfluidic cell sorting. N = 3 independent donors. Error bars = Standard deviation. DDCt was compared against BActin as a method to normalize for differences in cell number at each outlet.

4.5 Discussion

Currently, autologous cell therapies are under development for a wide variety of conditions, ranging from cancer to neurodegenerative blindness. As stem cell-based cell replacement strategies enter the clinic, sophisticated cell sorting technologies designed to enrich the donor cell population for the preferred cell types will be desirable [76], [146], [166]. This is especially true considering that the majority of current stem cell differentiation protocols are designed to recapitulate embryonic development and therefore give rise to a variety of organ specific cell types that may not be required for the target

application. For instance, retinal differentiation protocols are very effective in generating photoreceptor cells but also produce contaminating retinal cell types including retinal pigment epithelial cells and bipolar neurons. For the treatment of patients with photoreceptor cell specific diseases, such as retinitis pigmentosa, who often retain all other retinal cell types until very late in disease, transplantation of non-photoreceptor cells will likely be unnecessary [158] and possibly detrimental.

The majority of the preclinical photoreceptor cell enrichment strategies published to date have been focused on identifying cell surface antigens and antibodies that can be used to capture specific cell populations using traditional ‘gold standard’ cell-sorting approaches, such as FACS and/or MACS. For instance, in 2012 Eberle and colleagues demonstrated that by using a primary antibody targeted against the cell surface antigen CD73, and a secondary antibody conjugated to MACS micro-beads, they could magnetically isolate with high efficiency rod photoreceptor precursor cells from dissociated neonatal mouse retinas [56]. Lakowski and colleagues later expanded on this work by identifying several other cell surface antigens, namely CD24, CD133 and CD47, that could be used in conjunction with CD73 to further enrich for transplantable photoreceptor precursor cells via FACS or MACS [57].

As efficient as FACS- and MACS-based enrichment approaches are, when cells are destined to be transplanted into patients, where all reagents and procedures must be guaranteed to be safe and reproducible in order to gain FDA approval, avoiding the use of antibodies and stains that can alter cell function and viability is desirable. Likewise, from a clinical production perspective, large specialized pieces of equipment such as FACS units that are difficult to adapt to cGMP conditions should be avoided when possible. Of interest,

one approach that has been used extensively by us and others for enrichment of specific cell populations post-differentiation, is drug based positive selection following lentiviral incorporation of an antibiotic resistance cassette. For instance, in a recent study we demonstrated how puromycin antibiotic resistance delivered in a homology directed repair construct could be used to select patient derived iPSCs following CRISPR correction and differentiation [91]. This approach could readily be adapted to cGMP and modified to select for PPCs as described in this study. That said, antibiotic selection strategies are most appropriate when the specific target is well defined, as was the case both here for forced PPC production and in the above cited CRISPR report. The ideal retinal graft is unlikely to contain only one cell type. Rather a mixture of rods, cones (red, green and blue) and even support cells such as Müller glia, may be beneficial. In such a case, enrichment of late stage retinal progenitor cells that are capable of giving rise to all photoreceptor cell populations and glial cells would be ideal. With that in mind, the purpose of this study was to develop a method for enriching retinal cell populations based on the cells' physical and mechanical characteristics (i.e., size, stiffness and viscosity) [76], [88], [89], [148], [166] rather than surface protein expression. The platform described in this study was designed such that cells are exposed to repeated compressions by a series of narrow gaps oriented diagonally to the direction of fluid flow. As cells interact with these gaps, which are chosen to be smaller than the cell's diameter, they deflect laterally to a degree that is related to their size and stiffness. The design of the gaps allows cell debris and aggregates to move along the diagonal fins into a gutter and to exit the device without causing clogs.

As designed, the device selectively deflects larger softer cells to the left toward outlets 1 and the smaller stiffer cells to the right toward outlet 5. The results of our two cell line

mixture experiment (Figure 16) led us to hypothesize that RPE cells would be deflected toward outlets on the left of the device (i.e., larger cells would be deflected into outlets 1–3) and photoreceptor cells would be sorted into outlets on the right of the device (i.e., smaller cells would be deflected into outlets 3–5). As shown in Figure 17, the majority of human primary RPE cells were indeed sorted into outlet 1. A sharp decline in RPE cell message was detected in the cells in outlet 2 and almost no message was detected in the cells from outlets 3–5. Likewise, almost no photoreceptor cells, as determined by a lack of recoverin and rhodopsin expression, were sorted into outlet 1. Rather, there was an equal distribution of recoverin-positive cells (i.e. rods and cones) in outlets 2–4 and a sharp decline in recoverin expressing cells in outlet 5. Interestingly, the number of cells expressing rhodopsin (rod specific marker) steadily increased beyond outlet 2, with peak expression detectable in outlet 4. As with recoverin expression, rhodopsin expression sharply dropped in outlet 5. These findings suggest that rod photoreceptor cells are smaller or softer than cone photoreceptor cells as one would predict based on histopathology [167], [168]. It would also suggest that by selecting only cells in outlet 2 one would have a population that is enriched for cone photoreceptor cells, whereas outlet 4 would be more heavily skewed toward rod photoreceptor cells. Interestingly, inner retinal neurons expressing PKC α (i.e. bipolar cells) were skewed toward outlet 4, while POU4F2 expressing cells (i.e. ganglion cells, which vary widely in size in the human retina) were distributed across all 5 outlets with a slight skew toward outlets 1–3 with lower numbers in outlet 4 and 5. Compared to RPE and photoreceptor cells, the amount of message attributed to these inner retinal neurons across all outlets was relatively low. We suspect that this is due to the fact that there are far fewer bipolar neurons and retinal ganglion cells

in the human retina than photoreceptor cells, and that more aggressive cellular dissociation techniques are required to liberate these cell types, which unlike the RPE are embedded within the inner plexiform and nerve fiber layers respectively. Regardless, from a cell replacement perspective, the fact that retinal ganglion cells, which during stem cell differentiation develop on the inner most surface of retinal organoids and often die before mature photoreceptor precursor cells are made [12], suggest that removal of this cell type will be less of a concern. Likewise, the numbers of bipolar cells generated and sustained during retinal differentiation is often low [12] and inclusion of a small number of bipolar interneurons in a photoreceptor cell replacement based-approach may actually be beneficial.

In addition to the application discussed above, this platform also has applicability to other tissue types, including isolation of limbal stem cells from the limbal region of the eye [162], undifferentiated stem cells from differentiated stem cells [146], and cancer cells from liquid patient samples [137]. We also believe that the device described in this paper could be enhanced to improve throughput by parallelizing individual flow channels and that sorting sensitivity/specificity could be further improved through additional optimization.

In summary, we believe that antibody-free sorting will be a favorable choice for clinical applications due to its low cost, high throughput and cGMP compatibility. In this work, we present a high-throughput, antibody-free platform capable of sorting pooled primary retinal cells into biologically relevant subpopulations. We have demonstrated that the device is sensitive to the differences between cell types common in the human retina, and thus should be capable of sorting cells desired for transplant from other, contaminating cell types. This

device represents a key technological advancement for the development of future cell therapies, including iPSC derived treatments for inherited retinal degeneration.

CHAPTER 5. USE MICROFLUIDICS TO DELIVER LARGE FUNCTIONAL CONSTRUCTS TO PATIENT-DERIVED IPSCS IN A ONE-STEP MECHANICAL PROCESS

5.1 Abstract

Autologous cell replacement therapies are at the forefront of recent efforts to treat patients with advanced inherited retinal degenerative blindness. While we and others believe it will be possible to use gene therapy to halt disease progression in patients who still have useful vision, treating patients who have already lost their sight will require cell therapies to replace tissue lost due to their condition. Recent advances in the manufacture of patient-derived photoreceptors is encouraging but has been hampered by a lack of technologies capable of efficiently delivering large macromolecules to patient-derived induced pluripotent stem cells (iPSCs). In this chapter, we will detail our effort to address this need using microfluidic devices capable of effecting convective delivery of large macromolecules to the interior of cells. In addition to detailing our progress to date, we will also describe our future plans to increase transfection efficiency by using multistage microfluidic systems to overcome the iPSC size heterogeneity that we have observed.

5.2 Introduction

In many forms of inherited retinal degenerative blindness, a disease-causing mutation causes photoreceptor cells to die over the course of a patient's life, causing their vision to degenerate, eventually leading to blindness. While it is theorized that gene therapies designed to correct the causative mutation in a patient's cells could halt the progression of

their disease, it is unlikely that this therapy will be effective in patients who have already lost most of their vision. In an attempt to develop treatments for these patients, we and others have been developing pipelines for the manufacture of patient-derived photoreceptors with the aim of eventually transplanting these cells into patients to replace the tissue they have lost and restore some of their vision [3]–[12]. While complicated in practice, the general approach can be described simply. First, fibroblasts are collected from a patient via a skin biopsy. Next, forced expression of several key transcription factors (OCT4, SOX2, KLF4 and C-MYC, commonly referred to as the Yamanaka factors) is used to transform these fibroblasts into iPSCs. While the resulting iPSCs could at this point be differentiated into patient-derived photoreceptors, they would still contain the mutation that caused the patient’s disease originally. Therefore, before differentiation, macromolecules must be delivered to the iPSCs to correct the patient’s disease-causing genetic variants. Genome editing of iPSCs has been achieved using a variety of different approaches (e.g., CRISPR, zinc finger nucleases, TALENs, etc.), all of which require some technology to facilitate their delivery to the cell’s interior [91]–[93]. After the patient’s disease causing mutation is corrected, the resulting iPSCs can be differentiated into patient derived photoreceptors suitable for transplant [12]–[42].

In order to be suitable for the correction of mutations in iPSCs destined for transplant after differentiation, transfection technologies must address two main challenges. First, any reagents used must be compatible with current good manufacturing practices (cGMP) and safe for use in human subjects. Second, they must be capable of delivering very large constructs at high efficiencies. The requirement that the technologies be safe is an obvious one, but it may be less clear why the use of large constructs is required. Current gene editing

technologies being considered for the correction of these mutations work in two steps. First, a double stranded DNA break within the cell's genome is made using one of several technologies capable of cutting DNA at prescribed locations (typically within close proximity to the patient's disease causing mutation) such as CRISPR, zinc finger nucleases or TALENs. After inducing this break in the genome, the cell's own DNA repair machinery will attempt to repair the damage via either non-homologous end joining (NHEJ), which is often imprecise, or the more accurate homology directed repair (HDR). With HDR, the cell will use a template homologous to the sequence near the induced DNA damage to replace any missing sequence and repair the break. By co-delivering wild-type sequence spanning the patient's mutation as a template, HDR can result in precise correction of the mutation in the cell's genome [43]–[45]. Unfortunately, the sequences required for nuclease generation, genome targeting, and HDR are collectively quite long. For instance, a single multicistronic CRISPR HDR construct for correcting USH2A mutations in use in our laboratory is over 14kb in length.

While many technologies such as electroporation, lipofection and viral transduction have been commercialized for delivering macromolecules to the interior of cells, none of these techniques are simultaneously cGMP compatible and capable of delivering large genome editing plasmids. Viral packaging size limitations mean that clinically-relevant viruses such as AAV cannot be used to deliver genome editing reagents. While lipofection has been used by our group and others to successfully correct disease-causing mutations in iPSCs, these reagents are not cGMP compatible. Further, given that the transfection efficiency associated with lipofection and electroporation drops with increasing construct size, the best transfection efficiencies we can currently reach are still less than 1%.

Recently, our group demonstrated a novel transfection technology that uses mechanical perturbations to induce convective delivery of macromolecules to cells [1], [2]. This technique does not require the use of any chemical reagents and is cGMP compatible. Further, given that payloads are delivered to cells using a convective mechanism, there is no substantial dependence of delivery efficiency on payload size, meaning that large constructs can be delivered with very high efficiency.

In this chapter, I will detail our recent work on applying this technology for the repair of disease-causing mutations in patient-derived iPSCs. While our initial results are promising, we believe that for this technique to reach its full potential it will be necessary to integrate this transfection platform into multistage microfluidic devices to overcome the high degree of size heterogeneity discovered in patient-derived iPSC populations.

5.3 Methods

5.3.1 Atomic force microscopy

Measurements of the viscous relaxation of individual cells during repeated compressions were performed using an MFP-3D AFM (Asylum Research) in concert with an inverted optical microscope (Nikon Ti) to optically align the AFM probe with the center of each cell. The probes used in this study were MLCT-O10-D probes with a nominal spring constant of 0.03 N/m. The AFM cantilever interacted with the cells via a 15- μm diameter PMMA microsphere. Cantilever calibration was performed using the thermal vibration method against a glass surface. K562 cells in culture media were adhered to the surface of a glass Fluorodish using Cell-Tak (Corning). The indentation depth was chosen to be 10 μm to simulate the strain imposed by a 5- μm gap in a microfluidic channel. The cell relaxation

constant was extracted from the decay of viscous forces acting on the probe while maintaining constant indentation for 2 s after compression.

5.3.2 iPSC culture and maintenance

iPSCs generated from human dermal fibroblasts via infection with non-integrating Sendai viruses designed to drive expression of the four transcription factors OCT4, SOX2, KLF4, and c-MYC (Invitrogen/Thermo Fisher Scientific, CytoTune-iPS Reprogramming Kit) were used in this study [12]. Following generation, clonal expansion and characterization, iPSCs were maintained on either Matrigel (10ug/mL, BD Bioscience) coated culture plates in mTseR1™ media (Stem Cell Technologies) or hLaminin521-coated (10ug/mL, BioLamina) culture plates in Human Essential 8™ (E8) media (Invitrogen/Thermo Fisher Scientific). Cells were passaged using ReLeSR™ (Stem Cell Technologies) as per the manufacturer's protocol.

5.3.3 Microscopic analysis

To evaluate culture confluence and cellular morphology, iPSC cultures were imaged via phase microscopy using an EVOS XL digital microscope.

5.3.4 iPSC size analysis

iPSC cells were first detached from their culture vessels and dissociated using ReLeSR™ (Stem Cell Technologies) as per the manufacturers protocol. Cells were then collected *via* centrifugation and resuspended in ISOTON II diluent (Beckman Coulter) for analysis. Before each day of measurements a size standard (Coulter CC Size Standard L10, Beckman Coulter) was used to calibrate the coulter counter used for analysis (Z2, Beckman Coulter)

as per the instrument documentation. After calibration, each sample was measured three times and the instrument was flushed between each sample. The instrument was programmed to only record objects between 6 and 25 microns in size, and population metrics such as median size and size standard deviation were recorded after each measurement.

5.4 Results

Like many microfluidic technologies, the performance of our transfection platform is dependent on the careful selection of device geometry and operating conditions. In our approach, cells are perturbed by forcing them to pass through periodic constrictions that cause them to alternately lose volume under the constrictions and then regain the lost volume in between [1], [2]. We believe that this volume exchange with the surrounding buffer is what leads to the convective transport of macromolecules across the cell membrane. Therefore, the most important parameters to optimize when using our technique are the size of the constrictions and the flow rate. In order to illustrate how these parameters can affect transfection efficiency it is helpful to imagine extreme cases. For instance, if the constrictions are so large that the cells do not have to deform in order to pass through them, no volume exchange will occur and thus no transfection will be observed. Conversely, if the constrictions are too small, the cells will either be destroyed or the device will clog, resulting in a failed procedure. One can also imagine extremes in flow rate. If the flow rate is very low, the hydrodynamic force acting on the cells will not be large enough to force them through the constrictions, resulting in no transfection. On the other hand, if the flow rate is very high, cells will not have enough time to recover their lost volume in between the constrictions, reducing the efficacy of the technique. The goal in optimizing these

parameters for a given application is to find a pair of constriction size and flow rate where the cells are adequately perturbed to effect transfection, do not clog the device, and have sufficient time between constrictions to recover any volume lost while compressed.

To aid in the design of convective microfluidic transfection devices for delivery of macromolecules to iPSCs, we designed a simple mechanistic model of how we hypothesize delivery occurs in these devices. As shown in Figure 18a, we assumed that cells enter the device at some initial volume V_0 , which reduces to V_c when under a constriction. We further assumed that after being compressed, the cell volume would increase between the ridges, asymptotically approaching V_0 at a rate governed by the time constant τ . Initially, this time constant was the only free parameter in the model, given that V_0 was measured experimentally and V_c was estimated by assuming that cells under a ridge have the shape of a truncated sphere with radius equal to the undeformed radius of the cells and height set by the constriction size. We then assumed that macromolecule concentration in the surrounding buffer was constant, that the interior of the cells were well mixed, and that transport across the membrane was due to pure convection, allowing us to use our volume change model to predict intracellular macromolecule concentration.

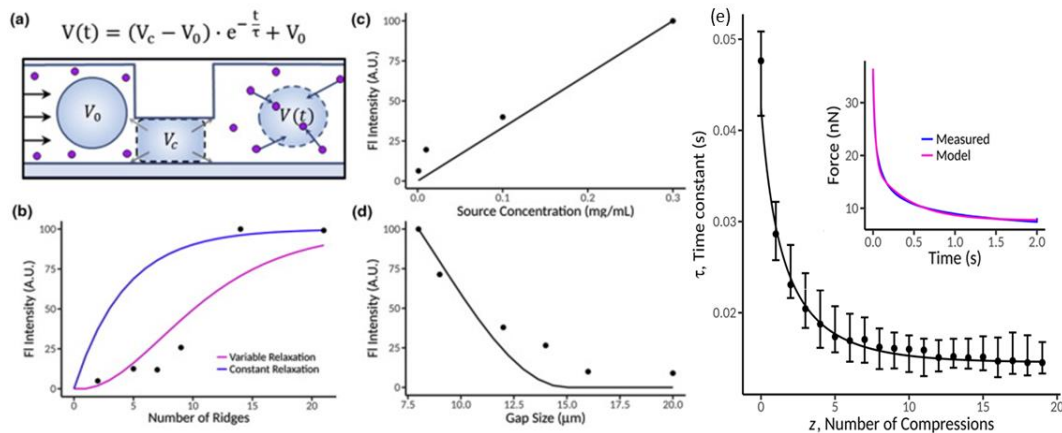


Figure 18. Mechanistic model of convective microfluidic delivery of macromolecules to cells. (a) Model overview. (b) Best model fit assuming variable cell relaxation rate or constant cell relaxation rate plotted against experimental data for fluorescent intensity vs. number of constrictions. (c) Best model fit plotted against experimental data for fluorescent intensity vs. macromolecule concentration. (d) Best model fit plotted against experimental data for fluorescent intensity vs. constriction size. (e) Time constant governing cell relaxation vs. compression number. This result shows that K562 cells relax more quickly after repeated compressions.

As shown in Figure 18b, our initial model, which assumes that cell relaxation rate is constant after each constriction, did not fit well to our data, causing us to suspect that cell relaxation rate may in fact change after repeated compressions. To test this hypothesis, we proceeded to use an atomic force microscope to repeatedly compress K562 cells and measure the relaxation rate of the cell after each compression. As shown in Figure 18e, this experiment found that K562 cells relax more quickly after repeated compressions, perhaps due to disruption of the cytoskeleton or the formation of pores in the cell membrane. While the rate of compression in our AFM experiment was orders of magnitude slower than that which occurs in our microfluidic device, it seemed plausible that similar behavior could be happening in our microfluidic device. We then replaced our single free parameter, τ with three parameters: τ_0 , the rate of cell relaxation after being compressed once, τ_∞ , the rate of cell relaxation after many compressions, and ζ , the rate constant governing how cell

relaxation rate asymptotically approaches τ_∞ from τ_0 . As shown in Figure 18, this model fit well to our experimental data for delivery of fluorescent dextran to K562s as a function of number of constrictions, macromolecule concentration and constriction size.

In an attempt to find such an optimal device geometry and operating condition for the transfection of iPSCs, we attempted to deliver large, multicistronic gene editing constructs to iPSCs using devices with several different constriction sizes at a variety of flow rates. While we were able to demonstrate successful delivery to iPSCs, as shown in Figure 19, the efficiency of our platform was no better than lipofectamine.

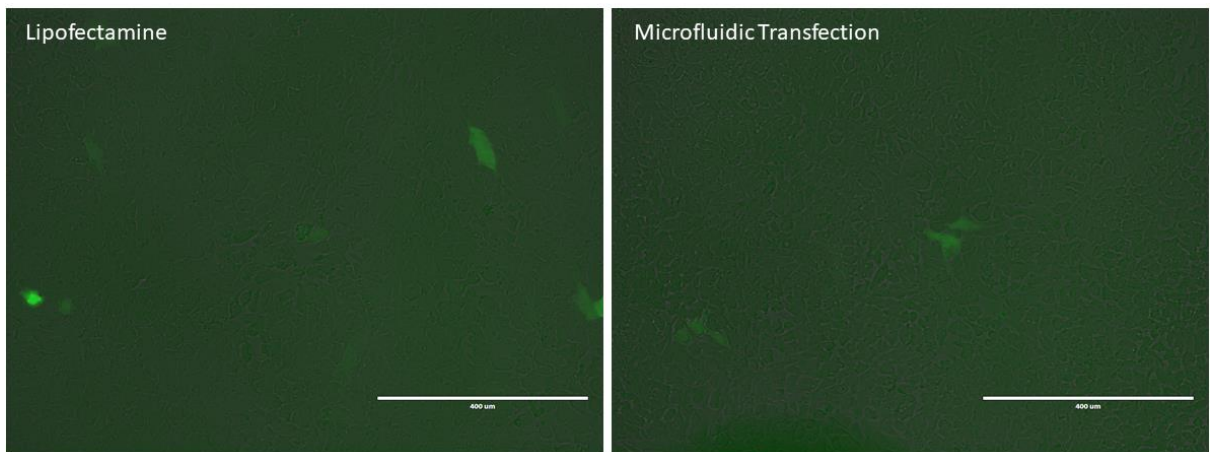


Figure 19. Microfluidic transfection as compared to lipofectamine. While we were able to use our microfluidic platform to deliver large plasmids to iPSCs, transfection efficiency was no better than lipofectamine. Scale bar is 400 microns.

To investigate what might be causing our lower than expected transfection efficiencies, we performed extensive characterization of iPSC size while varying many key conditions such as patient of origin, plating density (see Figure 20), choice of adhesion protein, cell culture media and time in suspension. Overall, these results were very consistent. As shown in Figure 21, we saw no substantial difference in the size of iPSCs derived from different

doners, which leads us to believe that a system capable of transfecting cells from one patient would constitute a general-use tool capable of working across any iPSCs generated using standard protocols. Further, as shown in Figure 22 there seems to be little effect of culture conditions on the size of iPSCs, provided the cultures are not allowed to become massively over-confluent. Specifically we did not find any marked difference in the size of iPSCs cultured on Lamin-coated dishes in E8 media as compared to those cultured on Matrigel-coated dishes in mTseR1 media. Finally, as displayed in Figure 23, we showed that the amount of time cells are left in suspension also does not have an effect on cell size, implying that overall processing time does not need to be tightly controlled to allow for successful transfection. Unfortunately, while the median cell size across our measured conditions was very consistent, significant amounts of heterogeneity in terms of size was observed across all of the iPSC populations measured. Standard deviations in size of the populations measured ranged from ~2.5 to ~3.3 microns, corresponding to ~20% of the median cell sizes measured. For comparison, the standard deviation of T cell size in most humans is reported to be ~10% of the mean cell diameter [169].

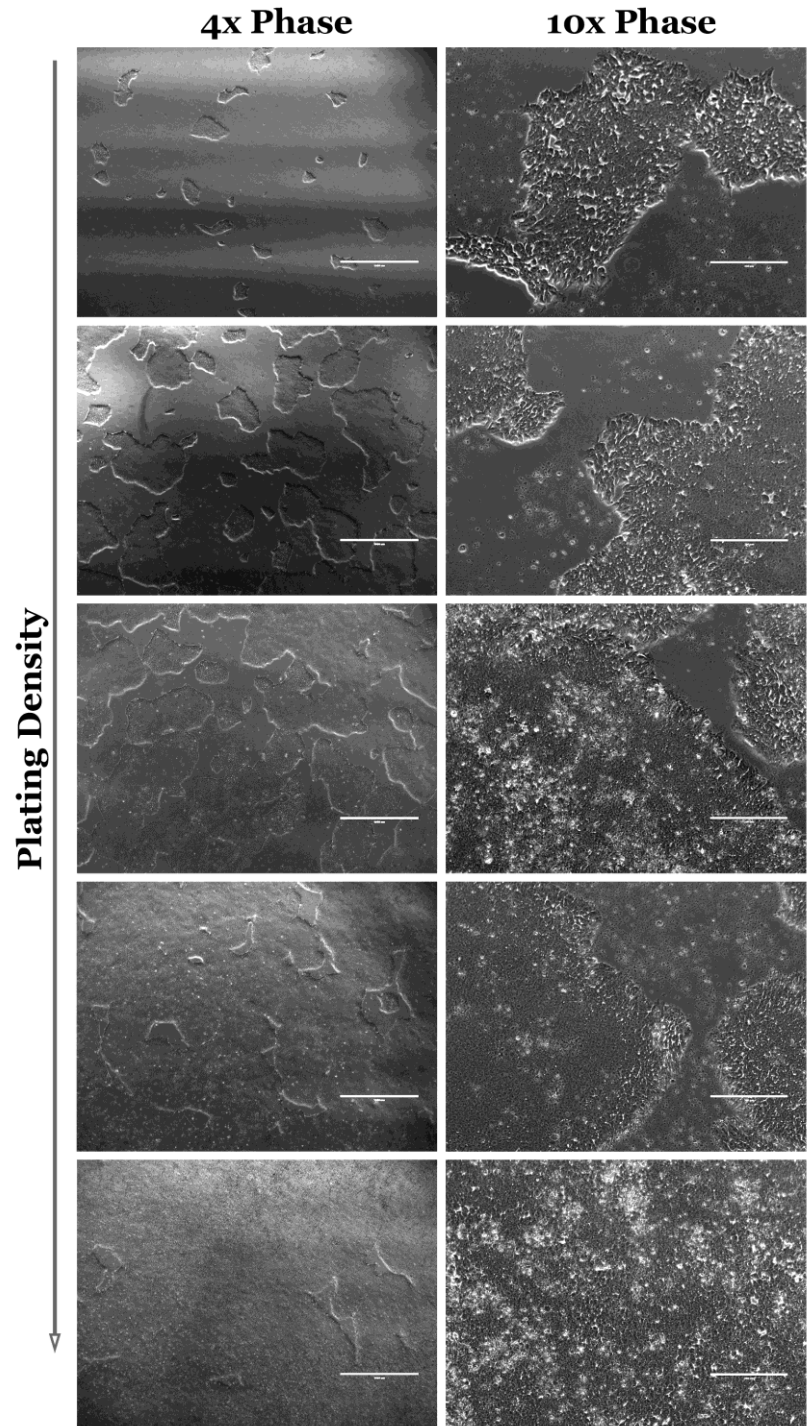


Figure 20. iPSC Morphology at various cell densities. Scale bar is 1000 microns for 4x images, 200 microns for 10x images.

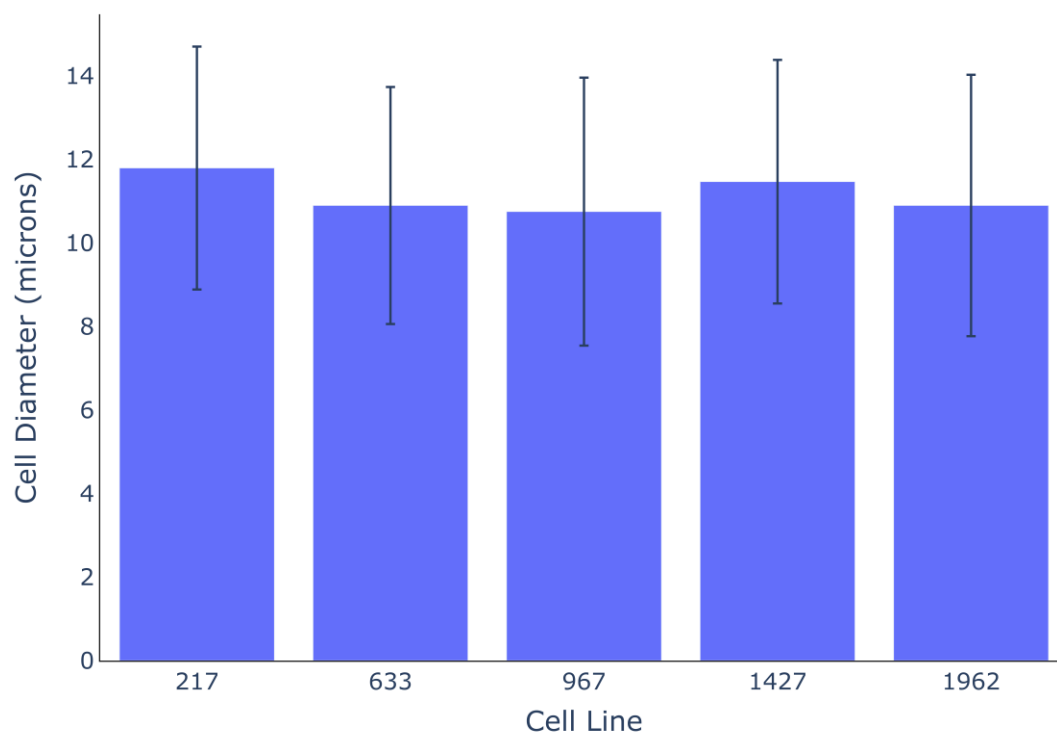


Figure 21. Measured iPSC size for iPSCs derived from several different patients. No substantial difference in median cell size was observed between iPSCs derived from 5 different patients. Error bars represent the standard deviation of size within each sample.

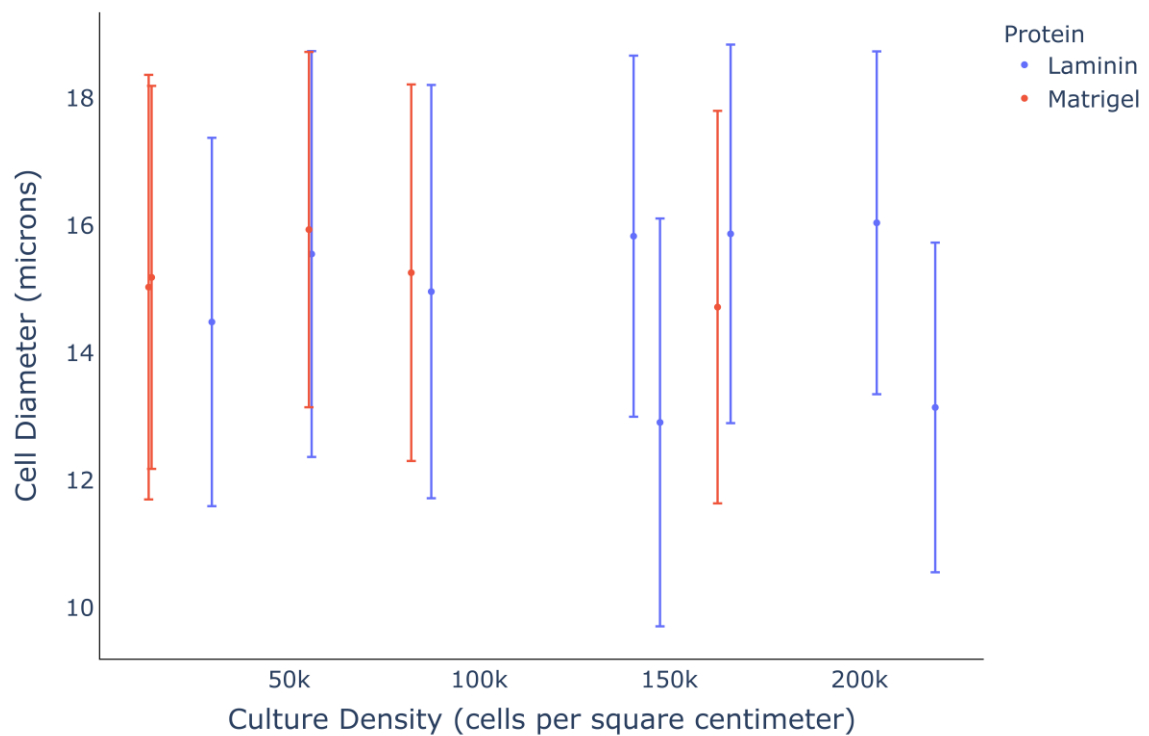


Figure 22. iPSC size at various culture conditions. The size of iPSCs grown on laminin and Matrigel were measured at several different culture densities. While no substantial trends were observed, there was significant size heterogeneity at all measured conditions. Error bars represent the standard deviation of size within each sample.

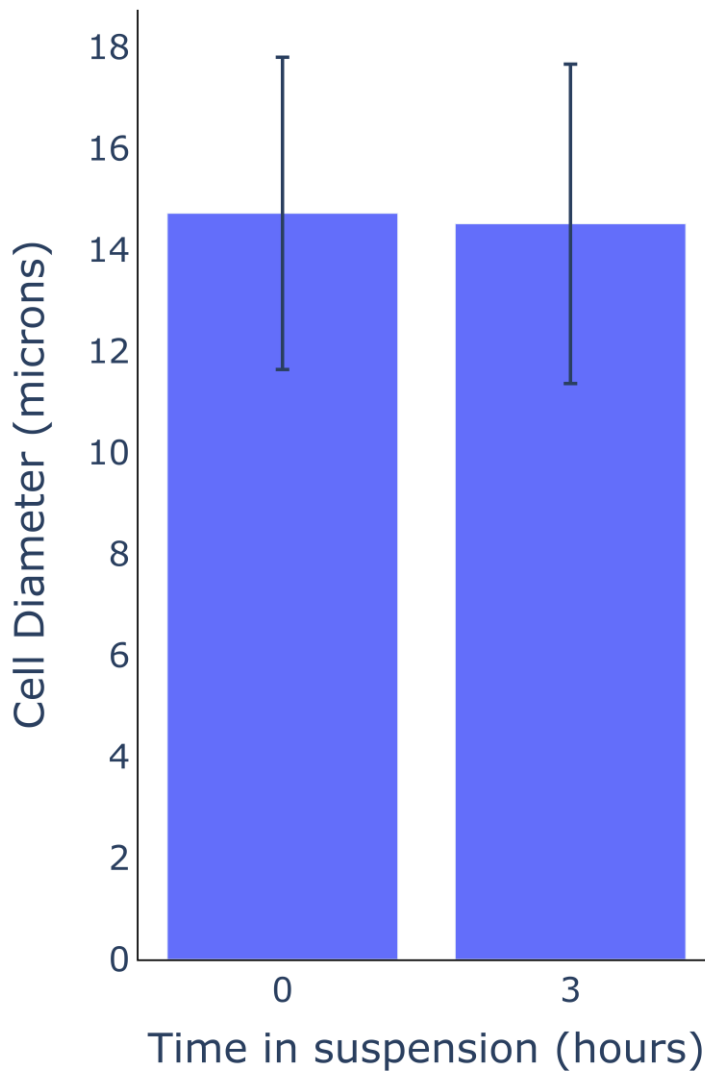


Figure 23. iPSC size immediately after dissociation and after 3 hours in suspension. No substantial change in size was observed after allowing cells to rest in suspension for 3 hours. This indicates that processing time should not have a large impact on device performance. Error bars represent the standard deviation of size within each sample.

This size heterogeneity appears to be a property of iPSCs and may be due to the way in which they grow in vitro. iPSCs generally grow in colonies, and as shown in Figure 24, cells growing at the edges of the colonies seem to be larger than their companions in the center. This suggests a naïve method of reducing heterogeneity, simply expanding the cells

until they are fully confluent (removing the distinction between cells on the edge of a colony and those in the center). Interestingly, we did find that when cultures were allowed to become massively overconfluent the average cell size and standard deviation from the mean did decrease slightly. Unfortunately, as overconfluence of iPSC cultures often results in spontaneous differentiation and a loss of potency, this should be avoided.

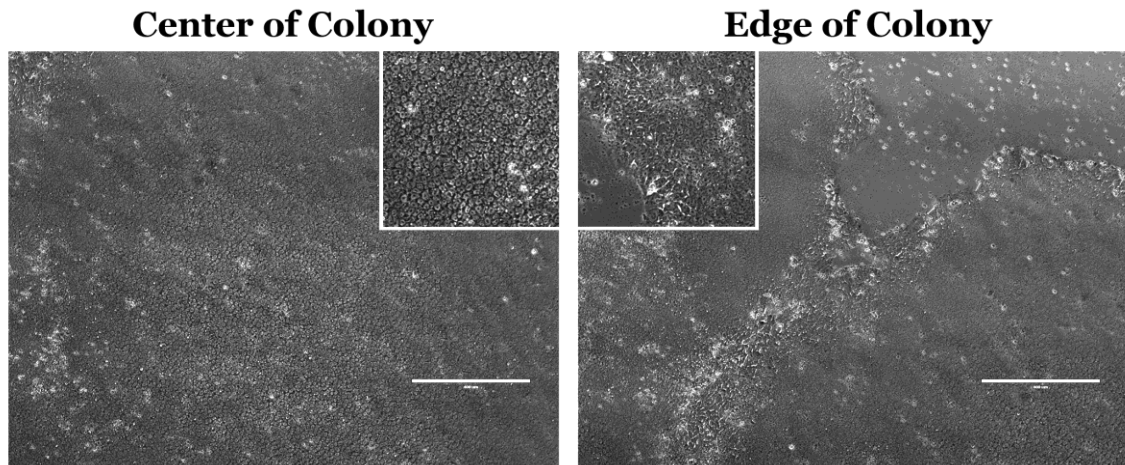


Figure 24. iPSC morphology at the center and edge of iPSC colonies. iPSCs in the center of colonies (**left**) appear to be smaller and more uniform in size than those at the edges of colonies (**right**). Scale bars are 400 microns.

The observed heterogeneity in terms of size presents a significant obstacle to our goal of microfluidic enhancement of transfection. As stated above, the performance of this transfection platform depends on careful tuning of device geometry to cause significant compression of cells without clogging, a task that is made very difficult if there is significant variation in cell size. For example, a device that could perform perfectly on cells close to the mean size in a population may become clogged due to larger cells present in the mixture and may not compress smaller cells enough to cause transfection.

To address this issue, we envision a modification of our device that will integrate a size-based sorter upstream of the transfection platform. We hypothesize that by splitting a heterogeneous iPSC population into subpopulations of more uniform size, we will dramatically improve the performance of our device and achieve transfection efficiencies significantly higher than those that are possible using existing approaches, such as lipofectamine.

5.5 Conclusions

In order to enable the development of autologous cell therapies for degenerative inherited conditions, transfection platforms are needed that are safe and capable of delivering large gene editing constructs to the interior of iPSCs. To meet this need, we propose adapting a microfluidic transfection technology developed in our group to iPSC transfection. Although we successfully used this platform to deliver large CRISPR/HDR constructs to patient-derived iPSCs, our progress has been hampered due to the large degree of size heterogeneity present in these cell lines. To address this issue, we propose a multistage microfluidic device capable of first presorting a heterogeneous iPSC mixture into subpopulations that are relatively homogeneous in size, which can then be processed efficiently using our microfluidic sorting platform. We believe that when complete, this multistage device will be capable of delivering large constructs to iPSCs much more efficiently than current techniques and in a manner that is compliant with cGMP. This will have the potential to increase the utility and safety of current cell manufacturing pipelines and make the production of patient-derived cell therapies safer, simpler and less expensive.

CHAPTER 6. CONCLUSIONS

Microfluidic cell processing has the potential to revolutionize the areas of personalized and regenerative medicine. In this thesis, I have shown how microfluidic cell sorting and transfection could increase the safety and potency of manufactured cell therapies while simultaneously making cell manufacturing pipelines simpler and cheaper to operate. I have further shown that microfluidic cell sorting has the promise to increase the efficacy of modern personalized medicine techniques by purifying cancer cells in noninvasively obtained liquid biopsies. In this chapter, I will summarize the contributions I have made towards applying microfluidic cell processing for personalized and regenerative medicine in the pursuit of three specific aims.

6.1 Aim 1: Label-free microfluidic enrichment of cancer cells from non-cancer cells in ascites

6.1.1 Summary

Personalized medicine promises to revolutionize the treatment of cancers by using functional and molecular characterization of a patient's own cancer cells to inform treatment decisions. While these approaches show great promise, it is currently difficult to obtain pure populations of a patient's cancer cells, an issue that must be solved before personalized medicine techniques can reach their full utility. While cells from a patient's primary tumor can be collected via biopsy, these operations are often quite invasive. In order to avoid performing invasive procedures on cancer patients who are often in poor health, recent approaches have explored the use of 'liquid biopsies', in which liquid

samples containing metastatic cancer cells (such as a patient's blood or abdominal fluid) are taken from patients in less invasive procedures. Unfortunately, these liquid biopsies do not result in pure populations of cancer cells. Instead, the malignant cells which are desired for functional and molecular characterization are generally mixed with contaminating blood and immune cells, which should be removed in order to increase the sensitivity of downstream assays. While many high throughput cell sorting technologies such as MACS and FACS have been commercialized, the dependence of these 'gold-standard' approaches on the presence of unique surface markers on cells of interest limit their utility for cancer applications. Given that every patient's cancer is unique, it is very difficult to depend on the presence of a specific marker to perform sorting using antibody-based techniques. To address this issue, we used a label-free microfluidic sorting platform to isolate cancer cells based on their size and stiffness, which has been shown to be a reliable marker for malignancy in many cancers. After exploring the feasibility of our technique using representative ovarian cancer cell lines we proceeded to isolate cancer cells from liquid biopsies taken from ovarian cancer patients. Analysis of our sorted populations using both immunocytochemistry and next generation sequencing techniques showed that our platform successfully enriched cancer cells from the mixed populations present in these liquid biopsies without relying on specific cell surface markers. These results show the great promise that our platform, and microfluidic label-free sorting in general, has for enabling high-sensitivity functional and molecular assays for personalized medicine applications.

6.1.2 *Future directions*

While our results for isolation of metastatic ovarian cancer cells from patient ascites were quite promising, there is work remaining before our sorting platform will be ready for clinical applications. First, experiments should be performed to determine how the sensitivity of personalized medicine assays change with increasing sample purity to determine the absolute purity that is required for these applications. Next, the purity of the samples generated using our platform should be quantified *via* histology to get a concrete number for the purity that is currently being achieved using our device. If higher purity is required, further optimization of the device could be performed, or a complete redesign could be undertaken. Given recent interest in the importance of circulating cancer cell clusters in metastasis, this redesign could focus on size-based sorting, which could be capable of sorting metastatic cancer cell clusters from single cells.

6.2 Specific Aim 2: Label-free microfluidic enrichment of photoreceptor cells

6.2.1 *Summary*

Induced pluripotent stem cell (iPSC) derived autologous cell therapies are a promising treatment for patients with a variety of conditions, including inherited degenerative blindness. In these treatment approaches, patient-derived iPSCs are generated from fibroblasts harvested from a patient via a skin biopsy. These iPSCs can then be differentiated into cells capable of regenerating tissue a patient has lost due to injury or disease. In the case of inherited degenerative blindness, our group and others are

developing pipelines for the manufacture of patient-derived photoreceptors which we hope will be capable of restoring a patient's vision after transplant. Unfortunately, current iPSC differentiation protocols do not result in pure populations of therapeutically relevant cells. Retinal differentiation protocols used for the production of photoreceptors result in a mixed population of many cell types present in the mature human retina, such as retinal pigment epithelium (RPE), glial, and photoreceptor cells. In order to increase the potency of cell therapies produced using these pipelines, a cell sorting approach is required to purify cells desired for transplant from other contaminating cells.

While very selective, gold-standard approaches such as FACS and MACS are not well suited to this application. Conjugation of animal-derived antibodies to cells destined for transplant into patients poses significant safety risks, and the use of expensive FACS sorters to isolate cells destined for transplant into multiple patients increases the risk of contaminating cells manufactured for one patient with those intended for others. Label-free microfluidic sorting systems can be implemented as single-use, disposable chips which drastically reduce the risk of product contamination and can be operated without the use of reagents, such as monoclonal antibodies, which could compromise the safety and increase the regulatory burden associated with these treatments.

To demonstrate how label-free microfluidic sorting systems could be used to increase the potency and safety of iPSC-derived autologous cell therapies, we applied our microfluidic sorting platform to the isolation of photoreceptors from the mixture of cell types found in the human retina. After performing mechanical characterization of representative cell lines to show that target photoreceptors and contaminating cells are mechanically distinct and sortable using our approach, we proceeded to isolate photoreceptors from dissociated

whole human retina. We then examined the gene expression profiles of our sorted populations, which showed that our device was capable of enriching photoreceptors from the mixture of cell types present in whole human retina. We believe that this result indicates that label-free microfluidic sorting should be capable of isolating photoreceptors from contaminating cells produced during iPSC differentiation protocols, thereby increasing the potency and safety of the resulting cell therapy.

6.2.2 Future directions

While our results showing enrichment of cone photoreceptors from dissociated post-mortem human retina indicate that our platform should be capable of isolating photoreceptors from patient iPSC derived retinal organoids, our next step is to prove that it is. The first step in this process will be to perform detailed size and mechanical characterization of the populations present in mature iPSC derived retinal organoids, after which our device will need to be redesigned and reoptimized for this application.

6.3 Specific Aim 3: Use microfluidics to deliver large functional constructs to patient derived iPSCs in a one-step mechanical process

6.3.1 Summary

When manufacturing cell therapies for the treatment of inherited conditions, it is likely that any disease-causing mutations will need to be corrected in patient-derived iPSCs before differentiating them into the cell types relevant for therapy. In practice, this means that technologies capable of delivering large gene editing constructs at high efficiency are needed. While many cell transfection technologies such as electroporation, lipofection and

viral transduction have been developed previously, none of them are ideal for correcting mutations in genes in patient-derived iPSCs. Packaging size limitations make it impossible to use clinically-relevant viruses for this application, and while both lipofectamine and electroporation have been used to correct mutations in iPSCs previously, both suffer from very low transfection efficiencies when delivering large constructs.

Recently, our group developed a reagent-free microfluidic transfection platform capable of delivering large payloads to cells using convective transport. As this technology accomplishes delivery using an active (convective) transport mechanism, it is capable of delivering very large macromolecules to cells with very high efficiency, making it ideal for use in this application.

While we demonstrated transfection with efficiencies comparable to lipofectamine, we believe that this is not the highest possible transfection efficiency achievable with our platform. One drawback of this microfluidic transfection platform is that it does not perform well when used to process cell populations that are heterogeneous in terms of size. To determine if this would be an issue in our case, we performed extensive characterization of how iPSC size changes with different culture conditions, such as plating density and choice of adhesion protein. This characterization revealed that there exists significant size heterogeneity in iPSC populations even when these parameters are controlled for.

6.3.2 Future directions

In order to address the previously unreported size heterogeneity of iPSCs, our next step is the design of a multistage microfluidic device capable of splitting heterogeneous iPSC populations into homogeneous subpopulations through size based sorting upstream of

transfection. Each of these subpopulations could then be transfected using channels optimized for that population. We believe that such a device will be capable of transfecting iPSCs at very high efficiencies, simplifying iPSC manufacturing pipelines for regenerative medicine applications.

6.4 Summary

In this thesis, I have demonstrated how microfluidic cell processing can be used to improve current methodologies for both personalized and regenerative medicine. In aim one, I showed how label-free microfluidic cell sorting can be used to improve personalized medicine workflows by enabling isolation of metastatic cancer cells from liquid biopsies without relying on antibody labels. In aim two, I demonstrate that microfluidic cell sorting can be used to isolate photoreceptors from other retinal cell populations to improve the safety and potency of cell therapies for inherited degenerative blindness. Finally, in aim three, I demonstrate successful delivery of a large multicistronic CRISPR construct to patient derived iPSCs at efficiencies comparable to lipofectamine, a standard in the field. In addition, I performed the first in depth characterization of iPSC cell size, with the end goal of designing a new microfluidic platform capable of enhancing the efficiency with which large gene editing constructs can be delivered to patient-derived iPSCs. Taken as a whole, this work demonstrates the central role microfluidic cell processing will play in personalized and regenerative therapies for cancer, inherited blindness and other conditions.

APPENDIX A. OPTIMIZATION OF MICROFLUIDIC SORTING DEVICES

Currently, our microfluidic sorting platform must be reoptimized for every application. While this procedure is laborious and requires a decent amount of intuition, it can be approached in a semi-systematic way, as shown in Figure X. The crucial, first step in this process is exhaustive characterization of the size and mechanics of the populations to be sorted to ensure that there are differences to exploit. For the work contained in this thesis, I performed mechanical characterization using atomic force microscopy (AFM) and size characterization using light microscopy and a coulter counter. While light microscopy is an acceptable method for measuring cell size, coulter counters are preferable, given that they are much higher throughput while being highly quantitative with respect to size.

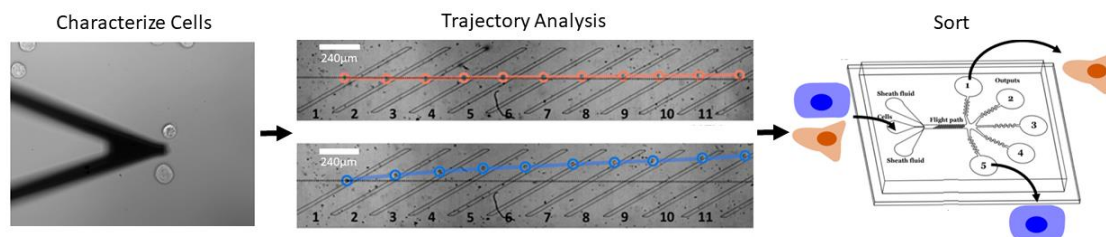


Figure 25. Optimization scheme for label-free microfluidic cell sorting. My optimization workflow starts with detailed size and mechanical characterization of cell populations to be sorted. Next, detailed trajectory analysis should be performed while varying device geometry and flow rates. The operation conditions that result in the biggest difference in characteristic trajectory of cells to be sorted can then be used to sort the cells of interest.

After performing characterization of the populations to be sorted, devices with a variety of ridge gaps should be fabricated. A good initial guess for an appropriate constriction size is 50-75% of the diameter of the largest cells to be sorted. These devices should then be tested

to find a constriction size/flow rate combination that results in qualitative differences in behavior between large/stiff and small/soft populations. Once this rough optimization has been completed, detailed trajectory information for each population to be sorted should be captured using high speed microscopy. This trajectory information should be captured while varying flow rate, ridge spacing and constriction size. Analysis of this data will allow the operator to discover the optimum device and flow rate which results in the largest difference between the characteristic trajectories of the populations to be sorted.

Finally, a sort should be attempted. The relative flow rates of the cell and sheath inlets should then be tuned (while keeping the total flow rate constant) to accomplish three goals. First, the cell stream should be well focused, so that each cell contacts the first ridge at the same point. Second, the total cell concentration should be controlled to minimize interactions between cells within the device, which can lead to poor sorting or clogs. Lowering this cell concentration, however, directly reduces throughput so it should only be reduced when necessary. Third, the relative flow rate of the two sheath inlets should be tuned to bias the cell stream such that the cells are spread as evenly as possible between outlets.

APPENDIX B. DESIGN IMPROVEMENTS FOR TRANSFECTION DEVICES

Over the course of the work contained in this thesis, I made two key contributions to the design of our transfection devices. First, I designed the symmetric constrictions of our transfection platform, illustrated in Figure 26. In our initial exploration of convective macromolecule delivery, we simply used our sorting platform to perform the compressions required to mediate transfection. However, the asymmetric design of our sorting platform had some disadvantages for transfection applications. Most importantly, our sorting platform is designed to cause cells to move laterally in the device, which could cause cells to exit the active region of the device before being compressed by each ridge. The symmetric design is intended to direct relatively small/soft cells towards the center of the channel, while directing large aggregates, which interfere with the operation of our device, out of the active region. This ability to redirect cells to the center of our device's active region also decreases the reliance of our device on precise cell focusing, which allowed us to remove the sheath inlets used in early devices. Removal of the sheath inlets simplified operation of the device and reduced consumption of expensive reagents.

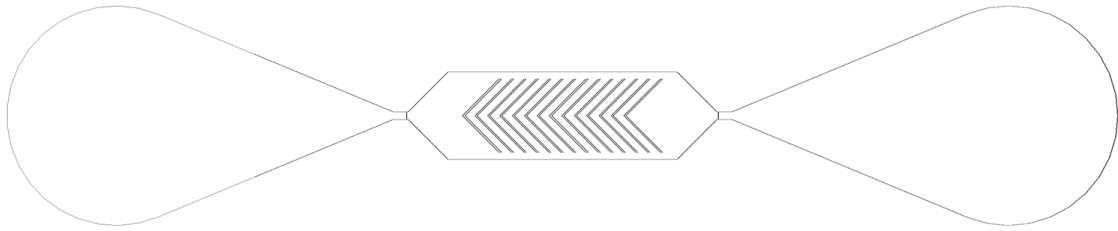


Figure 26. Symmetric constrictions for transfection devices. These symmetric constrictions are designed to focus single cells into the center of the transfection channel, while directing aggregates to the edges of the device.

While our redesigned transfection devices can be operated without any cell focusing, sheathless focusing would allow operators to ensure that every cell is successfully delivered to the active region of the device without wasting reagents by using sheaths. To this end, I introduced hydrodynamic focusing channels, illustrated in Figure X, at the inlets of our devices. These channels tend to concentrate cells with similar size into a single streamline, directing cells to the active region of our device without using sheaths [142]. Use of these focusing channels is now standard practice in our group.



Figure 27. Hydrodynamic focusing channels for sheathless operation of transfection devices. These channels tend to focus cells of similar size into a single streamline, allowing cells to be directed into the active area of our device without using sheath inlets.

APPENDIX C. LIST OF PUBLICATIONS

- **Nicholas E. Stone**, Andrew P. Voigt, Jessica A. Cooke, Joseph C. Giacalone, Srinivas Hanasoge, Robert F. Mullins, Budd A. Tucker, Todd Sulchek, Label-free microfluidic enrichment of photoreceptor cells, *Experimental Eye Research*, Volume 199, 2020, 108166, ISSN 0014-4835
- **Nicholas E. Stone**, Abhishek Raj, Katherine M. Young, Adam P. DeLuca, Fatima Ezahra Chrit, Budd A. Tucker, Alexander Alexeev, John McDonald, Benedict B. Benigno, Todd Sulchek, Label-free microfluidic enrichment of cancer cells from non-cancer cells in ascites, *Scientific Reports*, In press
- **Nicholas E. Stone**, Andrew P. Voigt, Robert F. Mullins, Todd Sulchek, Budd A. Tucker, Microfluidic processing of stem cells for autologous cell replacement, *Stem Cells Translational Medicine*, In press
- Islam, Muhymin, Hannah Brink, Sydney Blanche, Caleb DiPrete, Tom Bongiorno, **Nicholas Stone**, Anna Liu, et al. 2017. "Microfluidic Sorting of Cells by Viability Based on Differences in Cell Stiffness." *Scientific Reports* 7 (1): 1997. <https://doi.org/10.1038/s41598-017-01807-z>.
- Liu, Anna, Muhymin Islam, **Nicholas Stone**, Vikram Varadarajan, Jenny Jeong, Samuel Bowie, Peng Qiu, Edmund K. Waller, Alexander Alexeev, and Todd Sulchek. 2018. "Microfluidic Generation of Transient Cell Volume Exchange for Convectively Driven Intracellular Delivery of Large Macromolecules." *Materials Today* 21 (7): 703–12. <https://doi.org/10.1016/j.mattod.2018.03.002>.

- Liu, Anna, Tong Yu, Katherine Young, **Nicholas Stone**, Srinivas Hanasoge, Tyler J. Kirby, Vikram Varadarajan, et al. 2019. “Cell Mechanical and Physiological Behavior in the Regime of Rapid Mechanical Compressions That Lead to Cell Volume Change.” *Small*, November, 1903857. <https://doi.org/10.1002/sml.201903857>.

REFERENCES

- [1] A. Liu *et al.*, “Microfluidic generation of transient cell volume exchange for convectively driven intracellular delivery of large macromolecules,” *Mater. Today*, vol. 21, no. 7, pp. 703–712, 2018, doi: 10.1016/j.mattod.2018.03.002.
- [2] A. Liu *et al.*, “Cell Mechanical and Physiological Behavior in the Regime of Rapid Mechanical Compressions that Lead to Cell Volume Change,” *Small*, p. 1903857, Nov. 2019, doi: 10.1002/sml.201903857.
- [3] B. A. Tucker *et al.*, “Transplantation of adult mouse iPS cell-derived photoreceptor precursors restores retinal structure and function in degenerative mice,” *PloS One*, vol. 6, no. 4, p. e18992, Apr. 2011, doi: 10.1371/journal.pone.0018992.
- [4] D. A. Lamba, A. McUsic, R. K. Hirata, P.-R. Wang, D. Russell, and T. A. Reh, “Generation, purification and transplantation of photoreceptors derived from human induced pluripotent stem cells,” *PloS One*, vol. 5, no. 1, p. e8763, Jan. 2010, doi: 10.1371/journal.pone.0008763.
- [5] D. Zerti *et al.*, “Transplanted pluripotent stem cell-derived photoreceptor precursors elicit conventional and unusual light responses in mice with advanced retinal degeneration,” *Stem Cells Dayt. Ohio*, Mar. 2021, doi: 10.1002/stem.3365.
- [6] B. Lin *et al.*, “Retina Organoid Transplants Develop Photoreceptors and Improve Visual Function in RCS Rats With RPE Dysfunction,” *Invest. Ophthalmol. Vis. Sci.*, vol. 61, no. 11, p. 34, Sep. 2020, doi: 10.1167/iovs.61.11.34.
- [7] T. F. Santos-Ferreira, O. Borsch, and M. Ader, “Rebuilding the Missing Part-A Review on Photoreceptor Transplantation,” *Front. Syst. Neurosci.*, vol. 10, p. 105, 2016, doi: 10.3389/fnsys.2016.00105.
- [8] O. Goureau and G. Orioux, “[Photoreceptor cell transplantation for future treatment of retinitis pigmentosa],” *Med. Sci. MS*, vol. 36, no. 6–7, pp. 600–606, Jul. 2020, doi: 10.1051/medsci/2020097.
- [9] G. Gagliardi, K. Ben M’Barek, and O. Goureau, “Photoreceptor cell replacement in macular degeneration and retinitis pigmentosa: A pluripotent stem cell-based approach,” *Prog. Retin. Eye Res.*, vol. 71, pp. 1–25, Jul. 2019, doi: 10.1016/j.preteyeres.2019.03.001.
- [10] M. Mandai *et al.*, “Autologous Induced Stem-Cell-Derived Retinal Cells for Macular Degeneration,” *N. Engl. J. Med.*, vol. 376, no. 11, pp. 1038–1046, Mar. 2017, doi: 10.1056/NEJMoa1608368.

- [11] R. Sharma *et al.*, “Clinical-grade stem cell-derived retinal pigment epithelium patch rescues retinal degeneration in rodents and pigs,” *Sci. Transl. Med.*, vol. 11, no. 475, Jan. 2019, doi: 10.1126/scitranslmed.aat5580.
- [12] L. A. Wiley *et al.*, “cGMP production of patient-specific iPSCs and photoreceptor precursor cells to treat retinal degenerative blindness,” *Sci. Rep.*, vol. 6, Jul. 2016, doi: 10.1038/srep30742.
- [13] L. A. Wiley *et al.*, “Generation of Xeno-Free, cGMP-Compliant Patient-Specific iPSCs from Skin Biopsy,” *Curr. Protoc. Stem Cell Biol.*, vol. 42, no. 1, p. 4A.12.1-4A.12.14, Aug. 2017, doi: 10.1002/cpsc.30.
- [14] B. A. Tucker *et al.*, “Patient-specific iPSC-derived photoreceptor precursor cells as a means to investigate retinitis pigmentosa,” *eLife*, vol. 2, Aug. 2013, doi: 10.7554/eLife.00824.
- [15] X. Zhong *et al.*, “Generation of three dimensional retinal tissue with functional photoreceptors from human iPSCs,” *Nat. Commun.*, vol. 5, p. 4047, Jun. 2014, doi: 10.1038/ncomms5047.
- [16] J. S. Meyer *et al.*, “Optic Vesicle-like Structures Derived from Human Pluripotent Stem Cells Facilitate a Customized Approach to Retinal Disease Treatment,” *Stem Cells Dayt. Ohio*, vol. 29, no. 8, pp. 1206–1218, Aug. 2011, doi: 10.1002/stem.674.
- [17] J. S. Meyer *et al.*, “Modeling early retinal development with human embryonic and induced pluripotent stem cells,” *Proc. Natl. Acad. Sci. U. S. A.*, vol. 106, no. 39, pp. 16698–16703, Sep. 2009, doi: 10.1073/pnas.0905245106.
- [18] A. Kallman *et al.*, “Investigating cone photoreceptor development using patient-derived NRL null retinal organoids,” *Commun. Biol.*, vol. 3, Feb. 2020, doi: 10.1038/s42003-020-0808-5.
- [19] K. J. Wahlin, J. Maruotti, and D. J. Zack, “Modeling retinal dystrophies using patient-derived induced pluripotent stem cells,” *Adv. Exp. Med. Biol.*, vol. 801, pp. 157–164, 2014, doi: 10.1007/978-1-4614-3209-8_20.
- [20] K. Ueda, A. Onishi, S.-I. Ito, M. Nakamura, and M. Takahashi, “Generation of three-dimensional retinal organoids expressing rhodopsin and S- and M-cone opsins from mouse stem cells,” *Biochem. Biophys. Res. Commun.*, vol. 495, no. 4, pp. 2595–2601, Jan. 2018, doi: 10.1016/j.bbrc.2017.12.092.
- [21] J. Collin *et al.*, “CRX Expression in Pluripotent Stem Cell-Derived Photoreceptors Marks a Transplantable Subpopulation of Early Cones,” *Stem Cells Dayt. Ohio*, vol. 37, no. 5, pp. 609–622, May 2019, doi: 10.1002/stem.2974.
- [22] S. Reichman *et al.*, “From confluent human iPS cells to self-forming neural retina and retinal pigmented epithelium,” *Proc. Natl. Acad. Sci. U. S. A.*, vol. 111, no. 23, pp. 8518–8523, Jun. 2014, doi: 10.1073/pnas.1324212111.

- [23] C. B. Mellough, E. Sernagor, I. Moreno-Gimeno, D. H. W. Steel, and M. Lako, “Efficient stage-specific differentiation of human pluripotent stem cells toward retinal photoreceptor cells,” *Stem Cells Dayt. Ohio*, vol. 30, no. 4, pp. 673–686, Apr. 2012, doi: 10.1002/stem.1037.
- [24] T. J. Rowland, D. E. Buchholz, and D. O. Clegg, “Pluripotent human stem cells for the treatment of retinal disease,” *J. Cell. Physiol.*, vol. 227, no. 2, pp. 457–466, Feb. 2012, doi: 10.1002/jcp.22814.
- [25] A. La Torre, D. A. Lamba, A. Jayabalu, and T. A. Reh, “Production and transplantation of retinal cells from human and mouse embryonic stem cells,” *Methods Mol. Biol. Clifton NJ*, vol. 884, pp. 229–246, 2012, doi: 10.1007/978-1-61779-848-1_16.
- [26] B. A. Tucker *et al.*, “Exome sequencing and analysis of induced pluripotent stem cells identify the cilia-related gene male germ cell-associated kinase (MAK) as a cause of retinitis pigmentosa,” *Proc. Natl. Acad. Sci. U. S. A.*, vol. 108, no. 34, pp. E569–576, Aug. 2011, doi: 10.1073/pnas.1108918108.
- [27] Z.-B. Jin *et al.*, “Modeling retinal degeneration using patient-specific induced pluripotent stem cells,” *PloS One*, vol. 6, no. 2, p. e17084, Feb. 2011, doi: 10.1371/journal.pone.0017084.
- [28] T. A. Reh, D. Lamba, and J. Gust, “Directing human embryonic stem cells to a retinal fate,” *Methods Mol. Biol. Clifton NJ*, vol. 636, pp. 139–153, 2010, doi: 10.1007/978-1-60761-691-7_9.
- [29] F. Osakada *et al.*, “In vitro differentiation of retinal cells from human pluripotent stem cells by small-molecule induction,” *J. Cell Sci.*, vol. 122, no. Pt 17, pp. 3169–3179, Sep. 2009, doi: 10.1242/jcs.050393.
- [30] D. A. Lamba, J. Gust, and T. A. Reh, “Transplantation of human embryonic stem cell-derived photoreceptors restores some visual function in Crx-deficient mice,” *Cell Stem Cell*, vol. 4, no. 1, pp. 73–79, Jan. 2009, doi: 10.1016/j.stem.2008.10.015.
- [31] F. Osakada *et al.*, “Toward the generation of rod and cone photoreceptors from mouse, monkey and human embryonic stem cells,” *Nat. Biotechnol.*, vol. 26, no. 2, pp. 215–224, Feb. 2008, doi: 10.1038/nbt1384.
- [32] C. Boucherie, S. Mukherjee, E. Henckaerts, A. J. Thrasher, J. C. Sowden, and R. R. Ali, “Brief report: self-organizing neuroepithelium from human pluripotent stem cells facilitates derivation of photoreceptors,” *Stem Cells Dayt. Ohio*, vol. 31, no. 2, pp. 408–414, Feb. 2013, doi: 10.1002/stem.1268.
- [33] T. Nakano *et al.*, “Self-formation of optic cups and storable stratified neural retina from human ESCs,” *Cell Stem Cell*, vol. 10, no. 6, pp. 771–785, Jun. 2012, doi: 10.1016/j.stem.2012.05.009.

- [34] C. M. Fligor, K.-C. Huang, S. S. Lavekar, K. B. VanderWall, and J. S. Meyer, "Differentiation of retinal organoids from human pluripotent stem cells," *Methods Cell Biol.*, vol. 159, pp. 279–302, 2020, doi: 10.1016/bs.mcb.2020.02.005.
- [35] D. Zerti *et al.*, "Developing a simple method to enhance the generation of cone and rod photoreceptors in pluripotent stem cell-derived retinal organoids," *Stem Cells Dayt. Ohio*, vol. 38, no. 1, pp. 45–51, Jan. 2020, doi: 10.1002/stem.3082.
- [36] D. Hallam *et al.*, "Human-Induced Pluripotent Stem Cells Generate Light Responsive Retinal Organoids with Variable and Nutrient-Dependent Efficiency," *Stem Cells Dayt. Ohio*, vol. 36, no. 10, pp. 1535–1551, Oct. 2018, doi: 10.1002/stem.2883.
- [37] M. Eiraku *et al.*, "Self-organizing optic-cup morphogenesis in three-dimensional culture," *Nature*, vol. 472, no. 7341, Art. no. 7341, Apr. 2011, doi: 10.1038/nature09941.
- [38] W.-L. Deng *et al.*, "Gene Correction Reverses Ciliopathy and Photoreceptor Loss in iPSC-Derived Retinal Organoids from Retinitis Pigmentosa Patients," *Stem Cell Rep.*, vol. 10, no. 4, pp. 1267–1281, Apr. 2018, doi: 10.1016/j.stemcr.2018.02.003.
- [39] H. Liu *et al.*, "Human embryonic stem cell-derived organoid retinoblastoma reveals a cancerous origin," *Proc. Natl. Acad. Sci.*, vol. 117, no. 52, pp. 33628–33638, Dec. 2020, doi: 10.1073/pnas.2011780117.
- [40] S. Kim *et al.*, "Generation, transcriptome profiling, and functional validation of cone-rich human retinal organoids," *Proc. Natl. Acad. Sci.*, vol. 116, no. 22, pp. 10824–10833, May 2019, doi: 10.1073/pnas.1901572116.
- [41] D. Pan *et al.*, "COCO enhances the efficiency of photoreceptor precursor differentiation in early human embryonic stem cell-derived retinal organoids," *Stem Cell Res. Ther.*, vol. 11, no. 1, p. 366, Aug. 2020, doi: 10.1186/s13287-020-01883-5.
- [42] K. Homma, S. Usui, and M. Kaneda, "Knock-in strategy at 3'-end of Crx gene by CRISPR/Cas9 system shows the gene expression profiles during human photoreceptor differentiation," *Genes Cells*, vol. 22, no. 3, pp. 250–264, 2017, doi: <https://doi.org/10.1111/gtc.12472>.
- [43] Y.-Y. Jang and Z. Ye, "Gene correction in patient-specific iPSCs for therapy development and disease modeling," *Hum. Genet.*, vol. 135, no. 9, pp. 1041–1058, Sep. 2016, doi: 10.1007/s00439-016-1691-5.
- [44] E. R. Burnight *et al.*, "CRISPR-Cas9 genome engineering: Treating inherited retinal degeneration," *Prog. Retin. Eye Res.*, vol. 65, pp. 28–49, Jul. 2018, doi: 10.1016/j.preteyeres.2018.03.003.

- [45] N. Brookhouser, S. Raman, C. Potts, and D. A. Brafman, “May I Cut in? Gene Editing Approaches in Human Induced Pluripotent Stem Cells,” *Cells*, vol. 6, no. 1, Feb. 2017, doi: 10.3390/cells6010005.
- [46] R. E. MacLaren *et al.*, “Retinal repair by transplantation of photoreceptor precursors,” *Nature*, vol. 444, no. 7116, pp. 203–207, Nov. 2006, doi: 10.1038/nature05161.
- [47] K. Homma *et al.*, “Developing rods transplanted into the degenerating retina of Crx-knockout mice exhibit neural activity similar to native photoreceptors,” *Stem Cells Dayt. Ohio*, vol. 31, no. 6, pp. 1149–1159, Jun. 2013, doi: 10.1002/stem.1372.
- [48] T. Suzuki *et al.*, “Chondroitinase ABC treatment enhances synaptogenesis between transplant and host neurons in model of retinal degeneration,” *Cell Transplant.*, vol. 16, no. 5, pp. 493–503, 2007, doi: 10.3727/000000007783464966.
- [49] E. Aboualizadeh *et al.*, “Imaging Transplanted Photoreceptors in Living Nonhuman Primates with Single-Cell Resolution,” *Stem Cell Rep.*, vol. 15, no. 2, pp. 482–497, Aug. 2020, doi: 10.1016/j.stemcr.2020.06.019.
- [50] R. Kaewkhaw *et al.*, “Treatment Paradigms for Retinal and Macular Diseases Using 3-D Retina Cultures Derived From Human Reporter Pluripotent Stem Cell Lines,” *Invest. Ophthalmol. Vis. Sci.*, vol. 57, no. 5, pp. ORSF11–ORSF111, Apr. 2016, doi: 10.1167/iovs.15-17639.
- [51] P. T. Lam, C. Gutierrez, K. Del Rio-Tsonis, and M. L. Robinson, “Generation of a Retina Reporter hiPSC Line to Label Progenitor, Ganglion, and Photoreceptor Cell Types,” *Transl. Vis. Sci. Technol.*, vol. 9, no. 3, p. 21, Feb. 2020, doi: 10.1167/tvst.9.3.21.
- [52] G. Gagliardi *et al.*, “Characterization and Transplantation of CD73-Positive Photoreceptors Isolated from Human iPSC-Derived Retinal Organoids,” *Stem Cell Rep.*, vol. 11, no. 3, pp. 665–680, Sep. 2018, doi: 10.1016/j.stemcr.2018.07.005.
- [53] S. Reichman *et al.*, “Generation of Storable Retinal Organoids and Retinal Pigmented Epithelium from Adherent Human iPSCs in Xeno-Free and Feeder-Free Conditions,” *Stem Cells Dayt. Ohio*, vol. 35, no. 5, pp. 1176–1188, May 2017, doi: 10.1002/stem.2586.
- [54] T. Santos-Ferreira *et al.*, “Stem Cell-Derived Photoreceptor Transplants Differentially Integrate Into Mouse Models of Cone-Rod Dystrophy,” *Invest. Ophthalmol. Vis. Sci.*, vol. 57, no. 7, pp. 3509–3520, Jun. 2016, doi: 10.1167/iovs.16-19087.
- [55] T. Santos-Ferreira, K. Postel, H. Stutzki, T. Kurth, G. Zeck, and M. Ader, “Daylight vision repair by cell transplantation,” *Stem Cells Dayt. Ohio*, vol. 33, no. 1, pp. 79–90, Jan. 2015, doi: 10.1002/stem.1824.

- [56] D. Eberle, T. Santos-Ferreira, S. Grahl, and M. Ader, “Subretinal transplantation of MACS purified photoreceptor precursor cells into the adult mouse retina,” *J. Vis. Exp. JoVE*, no. 84, p. e50932, Feb. 2014, doi: 10.3791/50932.
- [57] J. Lakowski *et al.*, “Transplantation of Photoreceptor Precursors Isolated via a Cell Surface Biomarker Panel From Embryonic Stem Cell-Derived Self-Forming Retina,” *Stem Cells Dayt. Ohio*, vol. 33, no. 8, pp. 2469–2482, Aug. 2015, doi: 10.1002/stem.2051.
- [58] S. Nishimoto *et al.*, “CD140b and CD73 are markers for human induced pluripotent stem cell-derived erythropoietin-producing cells,” *FEBS Open Bio*, vol. 10, no. 3, pp. 427–433, Mar. 2020, doi: 10.1002/2211-5463.12800.
- [59] C. Estrela *et al.*, “Mesenchymal Stem Cell Marker Expression in Periapical Abscess,” *J. Endod.*, vol. 45, no. 6, pp. 716–723, Jun. 2019, doi: 10.1016/j.joen.2019.03.009.
- [60] A. P. Voigt *et al.*, “Molecular characterization of foveal versus peripheral human retina by single-cell RNA sequencing,” *Exp. Eye Res.*, vol. 184, pp. 234–242, Jul. 2019, doi: 10.1016/j.exer.2019.05.001.
- [61] Y. Lu *et al.*, “Single-Cell Analysis of Human Retina Identifies Evolutionarily Conserved and Species-Specific Mechanisms Controlling Development,” *Dev. Cell*, vol. 53, no. 4, pp. 473-491.e9, May 2020, doi: 10.1016/j.devcel.2020.04.009.
- [62] N. Y. Frank *et al.*, “Regulation of progenitor cell fusion by ABCB5 P-glycoprotein, a novel human ATP-binding cassette transporter,” *J. Biol. Chem.*, vol. 278, no. 47, pp. 47156–47165, Nov. 2003, doi: 10.1074/jbc.M308700200.
- [63] J. Ma *et al.*, “Isolation of tumorigenic circulating melanoma cells,” *Biochem. Biophys. Res. Commun.*, vol. 402, no. 4, pp. 711–717, Nov. 2010, doi: 10.1016/j.bbrc.2010.10.091.
- [64] B. J. Wilson *et al.*, “ABCB5 identifies a therapy-refractory tumor cell population in colorectal cancer patients,” *Cancer Res.*, vol. 71, no. 15, pp. 5307–5316, Aug. 2011, doi: 10.1158/0008-5472.CAN-11-0221.
- [65] K. Mulfaul *et al.*, “Stepwise differentiation and functional characterization of human induced pluripotent stem cell-derived choroidal endothelial cells,” *Stem Cell Res. Ther.*, vol. 11, no. 1, p. 409, Sep. 2020, doi: 10.1186/s13287-020-01903-4.
- [66] F. Zhang *et al.*, “Efficient endothelial and smooth muscle cell differentiation from human pluripotent stem cells through a simplified insulin-free culture system,” *Biomaterials*, vol. 271, p. 120713, Feb. 2021, doi: 10.1016/j.biomaterials.2021.120713.
- [67] S. Pars, K. Achberger, A. Kleger, S. Liebau, and N. Pashkovskaia, “Generation of Functional Vascular Endothelial Cells and Pericytes from Keratinocyte Derived

- Human Induced Pluripotent Stem Cells,” *Cells*, vol. 10, no. 1, Jan. 2021, doi: 10.3390/cells10010074.
- [68] S. Ota *et al.*, “Ghost cytometry,” *Science*, vol. 360, no. 6394, pp. 1246–1251, Jun. 2018, doi: 10.1126/science.aan0096.
- [69] C. Petchakup, K. H. H. Li, and H. W. Hou, “Advances in Single Cell Impedance Cytometry for Biomedical Applications,” *Micromachines*, vol. 8, no. 3, Mar. 2017, doi: 10.3390/mi8030087.
- [70] A. Mietke *et al.*, “Extracting Cell Stiffness from Real-Time Deformability Cytometry: Theory and Experiment,” *Biophys. J.*, vol. 109, no. 10, pp. 2023–2036, Nov. 2015, doi: 10.1016/j.bpj.2015.09.006.
- [71] M. Xavier *et al.*, “Label-free enrichment of primary human skeletal progenitor cells using deterministic lateral displacement,” *Lab. Chip*, vol. 19, no. 3, pp. 513–523, Jan. 2019, doi: 10.1039/c8lc01154k.
- [72] Z. Liu *et al.*, “Rapid isolation of cancer cells using microfluidic deterministic lateral displacement structure,” *Biomicrofluidics*, vol. 7, no. 1, Jan. 2013, doi: 10.1063/1.4774308.
- [73] C. I. Civin *et al.*, “Automated leukocyte processing by microfluidic deterministic lateral displacement,” *Cytometry A*, vol. 89, no. 12, pp. 1073–1083, 2016, doi: <https://doi.org/10.1002/cyto.a.23019>.
- [74] J. McGrath, M. Jimenez, and H. Bridle, “Deterministic lateral displacement for particle separation: a review,” *Lab Chip*, vol. 14, no. 21, pp. 4139–4158, Sep. 2014, doi: 10.1039/C4LC00939H.
- [75] D. Di Carlo, D. Irimia, R. G. Tompkins, and M. Toner, “Continuous inertial focusing, ordering, and separation of particles in microchannels,” *Proc. Natl. Acad. Sci. U. S. A.*, vol. 104, no. 48, pp. 18892–7, 2007, doi: 10.1073/pnas.0704958104.
- [76] S. C. Hur, T. Z. Brinckerhoff, C. M. Walthers, J. C. Y. Dunn, and D. D. Carlo, “Label-Free Enrichment of Adrenal Cortical Progenitor Cells Using Inertial Microfluidics,” *PLOS ONE*, vol. 7, no. 10, p. e46550, Oct. 2012, doi: 10.1371/journal.pone.0046550.
- [77] J. Sun *et al.*, “Double spiral microchannel for label-free tumor cell separation and enrichment,” *Lab. Chip*, vol. 12, no. 20, pp. 3952–3960, Sep. 2012, doi: 10.1039/C2LC40679A.
- [78] T. M. Geislinger, B. Eggart, S. Braunmüller, L. Schmid, and T. Franke, “Separation of blood cells using hydrodynamic lift,” *Appl. Phys. Lett.*, vol. 100, no. 18, p. 183701, Apr. 2012, doi: 10.1063/1.4709614.

- [79] B. A. Tucker *et al.*, “Patient-specific iPSC-derived photoreceptor precursor cells as a means to investigate retinitis pigmentosa,” *eLife*, vol. 2, p. e00824, Aug. 2013, doi: 10.7554/eLife.00824.
- [80] S. Reichman *et al.*, “From confluent human iPS cells to self-forming neural retina and retinal pigmented epithelium,” *Proc. Natl. Acad. Sci. U. S. A.*, vol. 111, no. 23, pp. 8518–8523, Jun. 2014, doi: 10.1073/pnas.1324212111.
- [81] X. Zhong *et al.*, “Generation of three-dimensional retinal tissue with functional photoreceptors from human iPSCs,” *Nat. Commun.*, vol. 5, p. 4047, Jun. 2014, doi: 10.1038/ncomms5047.
- [82] C. M. Fligor, K.-C. Huang, S. S. Lavekar, K. B. VanderWall, and J. S. Meyer, “Differentiation of retinal organoids from human pluripotent stem cells,” *Methods Cell Biol.*, vol. 159, pp. 279–302, 2020, doi: 10.1016/bs.mcb.2020.02.005.
- [83] D. Zerti *et al.*, “Developing a simple method to enhance the generation of cone and rod photoreceptors in pluripotent stem cell-derived retinal organoids,” *Stem Cells Dayt. Ohio*, vol. 38, no. 1, pp. 45–51, Jan. 2020, doi: 10.1002/stem.3082.
- [84] D. Hallam *et al.*, “Human-Induced Pluripotent Stem Cells Generate Light Responsive Retinal Organoids with Variable and Nutrient-Dependent Efficiency,” *Stem Cells Dayt. Ohio*, vol. 36, no. 10, pp. 1535–1551, Oct. 2018, doi: 10.1002/stem.2883.
- [85] A. Liu *et al.*, “Microfluidic generation of transient cell volume exchange for convectively driven intracellular delivery of large macromolecules,” *Mater. Today Kidlington Engl.*, vol. 21, no. 7, pp. 703–712, Sep. 2018, doi: 10.1016/j.mattod.2018.03.002.
- [86] N. E. Stone *et al.*, “Label-free microfluidic enrichment of photoreceptor cells,” *Exp. Eye Res.*, vol. 199, p. 108166, Oct. 2020, doi: 10.1016/j.exer.2020.108166.
- [87] G. Wang *et al.*, “Stiffness dependent separation of cells in a microfluidic device,” *PLoS One*, vol. 8, no. 10, p. e75901, 2013, doi: 10.1371/journal.pone.0075901.
- [88] B. Tasadduq, W. Lam, A. Alexeev, A. F. Sarioglu, and T. Sulchek, “Enhancing size based size separation through vertical focus microfluidics using secondary flow in a ridged microchannel,” *Sci. Rep.*, vol. 7, no. 1, p. 17375, Dec. 2017, doi: 10.1038/s41598-017-17388-w.
- [89] G. Wang, K. Crawford, C. Turbyfield, W. Lam, A. Alexeev, and T. Sulchek, “Microfluidic cellular enrichment and separation through differences in viscoelastic deformation,” *Lab. Chip*, vol. 15, no. 2, pp. 532–540, Jan. 2015, doi: 10.1039/c4lc01150c.

- [90] T. Bongiorno *et al.*, “Biophysical subsets of embryonic stem cells display distinct phenotypic and morphological signatures,” *PLoS One*, vol. 13, no. 3, p. e0192631, 2018, doi: 10.1371/journal.pone.0192631.
- [91] E. R. Burnight *et al.*, “Using CRISPR-Cas9 to Generate Gene-Corrected Autologous iPSCs for the Treatment of Inherited Retinal Degeneration,” *Mol. Ther. J. Am. Soc. Gene Ther.*, vol. 25, no. 9, pp. 1999–2013, Sep. 2017, doi: 10.1016/j.ymthe.2017.05.015.
- [92] L. R. Bohrer *et al.*, “Correction of NR2E3 Associated Enhanced S-cone Syndrome Patient-specific iPSCs using CRISPR-Cas9,” *Genes*, vol. 10, no. 4, Apr. 2019, doi: 10.3390/genes10040278.
- [93] J. C. Giacalone *et al.*, “CRISPR-Cas9-Based Genome Editing of Human Induced Pluripotent Stem Cells,” *Curr. Protoc. Stem Cell Biol.*, vol. 44, p. 5B.7.1-5B.7.22, Feb. 2018, doi: 10.1002/cpsc.46.
- [94] M. A. Zeballos C and T. Gaj, “Next-Generation CRISPR Technologies and Their Applications in Gene and Cell Therapy,” *Trends Biotechnol.*, Dec. 2020, doi: 10.1016/j.tibtech.2020.10.010.
- [95] J. C. Giacalone *et al.*, “Development of a Molecularly Stable Gene Therapy Vector for the Treatment of RPGR-Associated X-Linked Retinitis Pigmentosa,” *Hum. Gene Ther.*, vol. 30, no. 8, pp. 967–974, Aug. 2019, doi: 10.1089/hum.2018.244.
- [96] L. A. Wiley *et al.*, “Assessment of Adeno-Associated Virus Serotype Tropism in Human Retinal Explants,” *Hum. Gene Ther.*, vol. 29, no. 4, pp. 424–436, Apr. 2018, doi: 10.1089/hum.2017.179.
- [97] L. A. Wiley *et al.*, “Using Patient-Specific Induced Pluripotent Stem Cells and Wild-Type Mice to Develop a Gene Augmentation-Based Strategy to Treat CLN3-Associated Retinal Degeneration,” *Hum. Gene Ther.*, vol. 27, no. 10, pp. 835–846, Oct. 2016, doi: 10.1089/hum.2016.049.
- [98] A. V. Cideciyan *et al.*, “Effect of an intravitreal antisense oligonucleotide on vision in Leber congenital amaurosis due to a photoreceptor cilium defect,” *Nat. Med.*, vol. 25, no. 2, pp. 225–228, Feb. 2019, doi: 10.1038/s41591-018-0295-0.
- [99] S. Russell *et al.*, “Efficacy and safety of voretigene neparvovec (AAV2-hRPE65v2) in patients with RPE65-mediated inherited retinal dystrophy: a randomised, controlled, open-label, phase 3 trial,” *Lancet Lond. Engl.*, vol. 390, no. 10097, pp. 849–860, Aug. 2017, doi: 10.1016/S0140-6736(17)31868-8.
- [100] Y. Jin, Y. Shen, X. Su, N. L. Weintraub, and Y. Tang, “Effective restoration of dystrophin expression in iPSC Mdx-derived muscle progenitor cells using the CRISPR/Cas9 system and homology-directed repair technology,” *Comput. Struct. Biotechnol. J.*, vol. 18, pp. 765–773, 2020, doi: 10.1016/j.csbj.2020.03.012.

- [101] J.-P. Zhang *et al.*, “Different Effects of sgRNA Length on CRISPR-mediated Gene Knockout Efficiency,” *Sci. Rep.*, vol. 6, p. 28566, Jun. 2016, doi: 10.1038/srep28566.
- [102] H. W. Chu *et al.*, “CRISPR-Cas9-mediated gene knockout in primary human airway epithelial cells reveals a proinflammatory role for MUC18,” *Gene Ther.*, vol. 22, no. 10, pp. 822–829, Oct. 2015, doi: 10.1038/gt.2015.53.
- [103] J.-P. Zhang *et al.*, “Efficient precise knockin with a double cut HDR donor after CRISPR/Cas9-mediated double-stranded DNA cleavage,” *Genome Biol.*, vol. 18, no. 1, p. 35, Feb. 2017, doi: 10.1186/s13059-017-1164-8.
- [104] K. Lundstrom, “Viral Vectors in Gene Therapy,” *Diseases*, vol. 6, no. 2, p. 42, May 2018, doi: 10.3390/diseases6020042.
- [105] S. Kim, D. Kim, S. W. Cho, J. Kim, and J.-S. Kim, “Highly efficient RNA-guided genome editing in human cells via delivery of purified Cas9 ribonucleoproteins,” *Genome Res.*, vol. 24, no. 6, pp. 1012–1019, Jun. 2014, doi: 10.1101/gr.171322.113.
- [106] R. Mout *et al.*, “Direct Cytosolic Delivery of CRISPR/Cas9-Ribonucleoprotein for Efficient Gene Editing,” *ACS Nano*, vol. 11, no. 3, pp. 2452–2458, Mar. 2017, doi: 10.1021/acsnano.6b07600.
- [107] D. Sinha *et al.*, “Human iPSC Modeling Reveals Mutation-Specific Responses to Gene Therapy in a Genotypically Diverse Dominant Maculopathy,” *Am. J. Hum. Genet.*, vol. 107, no. 2, pp. 278–292, Aug. 2020, doi: 10.1016/j.ajhg.2020.06.011.
- [108] D. M. Hallow, R. A. Seeger, P. P. Kamaev, G. R. Prado, M. C. LaPlaca, and M. R. Prausnitz, “Shear-induced intracellular loading of cells with molecules by controlled microfluidics,” *Biotechnol. Bioeng.*, vol. 99, no. 4, pp. 846–854, Mar. 2008, doi: 10.1002/bit.21651.
- [109] A. Sharei *et al.*, “A vector-free microfluidic platform for intracellular delivery,” *Proc. Natl. Acad. Sci. U. S. A.*, vol. 110, no. 6, pp. 2082–2087, Feb. 2013, doi: 10.1073/pnas.1218705110.
- [110] S. M. Byrne and G. M. Church, “Crispr-mediated Gene Targeting of Human Induced Pluripotent Stem Cells,” *Curr. Protoc. Stem Cell Biol.*, vol. 35, p. 5A.8.1-5A.8.22, 2015, doi: 10.1002/9780470151808.sc05a08s35.
- [111] S. M. Byrne, P. Mali, and G. M. Church, “Genome editing in human stem cells,” *Methods Enzymol.*, vol. 546, pp. 119–138, 2014, doi: 10.1016/B978-0-12-801185-0.00006-4.
- [112] “Cancer of the Ovary - Cancer Stat Facts,” *SEER*. <https://seer.cancer.gov/statfacts/html/ovary.html> (accessed Oct. 05, 2020).
- [113] E. Lengyel, “Ovarian Cancer Development and Metastasis,” *Am. J. Pathol.*, vol. 177, no. 3, pp. 1053–1064, 2010, doi: <https://doi.org/10.2353/ajpath.2010.100105>.

- [114] K. E. Scarberry, E. B. Dickerson, Z. J. Zhang, B. B. Benigno, and J. F. McDonald, "Selective removal of ovarian cancer cells from human ascites fluid using magnetic nanoparticles," *Nanomedicine Nanotechnol. Biol. Med.*, vol. 6, no. 3, pp. 399–408, Jun. 2010, doi: 10.1016/j.nano.2009.11.003.
- [115] D. Antolovic *et al.*, "Heterogeneous detection of circulating tumor cells in patients with colorectal cancer by immunomagnetic enrichment using different EpCAM-specific antibodies," *BMC Biotechnol.*, vol. 10, no. 1, p. 35, Apr. 2010, doi: 10.1186/1472-6750-10-35.
- [116] A. Latifi *et al.*, "Isolation and Characterization of Tumor Cells from the Ascites of Ovarian Cancer Patients: Molecular Phenotype of Chemoresistant Ovarian Tumors," *PLOS ONE*, vol. 7, no. 10, p. e46858, Oct. 2012, doi: 10.1371/journal.pone.0046858.
- [117] E. Kipps, D. S. P. Tan, and S. B. Kaye, "Meeting the challenge of ascites in ovarian cancer: new avenues for therapy and research," *Nat. Rev. Cancer*, vol. 13, no. 4, pp. 273–282, Apr. 2013, doi: 10.1038/nrc3432.
- [118] A. Jemal *et al.*, "Cancer Statistics, 2006," *CA. Cancer J. Clin.*, vol. 56, no. 2, pp. 106–130, Mar. 2006, doi: 10.3322/canjclin.56.2.106.
- [119] B. A. Goff *et al.*, "Development of an ovarian cancer symptom index," *Cancer*, vol. 109, no. 2, pp. 221–227, Jan. 2007, doi: 10.1002/cncr.22371.
- [120] B. Davidson *et al.*, "Proteomic Analysis of Malignant Ovarian Cancer Effusions as a Tool for Biologic and Prognostic Profiling," *Clin. Cancer Res.*, vol. 12, no. 3, pp. 791–799, Feb. 2006, doi: 10.1158/1078-0432.CCR-05-2516.
- [121] V. Thomázy and L. Fésüs, "Differential expression of tissue transglutaminase in human cells," *Cell Tissue Res.*, vol. 255, no. 1, pp. 215–224, Jan. 1989, doi: 10.1007/BF00229084.
- [122] S. Suresh, "Elastic clues in cancer detection," *Nat. Nanotechnol.*, vol. 2, no. 12, Art. no. 12, Dec. 2007, doi: 10.1038/nnano.2007.397.
- [123] M. Lekka *et al.*, "Cancer cell detection in tissue sections using AFM," *Arch. Biochem. Biophys.*, vol. 518, no. 2, pp. 151–156, Feb. 2012, doi: 10.1016/j.abb.2011.12.013.
- [124] D. D. Carlo, "A Mechanical Biomarker of Cell State in Medicine:," *J. Lab. Autom.*, Jan. 2012, doi: 10.1177/2211068211431630.
- [125] E. C. Faria *et al.*, "Measurement of elastic properties of prostate cancer cells using AFM," *Analyst*, vol. 133, no. 11, pp. 1498–1500, Oct. 2008, doi: 10.1039/B803355B.
- [126] M. Lekka, P. Laidler, D. Gil, J. Lekki, Z. Stachura, and A. Z. Hryniewicz, "Elasticity of normal and cancerous human bladder cells studied by scanning force

- microscopy,” *Eur. Biophys. J.*, vol. 28, no. 4, pp. 312–316, May 1999, doi: 10.1007/s002490050213.
- [127] J. Guck *et al.*, “Optical Deformability as an Inherent Cell Marker for Testing Malignant Transformation and Metastatic Competence,” *Biophys. J.*, vol. 88, no. 5, pp. 3689–3698, May 2005, doi: 10.1529/biophysj.104.045476.
- [128] Yu Zhang, V. Yazdanpanah, Mo Yang, M. Ozkan, and C. S. Ozkan, “Normal and cancer breast epithelial cells endocytosis study of nanoparticles by combined AFM and NSOM microscopy,” in *2007 7th IEEE Conference on Nanotechnology (IEEE NANO)*, Aug. 2007, pp. 1028–1032. doi: 10.1109/NANO.2007.4601358.
- [129] M. Plodinec *et al.*, “The nanomechanical signature of breast cancer,” *Nat. Nanotechnol.*, vol. 7, no. 11, Art. no. 11, Nov. 2012, doi: 10.1038/nnano.2012.167.
- [130] A. Fuhrmann, J. R. Staunton, V. Nandakumar, N. Banyai, P. C. W. Davies, and R. Ros, “AFM stiffness nanotomography of normal, metaplastic and dysplastic human esophageal cells,” *Phys. Biol.*, vol. 8, no. 1, p. 015007, Feb. 2011, doi: 10.1088/1478-3975/8/1/015007.
- [131] M. Prabhune, G. Belge, A. Dotzauer, J. Bullerdiek, and M. Radmacher, “Comparison of mechanical properties of normal and malignant thyroid cells,” *Micron*, vol. 43, no. 12, pp. 1267–1272, Dec. 2012, doi: 10.1016/j.micron.2012.03.023.
- [132] T. W. Remmerbach, F. Wottawah, J. Dietrich, B. Lincoln, C. Wittekind, and J. Guck, “Oral Cancer Diagnosis by Mechanical Phenotyping,” *Cancer Res.*, vol. 69, no. 5, pp. 1728–1732, Mar. 2009, doi: 10.1158/0008-5472.CAN-08-4073.
- [133] V. Swaminathan, K. Mythreye, E. T. O’Brien, A. Berchuck, G. C. Blobe, and R. Superfine, “Mechanical Stiffness Grades Metastatic Potential in Patient Tumor Cells and in Cancer Cell Lines,” *Cancer Res.*, vol. 71, no. 15, pp. 5075–5080, Aug. 2011, doi: 10.1158/0008-5472.CAN-11-0247.
- [134] R. Mezencev *et al.*, “Molecular analysis of the inhibitory effect of N-acetyl-L-cysteine on the proliferation and invasiveness of pancreatic cancer cells,” *Anticancer. Drugs*, vol. 24, no. 5, pp. 504–518, Jun. 2013, doi: 10.1097/CAD.0b013e32836009d7.
- [135] M. J. Rosenbluth, W. A. Lam, and D. A. Fletcher, “Analyzing cell mechanics in hematologic diseases with microfluidic biophysical flow cytometry,” *Lab. Chip*, vol. 8, no. 7, pp. 1062–1070, Jun. 2008, doi: 10.1039/B802931H.
- [136] M. J. Rosenbluth, W. A. Lam, and D. A. Fletcher, “Force Microscopy of Nonadherent Cells: A Comparison of Leukemia Cell Deformability,” *Biophys. J.*, vol. 90, no. 8, pp. 2994–3003, Apr. 2006, doi: 10.1529/biophysj.105.067496.
- [137] W. Xu, R. Mezencev, B. Kim, L. Wang, J. McDonald, and T. Sulchek, “Cell Stiffness Is a Biomarker of the Metastatic Potential of Ovarian Cancer Cells,” *PLoS ONE*, vol. 7, no. 10, 2012, doi: 10.1371/journal.pone.0046609.

- [138] A. C. Rowat *et al.*, “Nuclear envelope composition determines the ability of neutrophil-type cells to passage through micron-scale constrictions,” *J. Biol. Chem.*, vol. 288, no. 12, 2013, doi: 10.1074/jbc.M112.441535.
- [139] S. E. Cross, J. Yu-Sheng, R. Jianyu, and J. K. Gimzewski, “Nanomechanical analysis of cells from cancer patients,” *Nat. Nanotechnol.*, vol. 2, no. 12, pp. 780–783, 2007, doi: 10.1038/nnano.2007.388.
- [140] S. E. Cross, Y.-S. Jin, J. Tondre, R. Wong, J. Rao, and J. K. Gimzewski, “AFM-based analysis of human metastatic cancer cells,” *Nanotechnology*, vol. 19, no. 38, pp. 384003–384003, 2008, doi: 10.1088/0957-4484/19/38/384003.
- [141] A. Kilimnik, W. Mao, and A. Alexeev, “Inertial migration of deformable capsules in channel flow,” *Phys. Fluids*, vol. 23, no. 12, p. 123302, Dec. 2011, doi: 10.1063/1.3664402.
- [142] D. Di Carlo, D. Irimia, R. G. Tompkins, and M. Toner, “Continuous inertial focusing, ordering, and separation of particles in microchannels,” *Proc. Natl. Acad. Sci. U. S. A.*, vol. 104, no. 48, pp. 18892–7, 2007, doi: 10.1073/pnas.0704958104.
- [143] W. Zhao *et al.*, “Label-free ferrohydrodynamic cell separation of circulating tumor cells,” *Lab. Chip*, vol. 17, no. 18, pp. 3097–3111, Sep. 2017, doi: 10.1039/C7LC00680B.
- [144] W. Zhang *et al.*, “Microfluidics separation reveals the stem-cell-like deformability of tumor-initiating cells,” *Proc. Natl. Acad. Sci.*, vol. 109, no. 46, pp. 18707–18712, Nov. 2012, doi: 10.1073/pnas.1209893109.
- [145] S. C. Hur, N. K. Henderson-MacLennan, E. R. B. McCabe, and D. D. Carlo, “Deformability-based cell classification and enrichment using inertial microfluidics,” *Lab. Chip*, vol. 11, no. 5, pp. 912–920, Mar. 2011, doi: 10.1039/C0LC00595A.
- [146] T. Bongiorno *et al.*, “Biophysical subsets of embryonic stem cells display distinct phenotypic and morphological signatures,” *PLOS ONE*, vol. 13, no. 3, pp. e0192631–e0192631, Mar. 2018.
- [147] N. E. Stone *et al.*, “Label-free microfluidic enrichment of photoreceptor cells,” *Exp. Eye Res.*, vol. 199, p. 108166, Oct. 2020, doi: 10.1016/j.exer.2020.108166.
- [148] G. Wang *et al.*, “Stiffness Dependent Separation of Cells in a Microfluidic Device,” *PLoS ONE*, vol. 8, no. 10, 2013, doi: 10.1371/journal.pone.0075901.
- [149] M. Satpathy, H. Nakshatri, and D. Matei, “Transglutaminase 2 is overexpressed in ovarian cancer and facilitates the adhesion of cancer cells to fibronectin,” *Cancer Res.*, vol. 66, no. 8 Supplement, pp. 800–800, Apr. 2006.
- [150] Y. Zhang, L. Cao, D. Nguyen, and H. Lu, “TP53 mutations in epithelial ovarian cancer,” *Transl. Cancer Res.*, vol. 5, no. 6, Art. no. 6, Sep. 2016, doi: 10.21037/9452.

- [151] M. Islam *et al.*, “Microfluidic Sorting of Cells by Viability Based on Differences in Cell Stiffness,” *Sci. Rep.*, vol. 7, no. 1, pp. 1997–1997, 2017, doi: 10.1038/s41598-017-01807-z.
- [152] M. Islam *et al.*, “Microfluidic cell sorting by stiffness to examine heterogenic responses of cancer cells to chemotherapy,” *Cell Death Dis.*, vol. 9, no. 2, Art. no. 2, Feb. 2018, doi: 10.1038/s41419-018-0266-x.
- [153] I. Sahly *et al.*, “Localization of Usher 1 proteins to the photoreceptor calyceal processes, which are absent from mice,” *J. Cell Biol.*, vol. 199, no. 2, pp. 381–399, Oct. 2012, doi: 10.1083/jcb.201202012.
- [154] E. E. Capowski *et al.*, “Reproducibility and staging of 3D human retinal organoids across multiple pluripotent stem cell lines,” *Dev. Camb. Engl.*, vol. 146, no. 1, Jan. 2019, doi: 10.1242/dev.171686.
- [155] D. A. Lamba, M. O. Karl, C. B. Ware, and T. A. Reh, “Efficient generation of retinal progenitor cells from human embryonic stem cells,” *Proc. Natl. Acad. Sci. U. S. A.*, vol. 103, no. 34, pp. 12769–12774, Aug. 2006, doi: 10.1073/pnas.0601990103.
- [156] S. Dalvi, C. A. Galloway, and R. Singh, “Pluripotent Stem Cells to Model Degenerative Retinal Diseases: The RPE Perspective,” in *Pluripotent Stem Cells in Eye Disease Therapy*, K. Bharti, Ed. Cham: Springer International Publishing, 2019, pp. 1–31. doi: 10.1007/978-3-030-28471-8_1.
- [157] K.-C. Huang *et al.*, “Morphological and Molecular Defects in Human Three-Dimensional Retinal Organoid Model of X-Linked Juvenile Retinoschisis,” *Stem Cell Rep.*, vol. 13, no. 5, pp. 906–923, Oct. 2019, doi: 10.1016/j.stemcr.2019.09.010.
- [158] R. F. Mullins *et al.*, “Autosomal Recessive Retinitis Pigmentosa Due To ABCA4 Mutations: Clinical, Pathologic, and Molecular Characterization,” *Invest. Ophthalmol. Vis. Sci.*, vol. 53, no. 4, pp. 1883–1894, Apr. 2012, doi: 10.1167/iovs.12-9477.
- [159] D. Eberle, S. Schubert, K. Postel, D. Corbeil, and M. Ader, “Increased integration of transplanted CD73-positive photoreceptor precursors into adult mouse retina,” *Invest. Ophthalmol. Vis. Sci.*, vol. 52, no. 9, pp. 6462–6471, Aug. 2011, doi: 10.1167/iovs.11-7399.
- [160] G. Gagliardi *et al.*, “Characterization and Transplantation of CD73-Positive Photoreceptors Isolated from Human iPSC-Derived Retinal Organoids,” *Stem Cell Rep.*, vol. 11, no. 3, pp. 665–680, Sep. 2018, doi: 10.1016/j.stemcr.2018.07.005.
- [161] G. Wang, C. Turbyfield, K. Crawford, A. Alexeev, and T. Sulchek, “Cellular enrichment through microfluidic fractionation based on cell biomechanical properties,” *Microfluid. Nanofluidics*, vol. 19, no. 4, pp. 987–993, 2015, doi: 10.1007/s10404-015-1608-y.

- [162] T. Bongiorno, J. L. Chojnowski, J. D. Lauderdale, and T. Sulchek, “Cellular Stiffness as a Novel Stemness Marker in the Corneal Limbus,” *Biophys. J.*, vol. 111, no. 8, pp. 1761–1772, Oct. 2016, doi: 10.1016/j.bpj.2016.09.005.
- [163] K. Haase and A. E. Pelling, “Investigating cell mechanics with atomic force microscopy,” *J. R. Soc. Interface*, vol. 12, no. 104, pp. 20140970–20140970, Mar. 2015, doi: 10.1098/rsif.2014.0970.
- [164] S. Moreno-Flores, R. Benitez, M. dM Vivanco, and J. L. Toca-Herrera, “Stress relaxation and creep on living cells with the atomic force microscope: a means to calculate elastic moduli and viscosities of cell components,” *Nanotechnology*, vol. 21, no. 44, pp. 445101–445101, Nov. 2010, doi: 10.1088/0957-4484/21/44/445101.
- [165] J. Jeong, N. J. Frohberg, E. Zhou, T. Sulchek, and P. Qiu, “Accurately tracking single-cell movement trajectories in microfluidic cell sorting devices,” *PLOS ONE*, vol. 13, no. 2, p. e0192463, Feb. 2018, doi: 10.1371/journal.pone.0192463.
- [166] M. Du, D. Kavanagh, Z. Zhang, and N. Kalia, “Designing Microfluidic Devices to Sort Haematopoietic Stem Cells Based on Their Mechanical Properties,” *Stem Cells Int.*, vol. 2019, p. e8540706, Sep. 2019, doi: 10.1155/2019/8540706.
- [167] C. A. Curcio, K. R. Sloan, O. Packer, A. E. Hendrickson, and R. E. Kalina, “Distribution of cones in human and monkey retina: individual variability and radial asymmetry,” *Science*, vol. 236, no. 4801, pp. 579–582, May 1987, doi: 10.1126/science.3576186.
- [168] C. A. Curcio, C. L. Millican, K. A. Allen, and R. E. Kalina, “Aging of the human photoreceptor mosaic: evidence for selective vulnerability of rods in central retina.,” *Invest. Ophthalmol. Vis. Sci.*, vol. 34, no. 12, pp. 3278–3296, Nov. 1993.
- [169] V. A. Loiko *et al.*, “Morphometric model of lymphocyte as applied to scanning flow cytometry,” *J. Quant. Spectrosc. Radiat. Transf.*, vol. 102, no. 1, pp. 73–84, Nov. 2006, doi: 10.1016/j.jqsrt.2006.02.069.